Dipartimento di Scienze della Vita

Dottorato in Scienze della Vita-Life Sciences

38° Ciclo

Coordinatrice: Prof.ssa Simona Maccherini

Characterization of a Preterm Rabbit Model Exposed to Hyperoxia for Preclinical Studies of Bronchopulmonary Dysplasia (BPD)

MEDS_02/A

Candidato

Simone De Meo

Sede di attività Università degli studi di Siena

Firma digitale del candidato

Firmato il 26/02/2026 6:06 PM
SIMONE DE MEO (simone.demeo@student.unisi.it)

Certificato da yousign

Supervisore

Dr.ssa Monica Lucattelli

Ente di appartenenza Università degli studi di Siena

Co-supervisori

Dr.ssa Chiara Catozzi

Dr.ssa Francesca Ricci

Ente di appartenenza Chiesi Farmaceutici S.p.A.

Anno accademico di conseguimento del titolo di Dottore di ricerca

2024/25

Abstract

Background: Bronchopulmonary dysplasia (BPD) is the most common long-term respiratory complication of prematurity. Its pathogenesis is multifactorial, with several pre- and post-natal insults contributing to the arrest of normal lung development. Due to the limited availability of lung samples from patients with BPD, animal models still play an essential role for investigating the pathogenic mechanisms and evaluating potential pharmacological interventions. Among the existing animal models, the preterm rabbit represents a good compromise between small (mice and rats) and large (baboons and lambs) animal species. Hyperoxia exposure remains the most common postnatal insult, used in combination with preterm birth, to reproduce key aspects of BPD pathophysiology. At Chiesi's Research Centre, the preterm rabbit model exposed to hyperoxia (95% O_2) for seven days has been set-up and validated. This thesis aimed to assess the effects of prematurity and hyperoxia exposure on postnatal lung development through functional, histological and biomolecular analyses, providing a comprehensive characterization of the hyperoxia-exposed preterm rabbit model of BPD.

Materials and Methods: Preterm rabbit pups were delivered by cesarean section (C-section) on gestational day 28 and randomized to hyperoxia (95% O_2) and normoxia (21% O_2) for three and seven days. Pups born at term on gestational day 31 and those left with their mothers at room air for four days after natural delivery were included as age-matched controls for physiological postnatal development. At the end of each experimental period, lung function was measured using the flexiVent™ system. Histological analyses were performed through conventional morphometric techniques and an innovative Artificial Intelligence (AI)-based software (Visiopharm®). Immunohistochemistry (IHC) for Surfactant Protein-C (SP-C) and α-Smooth Muscle Actin (α-SMA) was performed by using an automated research stainer. Two applications were developed: one for the quantification of SP-C positive type II alveolar epithelial (AT II) cells and another for the measurement of the thickness of α-SMA positive *tunica media* in small

pulmonary blood vessels. Ultrastructural alterations in the alveolar epithelium and in the pulmonary vascular wall were analyzed by Transmission Electron Microscope (TEM). Functional and histological data were then integrated with biomolecular analysis by quantitative Real Time-PCR (qRT-PCR) to assess the mRNA expression level of genes involved in vascular development and inflammatory response.

Results: Preterm pups exposed to hyperoxia exhibited significantly impaired lung function, as evidenced by decreased inspiratory capacity and static compliance and increased tissue damping and tissue elastance. Morphologically, hyperoxic lungs showed histopathological features characteristic of BPD, including enlarged airspaces, thickened alveolar septa, infiltration of inflammatory cells, accumulation of proteinaceous debris and disrupted elastic fiber architecture. Conventional morphometric analyses demonstrated a significant increase in Mean Linear Intercept (MLI), Acute Lung Injury (ALI) score, together with a decrease in Secondary Crests (SCs) count and Radial Alveolar Count (RAC) after postnatal exposure to hyperoxia. AI-based quantitative analysis confirmed the reduction in SCs count and showed a significant increase in Septal Thickness (ST). Moreover, in preterm pups exposed to hyperoxia, a significantly decreased number of AT II cells and increased thickness of the *tunica media* of small pulmonary blood vessels were observed. These results were subsequently confirmed by ultrastructural analysis, which showed morphological alterations in the vascular wall, as well as a reduction in the number of mature AT II cells. Postnatal exposure to hyperoxia also induced an imbalance of angiogenesis-regulating genes favoring anti-angiogenic factors and an upregulation of genes coding for pro-inflammatory cytokines.

Conclusions: The preterm rabbit model exposed to hyperoxia successfully mimics functional, structural and biomolecular features of the human disease, highlighting its translational relevance for preclinical studies of BPD.

Table of contents

List of abbreviations

AI: Artificial Intelligence

ALI: Acute Lung Injury

Ang: Angiopoietin

ANGPT-1: Angiopoietin-1

ANGPT-2: Angiopoietin-2

AoP: Apnea of Prematurity

AT I: Alveolar Type I

AT II: Alveolar Type II

ATS: American Thoracic Society

BPD: Bronchopulmonary Dysplasia

BW: Birth Weight

COD: Coefficient of Determination

COPD: Chronic Obstructive Pulmonary Disease

CP: Cerebral Palsy

C-section: Cesarean-section

Cst: Static Compliance

CXCL-8: Interleukin-8

DAB: 3,3' diaminobenzidine

DL: Deep Learning

ER1: Epitope Retrieval 1

ER2: Epitope Retrieval 2

ET: Endotracheal Tube

EVs: Extracellular Vesicles

FEV_1: Forced Expiratory Value in 1 second

FVC: Forced Vital Capacity

G: Tissue Damping

GA: Gestational Age

H&E: Hematoxylin and Eosin

H: Tissue Elastance

HRP: Horseradish Peroxidase

IC: Inspiratory Capacity

IGF-1: Insulin-like Growth Factor-1

IHC: Immunohistochemistry

IL-1R: Interleukin-1 Receptor

IL-1Ra: Interleukin-1 Receptor antagonist

IL-1β: Interleukin-1β

IUGR: Intra-Uterine Growth Restriction

LISA: Less Invasive Surfactant Administration

LPS: Lipopolysaccharide

ML: Machine Learning

MLI: Mean Linear Intercept

MSCs: Mesenchymal Stromal Cells

MV: Mechanical Ventilation

nCPAP: nasal Continuous Positive Airway Pressure

NICHD: National Institute of Child Health and Human Development

NICU: Neonatal Intensive Care Unit

NIV: Non-Invasive Ventilation

NRDS: Neonatal Respiratory Distress Syndrome

OS: Oxidative Stress

PDA: Patent Ductus Arteriosus

PDGFR-α: Platelet Derived Growth Factor Receptor-α

PDGF-α: Platelet Derived Growth Factor-α

PEEP: Positive End Expiratory Pressure

PH: Pulmonary Hypertension

PMA: Post-Menstrual Age

PPROM: Preterm Premature Rupture of the Membranes

qRT-PCR: quantitative Real Time-PCR

RAC: Radial Alveolar Count

RDS: Respiratory Distress Syndrome

ROI: Region Of Interest

ROS: Reactive Oxygen Species

RTU: Ready To Use

SCMFs: Secondary Crests Myofibroblasts

SCs: Secondary Crests

SP-C: Surfactant Protein-C

SMCs: Smooth Muscle Cells

SRT: Surfactant Replacement Therapy

ST: Septal Thickness

TEM: Transmission Electron Microscope

THBS-1: Thrombospondin-1

Tie: Tyrosine kinase with immunoglobulin-like and EGF-like domains

TNF-α: Tumor Necrosis Factor-α

VEGF: Vascular Endothelial Growth Factor

VEGFR-1: Vascular Endothelial Growth Factor Receptor-1

VEGFR-2: Vascular Endothelial Growth Factor Receptor-2

VILI: Ventilation-Induced Lung Injury

vSMCs: vascular Smooth Muscle Cells

WHO: World Health Organization

α-SMA: α-Smooth Muscle Actin

1. Introduction

1.1 Stages of human pulmonary development

Human lung development is a well-orchestrated process which includes three stages: embryonic, fetal and postnatal period. During the embryonic stage, lung organogenesis occurs. Fetal lung development includes the pseudoglandular, canalicular and saccular stages. The postnatal period consists of the processes of alveolarization and microvascular maturation [1]. The pulmonary circulation develops in parallel to the airways (Figure 1).

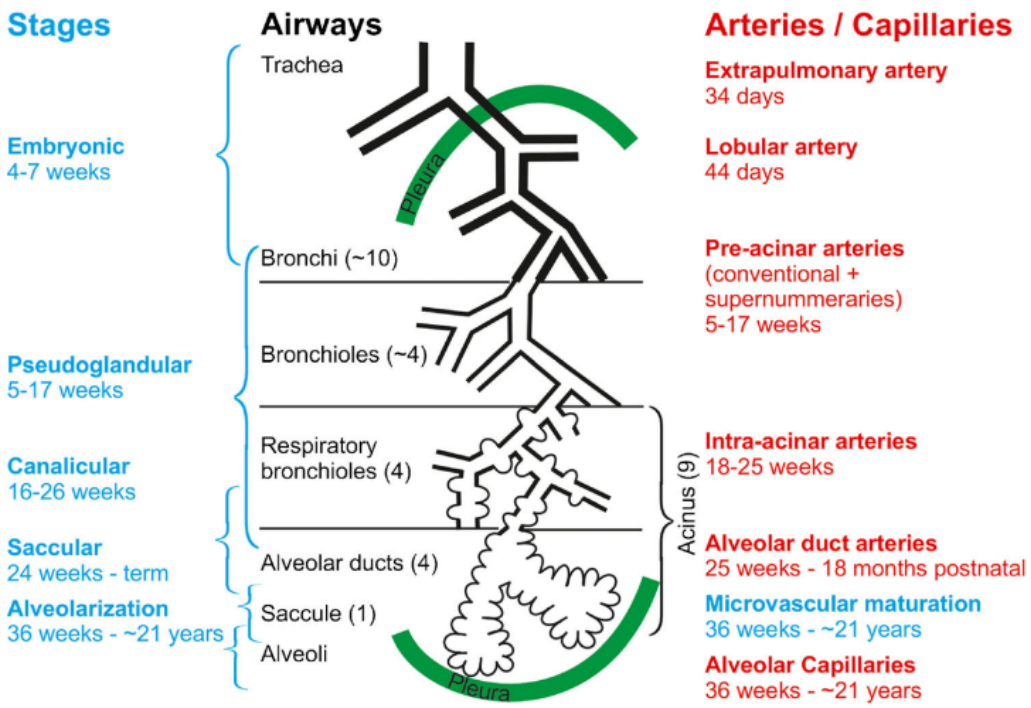

Figure 1. Stages of human lung development (from Schittny, 2017) [1].

Embryonic period (from the 1st to the 7th week): In humans, lung organogenesis begins around day 26-27 after fertilization and the anlage of the left and right lungs appears from the ventral surface of the primitive foregut. Both pulmonary buds undergo repetitive cycles of branching and outgrowth into the surrounding mesenchyme, leading to the formation of primary bronchi, which subsequently develop into the lobar and segmental bronchi. This process is a critical phase of lung

development and is finely regulated by a crosstalk between epithelial and mesenchymal cells [2]. The pulmonary vasculature starts to develop around the airway buds to ensure an adequate nutrient supply during this period [3].

Pseudoglandular period (from the 5th to the 17th week): During this stage, the lung resembles a tubular gland. The pulmonary buds continue to extend into the surrounding mesenchyme, where they undergo dichotomous branching, leading to the development of the future airways [1]. In humans, the first 20 generations of the future airways are formed during the pseudoglandular period and by the end of this stage, the level of the future alveolar ducts is reached [4].

Canalicular period (from the 16th to the 26th week): This stage is characterized by the differentiation of cuboidal epithelial cells into type I and type II alveolar epithelial cells. Alveolar Type I (AT I) cells are flattened cells that cover about 95% of the alveolar surface, ensuring an efficient gas exchange and maintaining the physiological structure of the lung tissue. Alveolar Type II (AT II) cells cover the remaining 5% of the alveolar surface, have a different morphology and are characterized by the presence of lamellar bodies. Their major function is the production of pulmonary surfactant, which prevents alveolar collapse by reducing alveolar surface tension. AT II cells are also responsible for maintaining alveolar epithelium integrity, as they are progenitors of AT I cells [5]. Furthermore, the mesenchymal capillary network comes into close contact with the epithelium to form the future air-blood barrier.

Saccular period (from the 24th to 38th week): At the beginning of this stage, the widening of the terminal airways forms clusters of larger airspaces: the so-called ‘sacculi’ [1], which will produce the alveolar sacs during the last phase of human lung development. Moreover, the production and secretion of pulmonary surfactant by AT II cells increases, as well as the possibility of survival after preterm birth [6].

Alveolar period (from the 36th week until 2 years of life): This is the final stage of lung development, during which the surface of gas exchange increases dramatically.

At birth, the maturity state of the lungs differs across animal species. In rats, alveoli formation occurs entirely during the first two weeks of postnatal life [7], [8]. In contrast, in other animal species, such as rabbits [9] or humans [10], alveolarization begins before birth and continues until approximately 2 years of postnatal life. At birth, the new alveoli form from the so-called 'primary septa', which appear thickened with a double layer of capillary network. Septation is the crucial process during the alveolar formation. It consists of the appearance of secondary crests (SCs), which protrude into the alveolar sacs, subdividing the pre-existing airspaces into new alveoli [10]. During this stage, secondary crests myofibroblasts (SCMFs) with contractile properties, also known as alveolar myofibroblasts, appear within the lung mesenchyme. SCMFs originate from a subpopulation of Platelet Derived Growth Factor Receptor-α (PDGFR-α) positive mesenchymal cells, which subsequently differentiate into α-Smooth Muscle Actin (α-SMA) positive cells [11]. These cells localize to the tips of the alveolar septa in close association with elastin deposits (Figure 2A), where they actively promote alveolar subdivision and the formation of new alveoli [11].

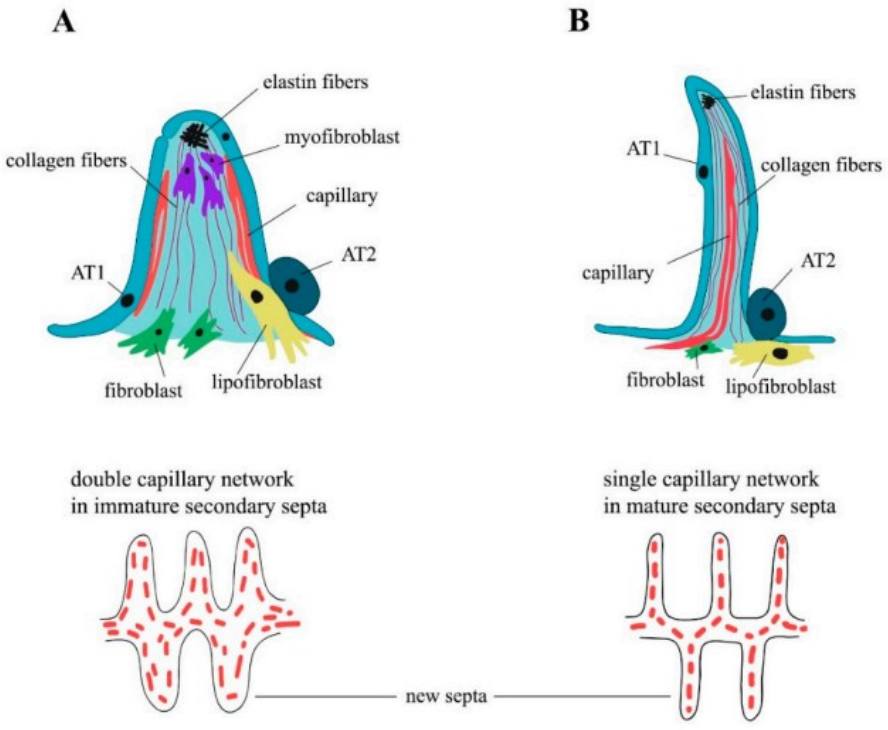

Figure 2. New alveoli formation (from Rippa *et al.*, 2021) [11]

It has been demonstrated that the Platelet Derived Growth Factor-α (PDGF-α) signaling pathway plays a pivotal role in alveolar development, as it is involved in smooth muscle cell migration and elastic fiber deposition [12]. Indeed, PDGF-α deficient mice exhibit a complete failure of alveolarization.

The term 'bulk alveolarization' refers to the process of massive production of new alveoli. It ends within the second week of postnatal age in rats and around two years in humans. After that, new alveoli are formed at a reduced rate until young adulthood [13]. In parallel to alveolarization, the interalveolar walls undergo significant structural changes to create a more efficient gas exchange surface. In the early stages of alveolar development, almost all secondary septa have a double-layered capillary network, so they are immature [11] (Figure 2B). On the contrary, in the adult lung, the mature septa are characterized by a single capillary layer. During the process of microvascular maturation, the two capillary layers fuse and the interstitial tissue decreases to form a single-layered capillary network in a thinner septum [11] (Figure 2B).

1.2 Vascular development

During the early stages of development, the formation of new blood vessels occurs through vasculogenesis. This is the process by which blood vessels are formed *de novo* by the differentiation of bone marrow-derived endothelial precursor cells. Once the initial vascular network is developed, angiogenesis takes over, leading to the formation of new blood vessels from the pre-existing ones, and allowing the vascular system to expand and remodel during development [14]. This process is finely regulated by several growth factors, among which the Vascular Endothelial Growth Factor (VEGF) is a key signaling factor that promotes cell migration, proliferation and survival by binding to Vascular Endothelial Growth Factor Receptor-1 (VEGFR-1 or Flt-1) and Vascular Endothelial Growth Factor Receptor-2 (VEGFR-2 or Flk-1) [15]. The lethality observed in embryos lacking VEGF after inactivation demonstrates its critical role during blood vessel development [16], [17].

The Angiopoietin-Tyrosine kinase with immunoglobulin-like and EGF-like domains (Ang-Tie) signaling pathway works in concert with VEGF and it is essential during the later stages of vascular development, especially in vascular maturation, remodeling and stability [18]. Angiopoietin 1 (ANGPT-1) and 2 (ANGPT-2) represent the two antagonistic ligands of the Tie 2 receptor: ANGPT-1 promotes vascular maturation by recruiting pericytes and associating endothelial cells with the surrounding extracellular matrix, stabilizing vascular structure [19]. On the contrary, ANGPT-2 acts as destabilizing factor, especially when vascular remodeling is necessary or in pathological conditions, such as inflammation or tumor growth [20]. The signaling pathway following ANGPT-2-Tie 2 interaction is strictly dependent on the surrounding environment. For example, it was demonstrated that the function of ANGPT-2 is modulated by growth factors, such as VEGF. Indeed, Lobov *et al.* [21] demonstrated that ANGPT-2 modulates capillary structure and promotes endothelial cell survival in a VEGF-dependent manner. Moreover, cytokines also play a critical role in determining the ANGPT-2 signaling pathway. Notably, ANGPT-2 has been shown to enhance cell adhesion and contribute to the inflammatory response by sensitizing endothelial cells to Tumor Necrosis Factor-α (TNF-α) [22]. Together, these findings highlight the versatile role of ANGPT-2 in vascular remodeling, enabling the vascular system to adapt to both physiological and pathological conditions through either blood vessel regression, stabilization or induction of inflammation.

1.3 Preterm birth

The World Health Organization (WHO) defines preterm birth as childbirth occurring before the 37th week of pregnancy [23]. Prematurity is considered one of the main risk factors of mortality in neonates aged under 5 years [24], with a global annual incidence of approximately 15 million cases, which represent 11% of all deliveries [25]. Prematurely born infants are classified according to the gestational age:

- Extremely preterm (less than 28 weeks' gestation)

- Very preterm (from 28 to less than 32 weeks' gestation)
- Moderate to late preterm (32 to 37 weeks' gestation)

The most common conditions leading to preterm birth include: 1) delivery due to maternal or fetal indications, where labour is induced or the infant is delivered by a cesarean section (C-section); 2) spontaneous preterm labour with intact membranes; and 3) preterm premature rupture of the membranes (PPROM). Several risk factors contributing to spontaneous preterm delivery have been identified and they are related to maternal aspects (nutritional status, smoking, alcohol and drugs use and other health conditions), sociodemographic aspects (race, type of work, absence of health insurance, lack of strong supportive economic and social safety net), pregnancy history (interpregnancy interval of less than six months, previous preterm delivery) and pregnancy characteristics (multiple gestations, vaginal bleeding, medical disorders, psychological and social stress, clinical depression, intra-uterine infections, bacterial vaginosis, uterine contraction frequency) [26].

Preterm birth may occur during the late canicular, saccular or early alveolar stages of lung development, when the alveolar epithelium is still differentiating, thus resulting in a partial deficiency of endogenous surfactant production, which is crucial to sustain extrauterine breathing. Surfactant deficiency is a key feature in the pathogenesis of neonatal respiratory distress syndrome (NRDS), as surfactant deficient prematurely born infants often struggle to initiate or sustain spontaneous breathing. Therefore, they require oxygen supplementation and ventilation support until the respiratory system is completely mature. Indeed, NRDS represents one of the most common conditions in neonates to be admitted into the neonatal intensive care units (NICUs). Although lifesaving, mechanical ventilation (MV) is an invasive technique which requires endotracheal intubation and can be associated with several complications, such as volutrauma, barotrauma, inflammation, pharyngeal and tracheal lesions. During recent years, thanks to the improvement of medical care, new respiratory support methods have been developed

and the technology of devices used for non-invasive ventilation (NIV) has significantly advanced [27]. Among them, nasal continuous positive airway pressure (nCPAP) is considered an effective and safer first-line intervention for early respiratory support in neonates since it reduces complications and mortality associated with the use of MV [28]. Nevertheless, in many cases, ventilation alone cannot fully support the underdeveloped lungs of preterm infants, who suffer from a deficiency of pulmonary surfactant. Considering the role of this deficiency in the pathogenesis of NRDS, surfactant replacement therapy (SRT) was developed to address this issue. Traditionally, exogenous surfactant was administered using an endotracheal tube (ET), followed by a period of MV. Nowadays, less invasive surfactant administration (LISA) techniques are being adopted. This strategy consists of administering exogenous surfactant while babies are supported with CPAP by advancing a thin catheter through the vocal cords, completely avoiding MV During the last years, this approach has gained popularity, since it improves outcomes in preterm infants affected with NRDS, minimizing short- and long-term complications associated with traditional methods [29], [30].

1.4 Bronchopulmonary dysplasia

During the past three decades, innovations like NIV methods and SRT have significantly improved survival rates and have pushed the boundaries of viability of prematurely born infants. Nevertheless, the increased survival of the most immature infants has also led to a higher incidence of respiratory complications, including bronchopulmonary dysplasia (BPD).

BPD results from an aberrant response to both antenatal and repetitive postnatal injury to developing lungs [31]. Due to its complex and multifactorial pathophysiology, the definition of BPD and its pathological features have evolved significantly over the years [32].

In 1967, Northway and colleagues described BPD as a chronic lung disease in preterm infants with NRDS who need supplemental oxygen for at least 28 days [33]. This definition focuses on

oxygen therapy as the main contributing factor for the development of the disease. Thanks to the advances in neonatal intensive care, including surfactant therapy and a gentler ventilation strategy, the diagnostic criteria started to change. Therefore, it was proposed that BPD can also be diagnosed in infants who require supplemental oxygen at 36 weeks postmenstrual age (PMA), highlighting long-term respiratory outcomes in preterm infants after birth [34]. In 2001, the National Institute of Child Health and Human Development (NICHD) proposed a new definition of BPD, according to which it is diagnosed in infants born before 32 weeks of gestation who require supplemental oxygen for at least 28 days and continue to require oxygen support at 36 weeks PMA. Moreover, a stratification system based on the severity of the disease was introduced. Indeed, BPD was classified into mild, moderate and severe forms, depending on supplemental oxygen requirement and type of respiratory support at 36 weeks PMA [35]. Briefly, the 2001 NICHD definition of BPD represents an important milestone in recognizing the multifactorial genesis of the disease. The ongoing evolution of BPD definition has raised an important dilemma, particularly regarding diagnostic criteria [36]. This is demonstrated by the wide reported range of global incidence of BPD, ranging from 10 to 89%. Such variability highlights the lack of a standardized diagnostic system and the need for a globally accepted diagnostic criterion to ensure uniformity in both clinical care and epidemiological research [37].

1.4.1 Pre- and post-natal risk factors

BPD is considered a multifactorial respiratory disease, and its development depends on a complex interplay between pre- and post-natal risk factors [38]. Among these, preterm birth and low birth weight represent the two main risk factors contributing to the development of the disease [31], [38]. Indeed, the incidence of BPD is inversely proportional to both gestational age (GA) and birth weight (BW). The Israeli Neonatal Network demonstrated that only 4,1% of infants born at 30-32 weeks of gestation develop BPD, while the incidence increases dramatically to 50% among

those born at 24-25 weeks of gestation [39]. In the same cohort, 29.3% of infants born with BW ranging from 1000g to 1500g and over 70% of infants with BW < 1000g develop BPD.

1.4.1.1 Pre-natal risk factors

Genetic predisposition: Studies conducted on preterm twins demonstrated the significant role of genetic predisposition in the development of BPD [40], [41]. Specifically, these studies have shown that the likelihood of developing BPD is higher in both monozygotic twins compared to dizygotic ones and that heritability accounts for a substantial portion of the risk of developing BPD. This evidence suggests that some preterm infants are genetically predisposed to develop BPD, with genetic factors playing a critical role in concert with environmental influences. Further studies have investigated genetic predisposition by analyzing the genomes of preterm infants. Several genes associated with pathways related to BPD have been identified. These include genes involved in lung development, maturation, inflammation, fibrosis, angiogenesis, oxidative stress (OS), or tissue injury and repair [42]. Identifying genetic factors associated with a higher risk of developing BPD is useful to better understand the pathophysiology of the disease. Moreover, as a future direction, researchers hope to develop targeted prevention strategies or personalized treatments for high-risk infants, based on their genetic profiles.

Intra-uterine growth restriction: Intra-Uterine Growth Restriction (IUGR) is an important cause of fetal and neonatal morbidity and mortality. It is defined as the rate of fetal growth below normal, considering the potential growth of that specific infant, as per the race and the sex of the fetus. The incidence of IUGR varies among countries, populations and races, with developing countries reporting the highest rate. IUGR is the result of maternal, fetal, placental or genetic risk factors [43]. This condition is associated with an increasing risk of developing both short- and long-term complications. Indeed, a higher prevalence of cardiovascular, renal, hepatic, metabolic and neurocognitive disorders has been observed in infants born after IUGR [44]. Moreover, it was demonstrated that chronic hypoxia associated with IUGR interrupts the normal lung development

and increases the risk of developing short- and long-term respiratory outcomes. In fact, prematurely born infants who have experienced IUGR during pregnancy are 45% more likely to be affected by BPD or die due to respiratory complications after birth as compared to well-grown infants [45].

Inflammation and chorioamnionitis: Prenatal inflammation is associated with an increased risk of spontaneous preterm delivery, since cytokines contribute to stimulate uterine contractions and to degrade the extracellular matrix of the fetal membranes, leading to PPROM [46]. Indeed, more than 50% of pregnancies that result in very preterm births (< 28 weeks of gestational age) show histological signs of chorioamnionitis (i.e., the inflammation of the fetal membranes and often the amniotic fluid) [31]. Chorioamnionitis principally results from intrauterine bacterial infections by *Ureaplasma sp*, even if several vaginal commensals and pathogens have also been identified [47]. It was broadly demonstrated that chorioamnionitis can accelerate lung maturation, reducing the risk of developing NRDS, but simultaneously induce lung injury, increasing the risk of developing BPD [48], [49].

Pregnancy-induced hypertensive disorders: Hypertensive disorders of pregnancy affect 2% to 8% of pregnancies worldwide and are responsible for 16% of maternal mortality [50]. The association between hypertensive disorders of pregnancy and the risk of developing BPD remains unclear. However, it was demonstrated that only pre-eclampsia showed a significant association with BPD, while the other disorders did not [51]. Pre-eclampsia is the most complex form of hypertensive disorder during pregnancy due to its multifactorial etiology and complicated pathogenesis. However, it is well known that patients with pre-eclampsia show an imbalance in angiogenic factors and OS markers [52]. These findings are strongly associated with adverse pregnancy outcomes, including IUGR, which is a risk factor for the development of BPD [52]. Several studies show that BPD is positively correlated with pre-eclampsia and IUGR, but not with maternal pre-eclampsia alone [38].

Tobacco: Tobacco exposure during pregnancy is associated with an increased risk of preterm birth. The mechanism by which it occurs is not yet fully elucidated. There are more than 3000 chemicals in cigarette smoke. Moreover, nicotine and carbon monoxide cause vasoconstriction, damaging the placenta and reducing the uteroplacental blood flow. This can result in fetal growth restriction [26]. Intrauterine cigarette smoke exposure has a significant impact on fetal lung development with permanent structural changes and altered lung function [53], increased risk of BPD [54], as well as long-term respiratory complications, such as wheeze and asthma [53].

1.4.1.2 Post-natal risk factors

Oxidative stress and hyperoxia: OS is one of the major risk factors for the development of BPD [38]. It occurs when the production of reactive oxygen species (ROS) exceeds the capacity of the antioxidant system. Preterm infants are more prone to develop OS, as they show an immature antioxidant system that is not able to neutralize the injurious effects of ROS, leading to tissue damage, inflammation and ultimately increasing the risk of BPD [55]. The exposure to high levels of oxygen causes OS, leading to oxidative damage with a significant impact on lung development [56]. Hyperoxia-induced acute lung injury is characterized by an influx of inflammatory cells into the lung parenchyma, which causes destruction of the alveolar-capillary barrier followed by an increased vascular permeability, release of inflammatory mediators, pulmonary edema and ultimately cell death [57], [58]. Prolonged exposure to hyperoxia not only amplifies OS but also sustains a persistent pro-inflammatory environment that disrupts normal postnatal lung development with effects that are dose dependent. This chronic inflammation has been shown to further exacerbate lung injury and play an essential role in the progression of BPD [58].

Mechanical ventilation: Even though MV is a lifesaving intervention, it can promote the development of the so-called 'Ventilation-Induced Lung Injury (VILI)'. For this reason, neonatologists aim to avoid prolonged ventilation and instead use lung-protective strategies to minimize VILI [59], [60]. Due to the multifactorial pathogenesis of VILI, it can be the result of a

complex interplay of ventilation-related and patient-related risk factors. The major ventilation-related factors are represented by volutrauma (caused by exposure to high tidal volume), barotrauma (by overstretching of the airways and alveoli), atelectrauma (by repeated alveolar collapse and expansion), oxygen toxicity (by excessive oxygen exposure) and biotrauma (by the release of inflammatory mediators); whereas patient-related factors include lung immaturity and surfactant deficiency [59]. MV disrupts both the alveolar epithelial and endothelial cells, leading to a breakdown of the alveolar-capillary barrier. This, in turn, increases vascular permeability and allows fluid and inflammatory mediators to leak into the alveolar spaces, causing pulmonary edema. Furthermore, MV induces an increase in pro-inflammatory cytokines in the lungs, which activate macrophages and neutrophils [61]. The increased vascular permeability, secondary to widespread tissue injury, allows pro-inflammatory mediators to leak into the systemic circulation. This can trigger an abundant systemic inflammatory response, leading to multiple system organ failure in some patients [62].

Infections: Prematurely born infants show more susceptibility to postnatal infections due to their immature immune system. Infections could either be localized to the lung or could be systemic, such as sepsis, whose risk increases proportionally to the degree of prematurity. Indeed, the incidence of early-onset sepsis, which develops within the first 72 hours of postnatal life, is about 2–3.5% in infants of < 28 weeks of gestational age. In contrast, late-onset sepsis, which occurs after 72 hours, affects 10% of infants born between 29 and 32 weeks of gestation, and can be as high as 41% in those born between 25 and 29 weeks of gestation [63]. It was demonstrated that an inflammatory response deriving from postnatal infections disrupts the normal lung development, increasing the risk of BPD and other neonatal conditions [64].

Patent ductus arteriosus: The ductus arteriosus is a blood vessel that plays a pivotal role in fetal blood circulation, as it connects the pulmonary artery to the descending aorta, allowing blood to bypass the lungs. After birth, the ductus typically closes within the first few days of postnatal life.

If its closure does not occur, a pathological condition called 'Patent Ductus Arteriosus (PDA)' may arise [65]. In preterm infants, PDA leads to increased pulmonary blood flow, resulting in elevated blood pressure, lung edema and decreased lung compliance [38]. As a result, patients with this condition often require respiratory support and MV, increasing the risk of developing BPD associated with pulmonary hypertension (PH) [66].

Respiratory microbial dysbiosis: Dysbiosis represents a condition that can be defined as an unbalanced structural complexity of microbial communities on or within the body [38]. The presence of a normal microbial population is crucial during the development of the immune system and its disruption can induce an abnormal inflammatory response, with consequent increased risk of BPD [67].

1.4.2 Pathophysiology of BPD

Along with the definition, the pathophysiology of BPD has also changed significantly over time, due to the recent advances in neonatal intensive care. The form of BPD described by Northway and colleagues [33], known as "old" BPD, was characterized by pulmonary fibrosis and abnormal arterial vascularization, often resulting from prolonged MV and oxygen therapy in more mature preterm babies. In recent years, the "old BPD" has been replaced by the "new BPD", which is associated with interference of the normal lung development in extremely preterm babies.

BPD histologically manifests as decreased septation, alveolar hypoplasia and dysregulated development of pulmonary vasculature [68], [69]. The decrease of alveolarization and the alteration of vascular growth represent the two main pathological features of the "new" BPD. It has long been known that pre- and postnatal risk factors, including exposure to high oxygen levels, can induce a damaging inflammatory response that disrupts the normal alveolar and vascular development in the immature lungs of premature infants with BPD. Thus, pulmonary inflammation represents a key pathogenic mechanism contributing to the functional and structural

impairments characteristic of the “new” BPD, as demonstrated by several studies [70], [71]. This inflammatory response is characterized by the accumulation of macrophages and neutrophils, the release of pro-inflammatory cytokines, and the proteolytic activity of enzymes such as neutrophil elastase and matrix metalloproteinases, which degrade extracellular matrix components critical for alveolar integrity, with consequent airspace enlargement and alveolar simplification [72]. Activated macrophages and neutrophils are also major sources of ROS, which contribute to OS and amplify pulmonary inflammation. Under physiological conditions, the activity of ROS is balanced by the endogenous antioxidant defense system [72]. However, preterm infants show an immature antioxidant defense system, making them particularly susceptible to ROS-induced lung injury following hyperoxia exposure [73] Moreover, this persistent pulmonary inflammation disrupts mesenchymal cell turnover, leading to an exaggerated fibroproliferative response characterized by thickened alveolar septa and impaired alveolar development, as demonstrated by Reyburn *et al.* in mechanically ventilated preterm lambs [74].

Although the mechanisms behind these developmental alterations are not yet fully understood, it has been suggested that the disruption of alveolarization and vascular growth are closely related, since these two processes occur in parallel during lung development [1]. According to the “vascular hypothesis” [75], disrupted angiogenesis during critical stages of lung development impairs alveolarization. This hypothesis has been supported by several studies on animal models of BPD. For instance, in newborn rats, the treatment with a VEGF-receptor inhibitor has been shown to impair alveolarization, leading to alveolar simplification and loss of pulmonary vasculature [76]. In contrast, VEGF gene therapy enhances survival, promotes angiogenesis and restores alveolar damage in a rat model of BPD exposed to hyperoxia [77]. In human studies, infants who died from BPD show disrupted pulmonary vasculature and decreased expression of angiogenic growth factors, such as VEGF and their receptors [78]. These findings underscore the crucial role of vascular growth in proper lung development and open potential possibilities of

therapeutic strategies that focus on promoting angiogenesis and restoring normal lung development [79]. However, further research is required to better understand the precise mechanisms underlying these disruptions and to develop targeted therapies aimed at enhancing lung development and reducing the long-term complications of BPD.

1.4.3 Long-term respiratory outcomes

BPD is associated with long-term respiratory outcomes, which may arise during childhood, adolescence and adulthood [80]. Epidemiological data show that re-hospitalization rate during the first year of postnatal life in infants with BPD is about 49%, and the mortality risk significantly correlates with the pulmonary complications of BPD [81]. Follow-up studies conducted on children and young adult survivors of BPD reveal compromised pulmonary function and defenses, asthma-like symptoms, PH and exercise intolerance [81]. In healthy subjects, lung function, measured as forced expiratory volume in 1 second (FEV_1), typically peaks in early adulthood, maintaining a relatively constant value for some years before starting to decrease with age, without reaching levels that cause disability. Conversely, BPD survivors, usually exhibit airflow limitation (i.e., lower FEV_1) and their lung function decline begins earlier in life compared to healthy individuals [82] (Figure 3).

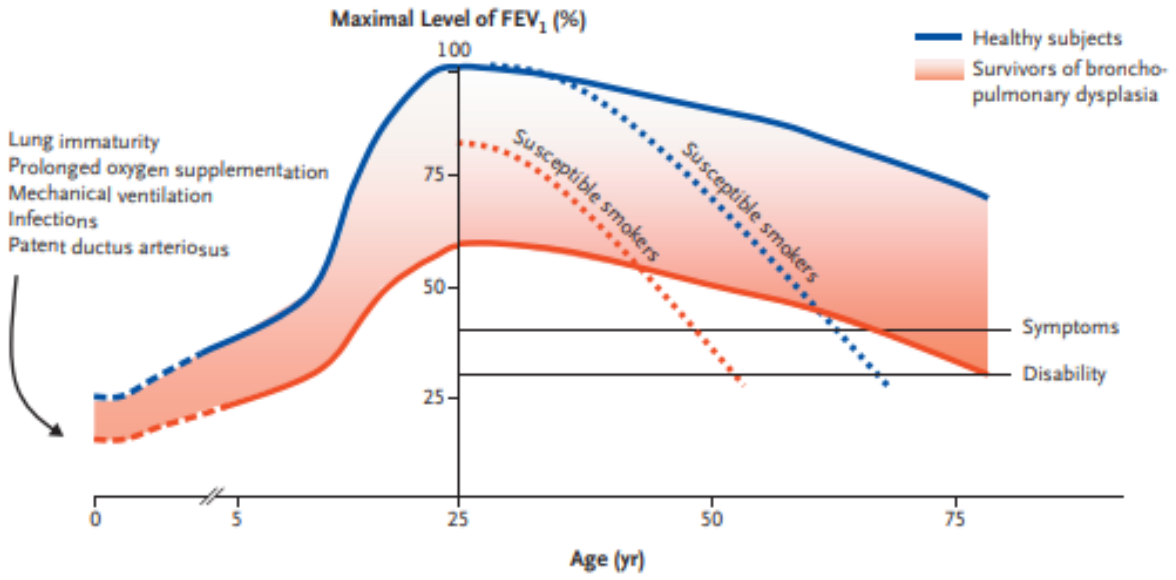

Figure 3. Changes in FEV_1 in survivors of BPD compared to healthy subjects (from Baraldi *et al.*, 2007) [82].

Studies have confirmed that subjects with a history of BPD show significantly lower values of FEV_1, forced vital capacity (FVC) and forced expiratory flow rate at 50% of FVC compared to those without BPD [83], [84]. Furthermore, preterm infants who have survived BPD show compromised pulmonary defenses, which make them more susceptible to pulmonary infections, that exacerbate their condition [81].

In a murine model of BPD, the combination of pre-natal inflammation induced by lipopolysaccharide (LPS) and post-natal exposure to hyperoxia has been shown to cause significant airway remodeling. This includes airway smooth muscle hypertrophy and airway narrowing, which increase the reactivity of the airways to environmental stimuli, such as allergens, viral infections, or pollutants [85]. In individuals with a history of BPD, the airway hyper-responsiveness can manifest through asthma-like symptoms (wheezing, cough, difficulty breathing), which often persist throughout childhood and into early adulthood, affecting exercise tolerance and overall quality of life [86]. Moreover, it was demonstrated that impaired lung development associated with BPD, along with genetic predisposition and subsequent environmental and infectious events during critical periods of postnatal life, significantly increases the risk of developing chronic obstructive pulmonary disease (COPD) in later life in BPD survivors [87].

Prematurely born infants with BPD are also at higher risk of developing PH, which is associated with elevated morbidity and mortality. According to the epidemiological data, 18% of extremely low birth weight infants develop this BPD-associated long-term sequela. Factors that increase the risk of PH include growth restriction at birth, the need for supplemental oxygen at 4 weeks of postnatal age and severe BPD [88]. Although PH has multifactorial pathogenesis, the inhibition of lung development represents one of the main contributing factors. In particular, the impaired lung and vascular growth lead to a reduced cross-sectional area of pulmonary vasculature.

Moreover, pulmonary blood vessels undergo significant changes, such as hypertrophy of vascular smooth muscle cells (vSMCs), resulting in increased vascular resistance and blood pressure [89].

In summary, even though the survival rate of preterm infants with BPD has increased over recent years, they still show a higher susceptibility for developing long-term complications. Therefore, it remains crucial to focus on preventing and minimizing neonatal lung injury. Additionally, long-term follow-up of BPD survivors is essential to ensure their ongoing health and well-being [80].

1.4.4 Pharmacological treatments

Despite recent advances in neonatal intensive care aimed at preventing or minimizing lung injury in preterm infants, the incidence of BPD has not substantially decreased [90]. This highlights the crucial need for a deeper understanding of the disease's pathogenesis and the development of more effective and targeted treatments. Over the last decades, several therapeutic strategies have been proposed (i.e., Vitamin A, Caffeine, and corticosteroids), which have not been efficient in covering the whole spectrum of BPD. Currently, novel therapeutic strategies (IGF-1/BP3 and extracellular vesicles) are under clinical development [91].

Caffeine: Caffeine belongs to the methylxanthines family, and it is routinely used in NICUs as treatment for apnea of prematurity (AoP). AoP, which is defined as cessation of breathing for more than 15 seconds followed by hypoxia or bradycardia, is highly frequent in preterm infants. It was demonstrated that caffeine can reduce the number of apneic attacks and the need for MV in the first seven days of treatment [92]. However, its exact mechanism of action is not fully elucidated. It has been hypothesized that methylxantines exert their effect by increasing chemoreceptor responsiveness, inducing generalized central nervous system excitation, and improving respiratory muscle performance [92]. Beyond the short-term management of apnea, caffeine also has a long-term therapeutic impact, particularly reducing the incidence of BPD in preterm infants with very low birth weight [93]. This protective effect is thought to be mediated

through its anti-inflammatory and anti-oxidant properties, as well as by promoting angiogenesis and improving pulmonary vascular remodeling [94]. Moreover, a study conducted on 11-year-old children with a birth weight < 1,251 g shows that subjects treated with caffeine during infancy have significantly higher expiratory flow rates than those treated with placebo [95].

Vitamin A: Vitamin A is a term used to refer to a group of fat-soluble retinoids that include retinol, retinal, retinyl esters and all-trans retinoic acid [96]. It plays a pivotal role during the early stages of lung development, promoting differentiation and maturation of epithelial cells [97]. Therefore, adequate vitamin A levels are essential for proper fetal lung development, while maternal vitamin A deficiency has been shown to be associated with impaired lung function, recurrent respiratory tract infections [98], and increased risk of developing BPD in very low birth weight infants [99]. Given its essential role during lung development, vitamin A supplementation has been studied as a strategy to prevent BPD. The systematic review and meta-analysis by Ding *et al.* [100] suggest that vitamin A supplementation can indeed prevent the development of BPD, although further studies are needed to confirm these findings.

Postnatal corticosteroids: Given the critical role of inflammation in the development of BPD, postnatal corticosteroids have been investigated as a potential treatment due to their anti-inflammatory properties. However, their use in BPD remains controversial, as corticosteroids have been linked to several adverse effects, such as cerebral palsy (CP) and abnormal neurological findings in the longer term [101]. This has led clinicians to carefully weigh the benefits versus the risks of using corticosteroids postnatally. Clinical research has focused on trying to find the optimal dosage and timing of treatment for a safe and efficacious treatment [101].

Dexamethasone and hydrocortisone are the two most commonly used corticosteroids in clinical practice. It has been shown that early (before the 8th day of postnatal life) systemic treatment with dexamethasone reduces the incidence of BPD, but it is associated with an increased risk of CP [102]. In contrast, early systemic treatment with hydrocortisone is not associated with long-term

neurological outcomes, but it is less effective in preventing BPD compared to dexamethasone [103].

Late systemic treatment with corticosteroids (after the 7th day of postnatal life) represents an alternative approach for preterm infants at risk of developing BPD. Although this strategy is not associated with adverse long-term neurological outcomes, it showed a lower effectiveness in preventing BPD, especially in infants at high risk of developing a severe form of the disease [104].

To avoid detrimental neurological effects associated with systemic corticosteroids, alternative routes of administration have been proposed. Inhaled corticosteroids, such as budesonide, have been shown to be associated with a lower rate of BPD at 36 weeks of postmenstrual age compared to the control group [105]. Moreover, a not significantly different rate of neurodevelopmental disability and a higher mortality rate were observed in the budesonide group [105]. Intratracheal administration of corticosteroids combined with surfactant emerged as an alternative to inhalation. Preclinical studies in a rabbit model of respiratory distress syndrome (RDS) suggest that this strategy is more effective in reducing pulmonary inflammation than using budesonide alone, as the surfactant provides budesonide to the distal airways [106]. Clinical studies have confirmed these findings, demonstrating that the intratracheal administration of budesonide with surfactant reduces the incidence of BPD [107], [108]. However, a more recent randomized clinical trial did not show any beneficial effect of intratracheal budesonide mixed with surfactant, compared with surfactant alone, on survival rate in extremely preterm infants [109]. Therefore, further studies are needed before it can be used as a standard care.

Mesenchymal stromal cells-based therapy: Mesenchymal stromal cells (MSCs) are multipotent adult cells that can differentiate into multiple mesenchymal cell types and expand significantly. They can be isolated from several locations, such as bone marrow, adipose tissue, placenta, umbilical cord and umbilical cord blood [110]. MSCs-based therapy showed a potential beneficial effect in the field of regenerative medicine, due to their innate immunomodulatory/anti-

inflammatory and reparative properties [110]. Rather than directly differentiating into the damaged tissue, MSCs exert their benefits through a paracrine effect. It seems to be mediated by the release of nano-sized extracellular vesicles (EVs), which have been recognized to be crucial components of cell-to-cell communication during normal cell homeostasis and disease processes [111]. The therapeutic potential of MSC-derived EVs has been tested in a murine model of BPD exposed to hyperoxia [112]. Here, it has been shown that a single dose of MSC-EVs results in improved lung function, decreased fibrosis and pulmonary vascular remodeling, and ameliorated PH. It has been hypothesized that these results are attributable to the capacity of MSC-EVs to promote the transition of macrophage phenotype from M1 (pro-inflammatory) to M2 (anti-inflammatory) [112].

Insulin-like growth factor-1: Insulin-like growth factor-1 (IGF-1) belongs to a class of polypeptides of the insulin family. It was demonstrated that IGF-1 plays a pivotal role during lung development by promoting cell proliferation and differentiation, particularly in the alveolar epithelial and airway basal cells [113]. Moreover, low serum IGF-1 levels have been shown to be associated with an increased risk of developing some complications, including BPD [114]. For this reason, IGF-1 is being considered as a potential therapeutic strategy for BPD, particularly in premature neonates. The recombinant human IGF-1 complexed with its binding protein (rhIGF-1/BP3) preserves lung growth and prevents the development of BPD and PH in preclinical models [115]. This therapy has proven beneficial not only in animal models but also in clinical trials. For instance, the clinical trial conducted on extremely preterm infants confirmed that rhIGF-1/BP3 significantly reduces the incidence of BPD, providing a promising way for the treatment of the disease [116]. Moreover, a phase 2b multicenter randomized study is ongoing to evaluate the efficacy of rhIGF-1/BP3 for the prevention of BPD.

Interleukin-1 receptor antagonist: It is widely accepted that increased activity of pro-inflammatory mediators, including interleukin-1 beta (IL-1β), contributes significantly to the

development of BPD in preterm infants [58]. IL-1β exerts its deleterious effects by binding to the IL-1 receptor (IL-1R). However, IL-1R antagonist (IL-1Ra) prevents IL-1 from exerting its activity. Moreover, it was demonstrated that in preterm infants, the imbalance of IL-1β and IL-1Ra may promote persistent inflammation, contributing to the pathogenesis of BPD [117]. In animal models, targeting the IL-1β signaling pathway by using IL-1Ra has been shown to have beneficial effects in reducing pulmonary inflammation and in preventing the development of BPD [118]. Currently, a clinical trial, also known as the Anakinra Pilot study, is ongoing to demonstrate the safety, feasibility and pharmacokinetics of IL-1Ra administration in preterm infants, aiming to evaluate its anti-inflammatory potential effect for the prevention of BPD [119].

1.5 Translation of BPD phenotype in animal models

Studies on lung tissue of patients with BPD are crucial for providing important information, but autopsy material has become increasingly rare and difficult to obtain, especially in the post-surfactant era, due to the improvement of survival rate in BPD patients [120], [121]. This challenge highlights the importance of animal models. A good animal model can increase the understanding of the pathophysiology of BPD and enable the development of novel therapeutic strategies [121]. Because of its complex etiology and heterogeneous phenotype, it is hard to mimic BPD in an animal model. Moreover, most of the pre-clinical models use only one injurious stimulus, neglecting the intricate combination of various insults on the developing lungs, such as prematurity, oxygen toxicity and infection [122]. Nevertheless, several animal models have been developed over time, including small and large animals.

1.5.1 Small animal models

Mice and rats represent the most commonly used animal species for BPD research. The reason why they are so extensively used is due to their several advantages: i) small size (birth weight mice: 0,5-1,5 g and rats: 5-6 g, ii) ease to house, iii) short gestation (21 days for mice, 22 days for

rats) with a large litter size, iv) availability of reagents and techniques [121], [123], [124]. However, both mice and rats are born at term at a phase of lung development equivalent to that of a very preterm human infant (i.e., saccular stage) (Figure 4). This means that they could be used to study alveolarization, but it is not feasible to induce preterm birth in these animal species [121]. Therefore, although at birth their lungs are considered structurally immature, mice and rats are fully capable of surviving, without developing the gas exchange limitations seen in preterm infants; this is possible thanks to a sufficient production of pulmonary surfactant at birth [123], [124]. Moreover, the small size of the pups restricts the possibility of performing long-term monitored experiments using MV [121]. In fact, postnatal exposure to hyperoxia represents the most widely used insult to reproduce human BPD phenotype in animal models, but the high oxygen levels often exceed those currently utilized in NICUs [123], [124]. Therefore, even though mice and rats are useful to study the pathophysiology of BPD, their limitations highlight the challenges in translating findings from these animal models to humans [121].

1.5.2 Large animal models

In BPD research, large animal models include preterm lambs and preterm baboons [125]. The most relevant advantage related to their use is that the lung development of lambs and especially baboons [126] recapitulates human lung development more closely, as they start alveolarization in utero, and the length of the developmental stages corresponds to the length in humans [121] (Figure 4). Moreover, they can be delivered prematurely (baboons: 125^{th} day of gestation and lambs: between 125^{th} and 142^{nd} day of gestation) and their large size enables long-term MV, which is a key feature in the clinical management of preterm infants with RDS [127]. The anatomical similarities between preterm lambs, preterm baboons and humans represent the reason why these animal species are so valuable to study BPD pathophysiology [126], [127]. Nevertheless, the complexity of care required, high costs and ethical issues, especially with non-human primates,

represent the major disadvantages and limit the use of these animal models in preclinical research on BPD [121].

1.5.3 The preterm rabbit model

The preterm rabbit model offers a good compromise between small and large animal models. The rabbit is a medium-sized animal whose lung development closely mirrors that of humans (Figure 4). Indeed, as in large animal models and humans, alveolarization starts in utero in rabbits and continues postnatally [121]. Other advantages related to its use are represented by large litter size, relatively short gestation, ease of handling and housing. However, a great difference with small animal models is the possibility of inducing preterm birth. Indeed, rabbits can be delivered prematurely by C-section at the 28^{th} day of gestation, during the saccular stage of lung development. It has been extensively demonstrated that preterm rabbits show an immature antioxidant [128] and surfactant system [129] when compared to those born at term. This lack of maturity makes preterm rabbits more susceptible to pulmonary oxygen toxicity when exposed to high oxygen levels and increases the risk of developing RDS. This underscores that prematurity represents the common risk factor of BPD. Salaets *et al.* [130] demonstrated that prematurity alone, without additional insults, affects lung structure (larger alveoli and thicker alveolar septa) and function, with a persistent effect on the developing lungs.

To enhance the translational value of the model, several pre- and postnatal insults have been used in combination with prematurity to better mimic the multifactorial etiology of the disease. Among these, postnatal exposure to hyperoxia represents the most commonly used additional injury in preterm rabbits. The first comprehensive description of hyperoxia-induced structural lung changes in the preterm rabbit model was provided by Mascaretti *et al.* [131]. In their study, preterm rabbits were exposed to high oxygen levels (95% O_2) for 11 days, resulting in significant structural lung alterations, including impaired alveolar development, lower collagen fiber density and evident disorganization of elastic fibers deposition. Subsequently, Manzano *et al.* [132]

investigated the influence of different gestational ages and oxygen concentrations on the severity of lung injury. Their study demonstrated that rabbit pups born on the 28th day of gestation and exposed to 95% of oxygen showed more severe structural lung injury and a higher mortality rate compared to those born at a more advanced gestational age and exposed to lower oxygen concentration. These findings highlight the critical influence of both lung immaturity at birth and oxygen levels on the extent of lung damage. The hyperoxia-exposed preterm rabbit model was further refined by Richter *et al.* [133], who provided a more comprehensive characterization of functional and structural changes resulting from postnatal hyperoxia exposure. Pups delivered by C-section on the 28th day of gestation were exposed to 95% O_2 for seven days. The study demonstrated a significant increase in mortality and a marked impairment of pulmonary function in preterm pups exposed to hyperoxia. Histological analyses confirmed these findings, showing that hyperoxia exposure led to alveolar simplification, associated with enlarged airspaces and thickened septa. Taken together, these studies underscore the translational value of the hyperoxia-exposed preterm rabbit model. It mimics not only the structural hallmarks of BPD but also the functional impairment characteristic of the disease.

In the last few years, this animal model has been set up and validated in Chiesi's Research Center, confirming results provided by scientific literature. Nevertheless, some limitations have been identified: exposure to high levels of oxygen (95%) is no longer used as the standard management strategy for preterm infants in NICUs. The continuous exposure to these elevated levels of oxygen could be too harmful to demonstrate any beneficial effect of pharmacological treatments [133]. Furthermore, while the 7-day exposure to hyperoxia is useful to study the acute lung injury, it could be too brief to fully simulate the chronic nature of BPD and its long-term effects. This limitation has prompted Chiesi's researchers to explore strategies to extend the experimental period up to postnatal day 14, which corresponds to the timeframe when BPD is typically diagnosed in human infants [134]. By adjusting the oxygen concentration and exploring multi-hit

strategies, the researchers aim to develop a preterm rabbit model that more closely mimics the progression of BPD in humans, enhancing the understanding of the disease's physiopathology and improving the model's ability to evaluate long-term pharmacological interventions [135].

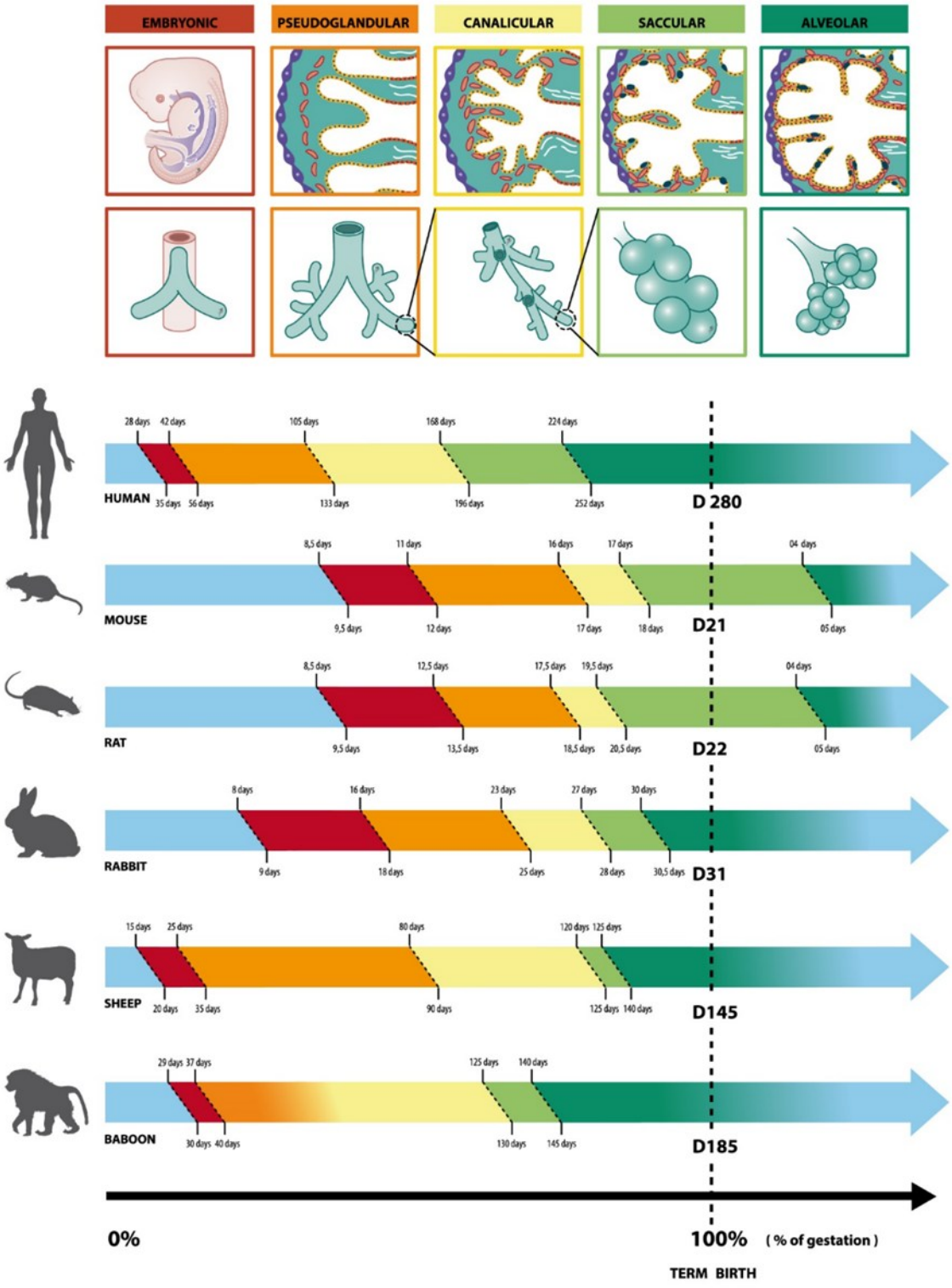

Figure 4. Lung development in different species of mammals (from Salaets *et al.*, 2017) [121]

1.6 The evolution of morphometric analyses: From traditional methods to emerging Artificial Intelligence (AI)-based approaches in BPD

The main histological hallmarks of BPD include impaired alveolar and vascular growth, as well as altered lung structure. The degree of lung development and pulmonary damage induced by the complex interplay between pre- and postnatal risk factors is typically assessed by performing morphometric analyses. This traditional approach involves the measurement and the quantification of specific lung tissue parameters. For instance, impaired alveolarization in animal models of BPD can be evaluated by measuring surface area, alveolar number and size.

Thurlbeck [136] proposed a quantitative method for evaluating lung tissue changes in emphysema by assessing internal surface area, a parameter directly associated with the lung's ability to perform gas exchange. This approach offers valuable insights that could be used to study other pulmonary diseases, including BPD, as decreased internal surface area often correlates with compromised lung function.

The Radial Alveolar Count (RAC) is a widely used histological method that consists of counting the number of saccules and alveoli crossed by a line drawn from the lumen of the terminal bronchiole to the nearest connective tissue or pleural margin [137], providing information on the degree of alveolarization.

Originally proposed to study the degree of lung emphysema [138], the Mean Linear Intercept (MLI) measurement can also be used to evaluate impaired alveolarization in BPD. This parameter is calculated by counting the number of times a reference line of known length intercepts the alveolar septa, offering insights into the extent of airspace enlargement and lung injury. In pulmonary diseases such as BPD, where alveolar septa are damaged and normal alveolar development is disrupted, MLI values are typically elevated. A higher value of MLI reflects fewer

and larger alveoli, indicating increased alveolar injury and impaired alveolarization. These structural changes result in a reduced lung surface area available for gas exchange, highlighting the functional deficits observed in this pathological condition.

Additionally, SCs formation has been shown to play a pivotal role during the alveolarization process, as these structures, after protruding from immature septa into the alveolar sacs, subdivide the pre-existing airspaces into new alveoli [11]. In the context of BPD, where the normal lung development is altered, the disruption to septation leads to simplified alveolar structure, further contributing to the impairment of lung function. Thus, counting the number of SCs is an alternative method that can be applied to assess the degree of alveolar development. This morphometric parameter is quantitatively assessed using the point counting method, as shown in Lucattelli *et al.* [139].

The Acute Lung Injury (ALI) score, which has been proposed by the American Thoracic Society (ATS) [140], can be used to evaluate the extent of pulmonary damage. This parameter is based on five different histological findings, such as neutrophils in the alveolar space, neutrophils in the interstitial space, hyaline membranes, proteinaceous debris and alveolar septal thickening, that are considered indicative of lung injury and inflammation. In the context of BPD, the ALI score is particularly valuable to better understand the pathogenetic mechanisms and lung structural changes induced by contributing risk factors to the development of the disease.

The maturation of alveolar septa, which typically occurs in the late canalicular or in the saccular stage of lung development, is of vital importance. As described by Burri [10], this process involves the reduction in septal thickness (ST) and the formation of mature capillary networks, both of which are essential for the creation of an efficient air-blood barrier. In pulmonary diseases like BPD, however, this maturational process is disrupted, leading to increased thickness of alveolar septa. This is a pathological feature caused by the interruption of the normal developmental process and is further exacerbated by a fibroproliferation response to the lung

inflammation. The fibroproliferative process involves the deposition of collagen and other extracellular matrix proteins, which ultimately contribute to compromised lung function [141]. For this reason, quantifying the thickness of alveolar septa is crucial in evaluating the degree of pulmonary damage in BPD.

The traditional approach, based on manual morphometric analysis, plays a critical role in understanding the pathogenesis of the disease, contributing to the development of targeted therapeutic strategies to mitigate pulmonary damage and promote tnormal lung growth. However, this approach has notable limitations. Indeed, manual morphometric analyses are time-consuming and could be operator dependent. Specifically, the operator-dependency means that results can vary depending on the individual performing the analysis, leading to lower reproducibility. This variability can introduce biases that can limit the reliability of data, making it more difficult to compare results across different studies. Moreover, the reduced ability to efficiently analyze large datasets represents another significant limitation related to manual morphometric analysis.

To overcome these limitations, there has been a growing interest in using an innovative Artificial Intelligence (AI)-based approach for histological analysis. AI, a broadly used term coined in 1950s, refers to the branch of computer science aimed at creating technologies that can mimic human-like actions and behavior. Machine Learning (ML)-based approaches represent a subtype of AI, where systems are designed to "learn" from provided data and make a prediction without explicit programming for each specific task. Deep Learning (DL), a more advanced form of ML, involves the use of artificial neural networks. These networks typically consist of multiple layers of interconnected nodes that process and interpret data, closely mimicking the brain's function [142]. The use of DL in histological analysis offers several key advantages over traditional methods. This innovative approach significantly improves the accuracy, efficiency, and reproducibility of histological data. By automating tasks such as the segmentation of tissue structures and pattern recognition, AI can reduce the time required for analysis, while enhancing

the consistency of results. Additionally, AI-based methods can help identify subtle patterns or variations in tissue samples that might be difficult for human observers to detect, leading to more accurate diagnostics and improved insights into disease progression [143]. However, there are several challenges that AI-based methods must address for broader adoption and better performance in digital pathology. Most DL algorithms require a large set of well-annotated images to be trained properly. This means that an operator needs to manually delineate the region of interest (ROI) in all images. In histology, obtaining high-quality labeled data can be time-consuming and expensive to generate. For pathologists, detailed annotation of a large number of images can be particularly challenging when working with low-resolution input datasets [144]. Moreover, variation in tissue preparation procedures, such as fixation, cutting and staining, across different laboratories represents an additional challenge to be addressed, potentially affecting the generalizability of AI-based methods [145].

In the context of BPD, the application of AI models, particularly ML algorithms, has shown considerable promise in improving the early identification of infants at risk of developing this condition. These prediction models have been developed by combining different antenatal risk factors with postnatal clinical, radiological and laboratory parameters [146]. A compelling example of AI's application in BPD diagnosis is found in the study of Chou *et al.* [147], which demonstrates the power of AI models in predicting the risk of BPD in preterm infants using chest radiographs. Chest X-rays are an important diagnostic tool in neonatal clinical practice, and AI algorithms can enhance the interpretation of these images, allowing for more precise identification of features indicative of early development of BPD. The AI-based approach can spot subtle lung abnormalities that may be missed by human observers, improving the accuracy and speed of diagnosis. Generally, early prediction of infants at high risk of BPD is crucial because it allows clinicians to take timely action to prevent or reduce the severity of the disease. In addition to the prediction models, AI is also being employed to interpret lung ultrasounds, a non-invasive and

increasingly important tool for monitoring lung health in preterm infants. AI algorithms can analyze lung ultrasound images to detect signs of lung injury or disease. These models have the potential to provide more accurate assessments compared to manual interpretation, improving the ability to monitor lung health and detect early signs of BPD [148]. Even though these AI-driven advancements in predicting and diagnosing BPD underscore its growing potential in neonatal care, it is important to acknowledge that there are still challenges and limitations to be addressed [146]. The integration of AI into histological analysis, instead, represents a less explored, promising research area. Histological examination of lung tissue at the microscopic level allows for the identification of structural and cellular changes that can contribute to the development and progression of BPD. Thus, AI-based models can enhance this process, potentially revolutionizing the way researchers and clinicians approach lung tissue analysis.

2. Aim of the study

BPD is the most prevalent chronic respiratory disease affecting premature infants. Despite recent advances in neonatal intensive care, no approved treatment exists, largely due to the disease's complex and heterogeneous pathophysiology. To better understand the mechanisms involved in BPD pathogenesis, several animal models have been developed. Among these, the hyperoxia-exposed preterm rabbit model has emerged as a promising tool. However, a comprehensive characterization of this animal model, integrating functional, histological and biomolecular outcomes and using an innovative AI-based approach for morphometric analyses, is still lacking.

The study aimed to characterize the preterm rabbit model by evaluating the impact of prematurity alone and in combination with hyperoxia exposure on postnatal lung development. Structural abnormalities observed in our experimental condition were assessed using an integrative approach that combined conventional morphometric techniques with AI-based quantitative analyses. Transmission Electron Microscope (TEM) was employed to investigate ultrastructural alterations in the alveolar epithelium and pulmonary vascular wall. Lung function measurements were performed to correlate morphological changes with impaired respiratory mechanics, providing a functional perspective on hyperoxia-induced injury. Moreover, the study examined the expression of genes involved in vascular development and inflammation, known to be affected by preterm birth and postnatal exposure to hyperoxia. By integrating functional, histological and biomolecular data, this study provides a comprehensive understanding of pathogenetic mechanisms contributing to the development of BPD in the preterm rabbit model, further confirming its translational relevance and supporting its use in preclinical studies.

3. Materials and methods

3.1 In vivo protocol

All experimental procedures were approved by the local animal ethics committee and were performed in accordance with the standard European regulations on animal research (n° 875/2021-PR). Pregnant New Zealand White rabbits were provided by Charles River (Domaine des Oncins, France) and kept in Chiesi's Research Centre facility, with food and water *ad libitum*, until C-section or natural delivery occurred. They were housed under controlled environmental conditions: temperature ranging from 15 to 21°C, relative humidity of 55 ± 15% and 12:12 hours dark/light cycles.

3.1.1 Custom-made incubators

At Chiesi's Research Centre, custom-made incubators (Okolab, Naples, Italy) were used to maintain an appropriate environment to rear the preterm rabbit pups. Incubators are placed under a walk-in hood (Weiss Technik ®, Germany) and connected to three gas lines: compressed air, nitrogen, and oxygen. Thanks to the presence of sensors inside them, Okolab incubators enable the control and recording of all experimental parameters (carbon dioxide, oxygen levels, relative humidity, and temperature) during the entire length of the experiment by using a PC monitor located outside the walk-in hood and equipped with the software DATALOG (Okolab). The three gas lines have a pressure reducer installed on the wall to keep the pressure below 2 bars. Each incubator is connected to a gas mixer (Okolab gas controller), a temperature controller (Okolab T Unit), a touch screen panel (OkoTouch), where all parameters of the incubator can be set, and a pedal to switch the lights on and off inside the incubator. Relative humidity can be manually adjusted by decreasing or increasing the volume of water inside metal water vessels located on a heated shelf. Moreover, each incubator is supplied with a constant flow of compressed air, which can be manually adjusted to modify carbon dioxide levels and relative humidity. Finally, the front

door of the Okolab incubator is characterized by the presence of three white diaphragm openings, which allow for performing daily experimental procedures, minimizing their impact on the parameters inside the incubator.

Figure 5. Okolab incubators (Naples, Italy).

3.1.2 C-section and experimental design

Preterm rabbits were delivered on the saccular phase on the 28th day of gestation (term 31 days). Firstly, does (3.8 ± 0.3 kg of body weight) were sedated with intramuscular (i.m.) injection of medetomidine 2 mg/kg (Domitor®, Orion Pharma, Finland). After ten minutes, 25 mg/kg of ketamine (Imalgene 1000®, Merial, France) and 5 mg/kg of xylazine (Rompun®, Bayer, Germany) were administered. Once they were properly sedated, does were placed in the supine position and shaved on their abdomen and euthanized with an overdose (100 mg/kg) of pentothal sodium (MSD Animal Health, USA) in the marginal ear vein. Then, a low midline abdominal incision was performed, and the uterus was exposed. After that, the pups were extracted by hysterotomy, they were dried, stimulated, and placed into Okolab incubators, where oxygen levels, relative humidity, and temperature were set according to the experimental conditions. Pups

that were unable to breathe on their own and died within the first hour of postnatal age were excluded from the experiment.

A total of 28 surviving pups from different experimental sessions were weighed, numbered, randomized into either normoxia (21% O_2) (n=17) or hyperoxia (95% O_2) (n=11), and placed into the incubators under specific conditions. Pups were further randomized to the following experimental groups:

- Normoxia (21% O_2) (N21% D28+3): pups were exposed to 21% oxygen for 3 days (n=10).
- Normoxia (21% O_2) (N21% D28+7): pups were exposed to 21% oxygen for 7 days (n=7).
- Hyperoxia (95% O_2) (H95% D28+3): pups were exposed to 95% oxygen for 3 days (n=3).
- Hyperoxia (95% O_2) (H95% D28+7): pups were exposed to 95% oxygen for 7 days (n=8).

Two additional experimental groups consisting of rabbit pups born at term and left with their mothers were included as age-matched controls for physiological postnatal lung development.

- Term (T31): pups born at term and sacrificed after natural delivery (n=5).
- Term (T31+4): pups born at term and maintained at room air with their mothers until postnatal day 4 (n=7).

When natural delivery at term (31st day of gestation) was allowed, does were placed in special cages equipped with an external box where they build their nest.

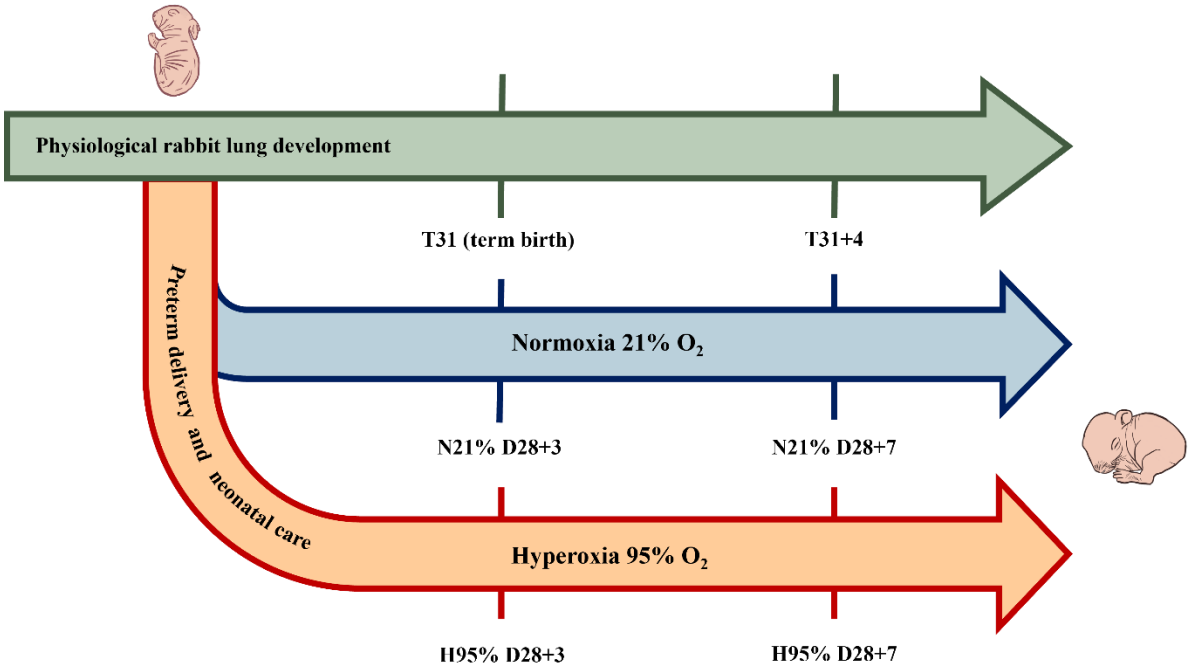

Figure 6. Scheme of the experimental timeline. Term pups were born at term on the 31st day of gestation and left at room air with their mothers until the lungs were collected at birth (T31) and 4 days after natural delivery (T31+4). Preterm pups were delivered through C-section on the 28th day of gestation and randomized into two groups exposed to normoxia (21% O_2) or hyperoxia (95% O_2). Pups were maintained under specific conditions in custom-made incubators until the lungs were collected on the 3rd (N21% D28+3; H95% D28+3) and on the 7th day of postnatal age (N21% D28+7; H95% D28+7).

3.1.3 Neonatal rabbit care

Preterm rabbits were housed in plastic containers covered by a double layer of soft and absorbent tissue with environmental enrichment inside the incubators, except during the feeding procedure. Housing materials were changed every day. Pups were fed twice a day via a 3.5 Fr orogastric tube (Vygon, France) placed prior to and removed as soon as the feeding was finished. The feeding included a milk replacer (Day One®, Protein 30%, Fat 50%; FoxValley, Illinois, US) melted with water (250 mg/ml) according to the manufacturer's directions. Probiotics (25 mg/ml) were added for all 7 days (Bio-Lapis®; Probiotics International Ltd, UK); instead, additional immunoglobulins were added only on the first 2 days of postnatal life (Col-o-Cat®, SanoBest, Netherlands). The total administered feed volume, divided into 2 daily feeds, was progressively increased starting from 80 ml/kg/day on day 0 up to 200ml/kg/day on days 3-7. Before being fed,

pups were stimulated to urinate. On day 2, vitamin K was administered i.m. (0.25 mg/kg, Konakion®; Roche, Switzerland).

3.1.4 Lung function measurements

At the end of each experimental period, invasive lung function testing was performed using a forced oscillation technique with the flexiVent™ system (Figure 7) equipped with module 2 or 3 (SCIREQ, Montreal, Canada) depending on the weight of pups (module 2 is used for rabbits weighing not more than 80 g, while module 3 is used for rabbits weighing more than 80 g). Pups were anesthetized through i.m. administration of ketamine (35 mg/kg) and xylazine (5 mg/kg). A tracheostomy was performed, and an 18-gauge metal cannula was inserted in the trachea and tied. Pups were connected to the volume-controlled MV of the flexiVent™ (tidal volume 10 ml/kg, frequency of 120 breaths/min, Positive End Expiratory Pressure - PEEP of 3 cmH_2O). The following parameters were measured: a) inspiratory capacity (IC), which represents the amount of air that can be inhaled after the end of a normal expiration; b) tissue elastance (H), which represents the ability of the tissue to retract and revert to its original shape; c) tissue damping (G), which is closely related to the tissue resistance and contains a contribution related to the resistance to air flow in the peripheral airways; d) static compliance (Cst), which reflects the intrinsic elastic properties of the respiratory system and the distensibility of the lungs. All measurements were performed until obtaining three consistent measurements, with a coefficient of determination (COD) of >0.95 as the limit to accept them. The average of three measurements was calculated and used in the results.

Figure 7. flexiVent^{TM} system (SCIREQ, Montreal, Canada).

3.1.5 Lung tissue collection

All pups were euthanized with an overdose of pentothal sodium. Lung samples were collected from preterm pups exposed to hyperoxia (95% O_2) on postnatal day 3 and day 7. Lungs from normoxia-exposed preterm pups were harvested on postnatal day 3 and day 7. Term rabbits were naturally delivered on gestational day 31 and maintained with their mothers at room air in individual cages until postnatal day 4. Lung samples from term pups were collected at birth (day 31) and on postnatal day 4, employed as age-matched controls for physiological lung development. Lungs were immediately removed, weighed, and selectively separated into the left and right lungs. Immediately after lung collection, an 18-gauge catheter was inserted in the trachea, and the left lungs were fixed with 4% buffered formalin (Sigma-Aldrich, Germany) for at least 4 hours under constant pressure (25 cmH_2O). To avoid heterogeneous fixation pressures, a custom-made device was used (Figure 8). After 4 hours of fixation, the lungs were left in formalin for at least 24 hours and then transferred to PBS until processing for the histological analysis. The right lungs, instead, were dedicated to the biomolecular analysis. Immediately after being removed, the right lungs were placed into RNA later (Sigma-Aldrich, USA) solution and stored at -20°C until RNA extraction was performed.

For ultrastructural analysis, left lungs were also collected from term pups maintained at room air with their mothers until postnatal day 4, and from preterm pups exposed to hyperoxia and

normoxia for seven days. After fixation with 4% formalin (Sigma-Aldrich, Germany) for at least 24 hours under constant pressure (25 cmH_2O), lung samples were transferred into 2.5% glutaraldehyde in 0.1 M cacodylate buffer (Sigma-Aldrich, Germany) at pH 7.4 and stored at 4°C until processing for the ultrastructural analysis. Post-fixation was performed in 1% osmium tetroxide in the same buffer for 60 minutes at room temperature. Lung samples were dehydrated through a graded ethanol series and embedded in Spurr's low viscosity resin (Electron Microscopy Sciences). Ultrathin sections were cut at 60-70 nm with an ultramicrotome and mounted on 150 mesh copper grids (Electron Microscopy Sciences). Lung samples were then examined using a Talos F200S G2 TEM (ThermoFisher Scientific, USA).

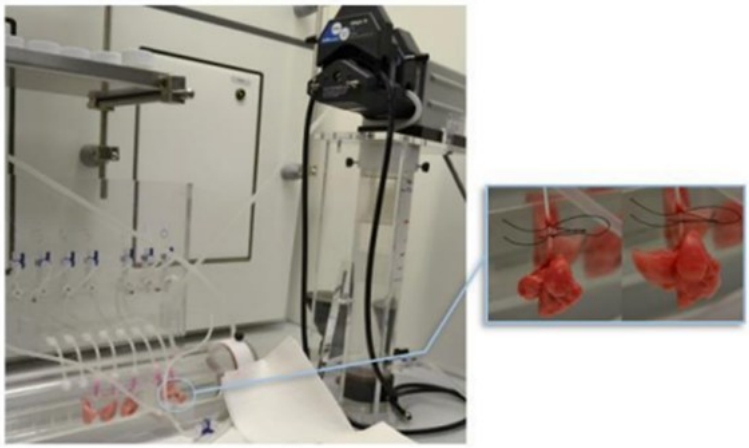

Figure 8. Custom-made device for constant pressure fixation.

3.2 Manual morphometric analysis

The left formalin-fixed lungs were dehydrated in graded alcohol solutions, xylene clarified, and paraffin-embedded. After that, samples were cut at 5 μm thickness with a rotary microtome (Slee Medical, Germany), placed on SuperFrost™ Microscope Slide (ThermoFisher Scientific, USA), and stained with Hematoxylin and Eosin (H&E) following standard histology protocols. The degree of postnatal alveolar development was manually assessed by the MLI, SCs count, and

RAC. The degree of the lung injury was evaluated using the ALI score. The distribution of elastic fibers was analyzed on pulmonary sections stained with Miller's staining.

3.2.1 Mean Linear Intercept (MLI)

Morphometric assessment of the extent of airspaces enlargement was performed by determining the MLI, a widely used quantitative parameter to study pulmonary diseases characterized by emphysematous lesions [138]. MLI is also commonly applied in the study of other conditions involving impaired alveolar development, such as BPD.

MLI measurement was performed using Dunnill's method [149]. A total of 40 histological fields per left lung were evaluated, both vertically and horizontally. The examination of such a number of fields ensures the assessment of the entire pulmonary section area. MLI measurement was determined by calculating the number of times a reference line of known length intercepts the alveolar septa. The analysis was manually performed by using an optical microscope on pulmonary sections stained with H&E at a magnification of 100x. The selected histological field was captured and projected onto the screen of a PC monitor, where two lines of the same length, corresponding to 200 μm, are superimposed. The value of MLI measurement was calculated by applying the following mathematical formula:

$$MLI = n \times L / \sum i$$

where n = number of lines counted, L = length of the reference line, $\sum i$ = total number of interalveolar intersections [149].

3.2.2 Secondary Crests (SCs) count

SCs count was manually performed by using an optical microscope on pulmonary sections stained with H&E. The selected histological field was captured and projected onto the screen of a PC monitor, where a 48-point "multipurpose" grid is superimposed. Morphometric analysis of SCs count was carried out by using the "point counting method" [139], which was performed at a

magnification of 200x by determining 20 randomly selected histological fields per left lung for a total of 960 points. The number of SCs was quantified by counting the points that fell on these structures, which was expressed as the density of SCs on lung parenchyma [150].

3.2.3. Radial Alveolar Count (RAC)

The degree of postnatal alveolar development was also evaluated by the RAC, a morphometric parameter proposed by Emery *et al.* [137] as an indicator of the alveolarization and, hence, of the changes in the alveolar number. The analysis was performed by drawing a perpendicular line from the lumen of the terminal bronchiole to the nearest connective tissue septum or pleural margin. The value of RAC was calculated by counting the number of saccules and alveoli crossed by this line [151].

3.2.4. Acute Lung Injury (ALI) score

The ALI score was proposed by the ATS in animal models of acute lung injury studies [140]. Because of the patchy distribution of lung injury, for each section, at least 20 random high-power histological fields at a magnification of 400x were independently scored in a blinded fashion. Moreover, at least 50% of each field must be occupied by lung alveoli, whereas fields that contain mainly the lumen of large airways or vessels were rejected. The ALI score was calculated by weighing the sum of each of the five independent variables, described above, according to the relevance ascribed to each feature by the committee, and normalizing them to the number of fields evaluated (Table 1). The resulting data is represented by a score between zero and one.

	Score per field		
Parameter	0	1	2
A. Neutrophils in the alveolar space	none	1–5	>5
B. Neutrophils in the interstitial space	none	1–5	>5
C. Hyaline membranes	none	1	>1
D. Proteinaceous debris filling the airspaces	none	1	>1
E. Alveolar septal thickening	<2x	2x–4x	>4x

Score = [(20 × A) + (14 × B) + (7 × C) + (7 × D) + (2 × E)]/(number of fields × 100)

Table 1. ALI scoring system (from Matute-Bello *et al.*, 2011) [140].

3.3 Morphometric analysis using an AI-based software

Manual morphometric analyses, although well established in scientific literature, show intrinsic limitations, such as being operator-dependent and time-consuming. They are typically performed in a predefined number of histological fields, chosen by the operator, which could not fully represent the entire tissue section. Consequently, subtle structural alterations could remain undetected.

To overcome these limitations, morphometric analyses were also performed using Visiopharm® (Visiopharm Integrator System, VIS, Hørsholm, Denmark), an AI-based software that allows the analysis of the entire tissue section fastly and accurately, minimizing operator-dependent variability and improving reproducibility. Visiopharm® enables the creation of custom applications (apps) for the detection and quantification of specific histological characteristics relevant to the disease studied. The creation of an app based on the DL-classification method requires a training phase. Although it could be time-consuming and required detailed manual annotation, this step is essential for training the software to accurately detect tissue structures, cellular components or morphological alterations and for ensuring the adaptability of the algorithm to variations in tissue morphology. Once properly trained, the app can automatically quantify the features of interest. Additional step-processing steps can be also applied to further refine and improve the accuracy of detection.

On pulmonary sections stained with H&E, two apps were developed: one for the measurement of ST and the other for the quantification of SCs.

3.3.1. Development of the app for the measurement of Septal Thickness (ST)

Pulmonary sections stained with H&E (Fig. 9a) were scanned using the Nanozoomer® (Hamamatsu, Japan) at a magnification of 20x, and the digitized pulmonary slices were uploaded

to Visiopharm® software. The app for the measurement of ST was developed using the DL-based classification method. During the training phase, the software was trained to recognize the alveolar septa, distinguishing them from surrounding tissue and background and assigning them a specific class within each ROI.

As shown in Figure 9b, an app to detect tissue section (green ROI) and another to exclude non-alveolar structures, such as bronchi and large blood vessels (black ROIs), were run. The combination of these two apps ensured that the measurement was restricted exclusively to alveolar regions, further reducing potential misdetection. The alveolar septa were detected (Figure 9d) and their thickness was automatically calculated by dividing the septal area by its length. ST values were expressed as mean thickness.

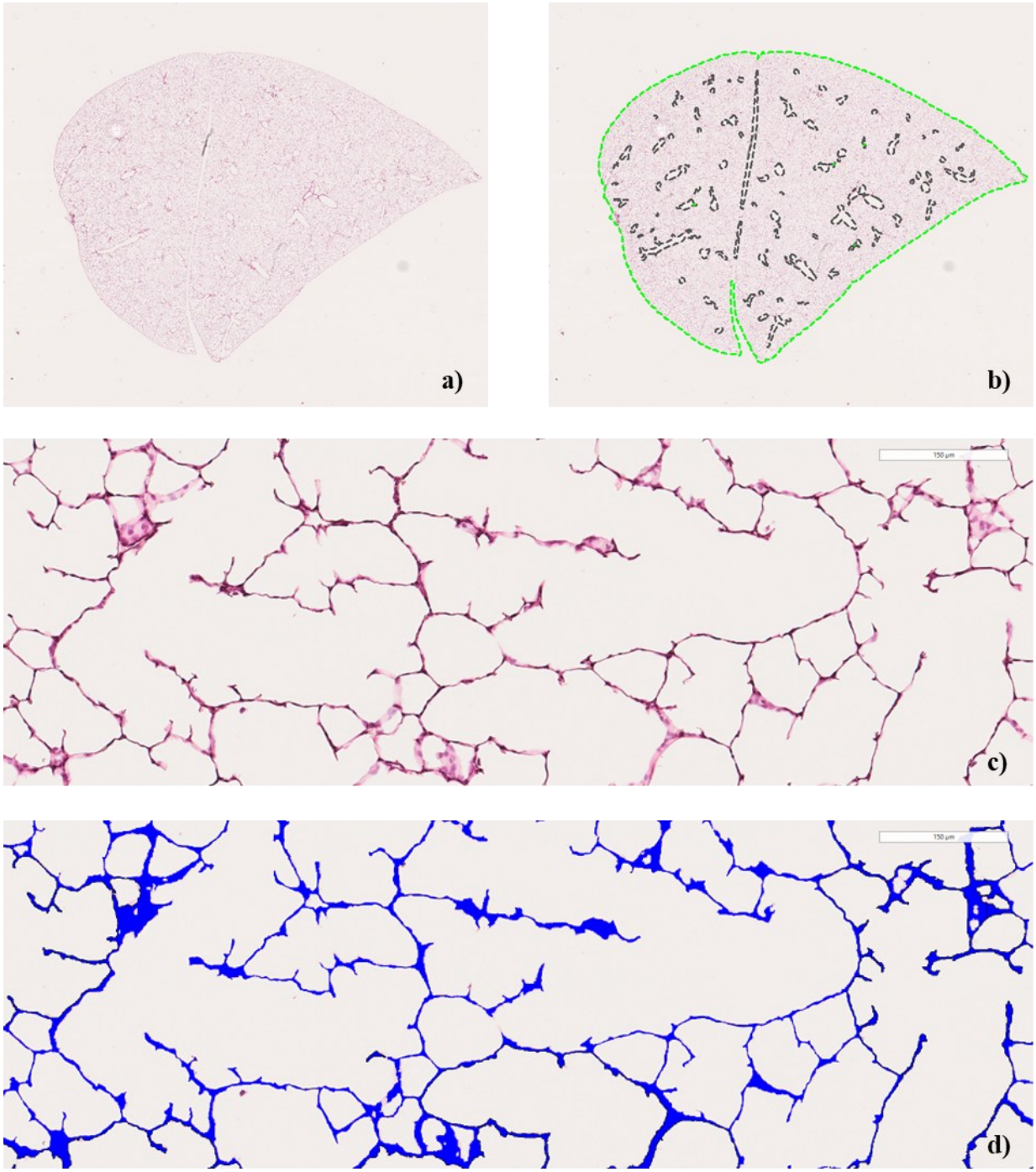

Figure 9. Detection of pulmonary tissue with exclusion of bronchi and large blood vessels and identification of alveolar septa. Figure a) shows a representative image of a lung section stained with H&E and scanned by Nanozoomer®. The digitized slice was uploaded to the software, which was trained to detect the contour of the pulmonary tissue (Figure b) in green, and to exclude bronchi and large blood vessels (Figure b) in black. Figure c) and Figure d) show a representative image of alveolar septa before and after the detection by the software (in blue).

3.3.2. Development of the app for Secondary Crests (SCs) count

Pulmonary sections stained with H&E (Figure 10a) were scanned using the Nanozoomer® (Hamamatsu, Japan) at a magnification of 20x, and the digitized pulmonary slices were uploaded to the Visiopharm® software. The app for SCs count was developed using the DL-based classification method. During the training phase, the software was trained to recognize SCs, distinguishing them from surrounding tissue and background and assigning them a specific class within each ROI.

As shown in Figure 10b, an app to detect tissue section (green ROI) and another to exclude non-alveolar structures, such as bronchi and large blood vessels (black ROIs), were run. The combination of these two apps ensured that the measurement was restricted exclusively to alveolar regions, further reducing potential misdetection. SCs were detected (Figure 10d) and automatically counted across the entire tissue section. SCs density was calculated by dividing the total number of SCs by the section area (green ROI, excluding black ROIs) expressed in mm^2.

The app for SCs count was validated by a manual morphometric analysis, which was performed by an expert pathologist on the same pulmonary section. Automated quantitative analysis was compared with manual morphometric analysis to evaluate the accuracy of detection, confirming that the app properly detected SCs.

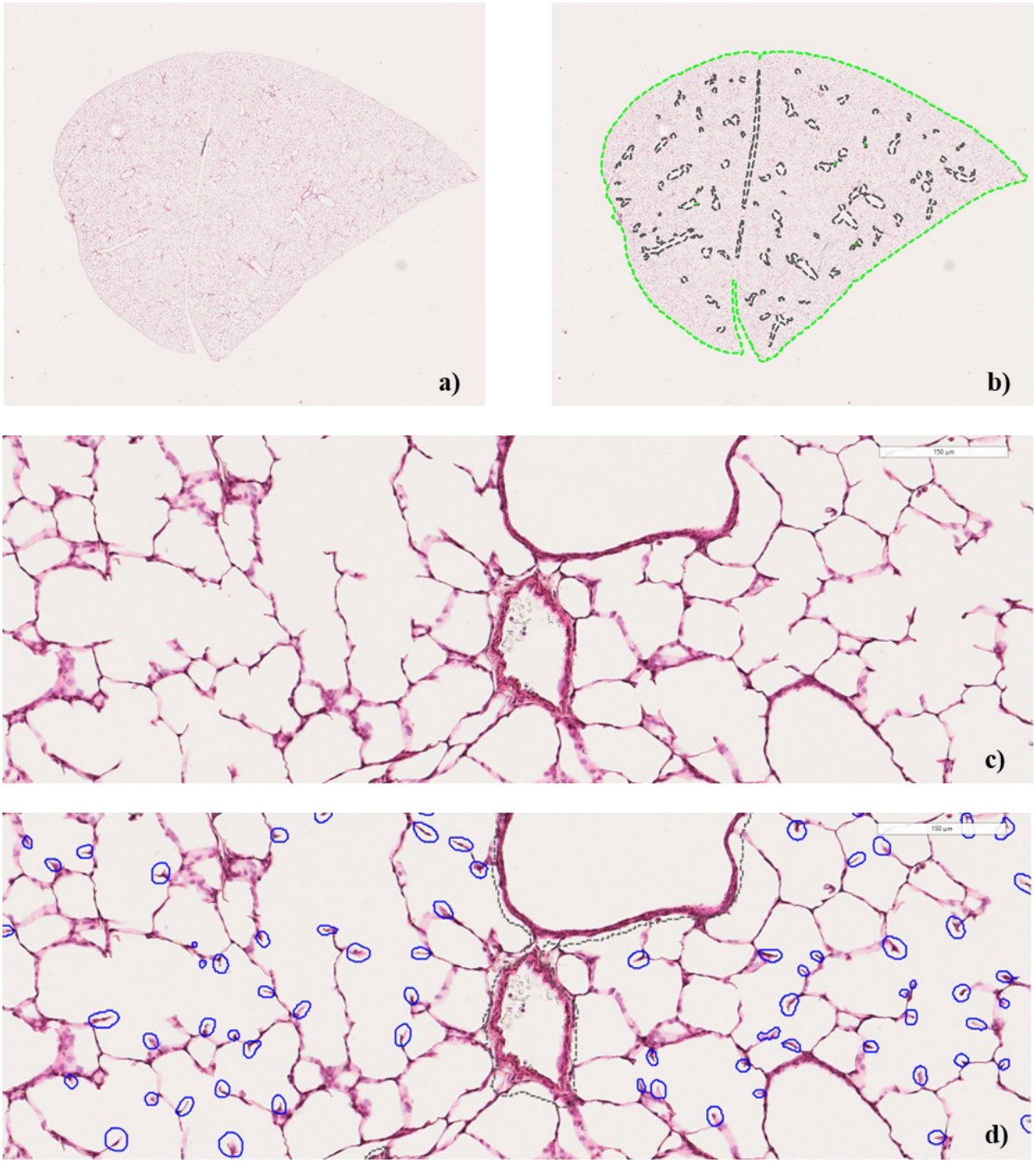

Figure 10. Detection of pulmonary tissue with exclusion of bronchi and large blood vessels and identification of SCs. Figure a) shows a representative image of a lung section stained with H&E and scanned by Nanozoomer®. The digitized slice was uploaded to the software, which was trained to detect the contour of the pulmonary tissue (Figure b) in green, and to exclude bronchi and large blood vessels (Figure b) in black. Figure c) and Figure d) show a representative image of SCs before and after the detection by the software (blue circles).

3.4 Immunohistochemistry (IHC)

Immunohistochemistry (IHC) was performed using a fully automated research stainer (Leica BOND RX, Leica Biosystems) (Figure 11). The BOND Intense R Detection System (DS9263) was used for the visualization of immunostaining. It is a peroxidase-based detection system optimized to be used on Leica BOND RX, and it contains peroxide block, streptavidin conjugated to horseradish peroxidase (HRP), 3,3'-diaminobenzidine (DAB) as chromogen, and hematoxylin. Before staining, lung sections were deparaffinized through incubation with BOND Dewax Solution (AR9222) at 72°C and rehydrated in ethanol. Heat-induced antigen retrieval was performed by applying citrate-based pH 6.0 buffer at 95° C for 20 minutes (Epitope Retrieval 1-ER 1) (AR9961). Since the detection system used is based on the enzymatic activity of peroxidase, lung sections were incubated for 10 minutes with peroxide block (Leica Biosystems) to block endogenous peroxidase. A non-immune serum diluted 1:10 with PBS+Triton X-100 and produced in the same host species as the secondary antibody was incubated for 60 minutes to block unspecific binding sites. Afterwards, lung sections were incubated for 1 hour with the primary antibody at room temperature. The following primary antibodies were used:

- Mouse monoclonal to Surfactant Protein-C (SP-C) (sc-518029, Santa Cruz Biotechonology) diluted 1:100 with goat serum.
- Goat polyclonal to α-SMA (ab21027, abcam) diluted 1:200 with horse serum.

For the detection of SP-C, lung sections were incubated for 40 minutes with biotinylated goat anti-mouse secondary antibody (Ready To Use, RTU) (BP-9200-50, Vector Laboratories). For the detection of α-SMA, lung sections were incubated for 40 minutes with biotinylated horse anti-goat secondary antibody (RTU) (BP-9500-50, Vector Laboratories). Then, streptavidin, a biotin-binding protein, covalently conjugated to HRP enzyme (Leica Biosystems), was incubated for 30 minutes on each lung sample. The reaction was visualized by using DAB as chromogen.

Figure 11. Leica BOND RX fully automated research stainer

3.5 Morphometric analysis on IHC-stained pulmonary sections using an AI-based software

On pulmonary sections stained by IHC for SP-C and α-SMA, two apps were developed: one to count the number of SP-C positive AT II cells and another to measure the thickness of α-SMA positive *tunica media* in small pulmonary blood vessels.

3.5.1 Development of the app for the quantification of Alveolar Type II (AT II) cells

Pulmonary sections stained by IHC with SP-C (Figure 12a), a specific marker of AT II cells, were scanned using Aperio VERSA (Leica Biosystems) at a magnification of 40x. The digitized lung slices were then visualized on Aperio Imagescope (Leica Biosystems) and uploaded to Visiopharm® software, where the app for the quantification of SP-C positive AT II cells was developed using the DL-based classification method. During the training phase, ROIs were drawn on pulmonary sections from different experimental conditions to ensure the adaptability of the algorithm to tissue variability and staining heterogeneity. Within each ROI, representative SP-C positive cells and background areas were manually annotated to create two distinct classes for

training. Additional post-processing steps were then added to the app workflow to further refine the accuracy of detection. The first post-processing step, named “Separate Object”, was applied to accurately distinguish individual cells in regions where adjacent SP-C positive cells were initially identified as a single object. Subsequently, the “Counting Frame” step was also added to ensure that only SP-C positive cells entirely located within a predefined frame were included in the quantification.

As shown in Figure 12b, an app to detect tissue section (blue ROI) and another to exclude non-alveolar structures, such as bronchi (red ROIs) and large blood vessels (yellow ROIs), were run. The combination of these two apps ensured that the measurement was restricted exclusively to alveolar regions, further reducing potential misdetection. SP-C positive cells were detected (Figure 12d) and automatically counted across the entire tissue section. Cell density was calculated by dividing the number of SP-C positive cells by the total section area (blue ROI, excluding red and yellow ROIs) expressed in mm^2.

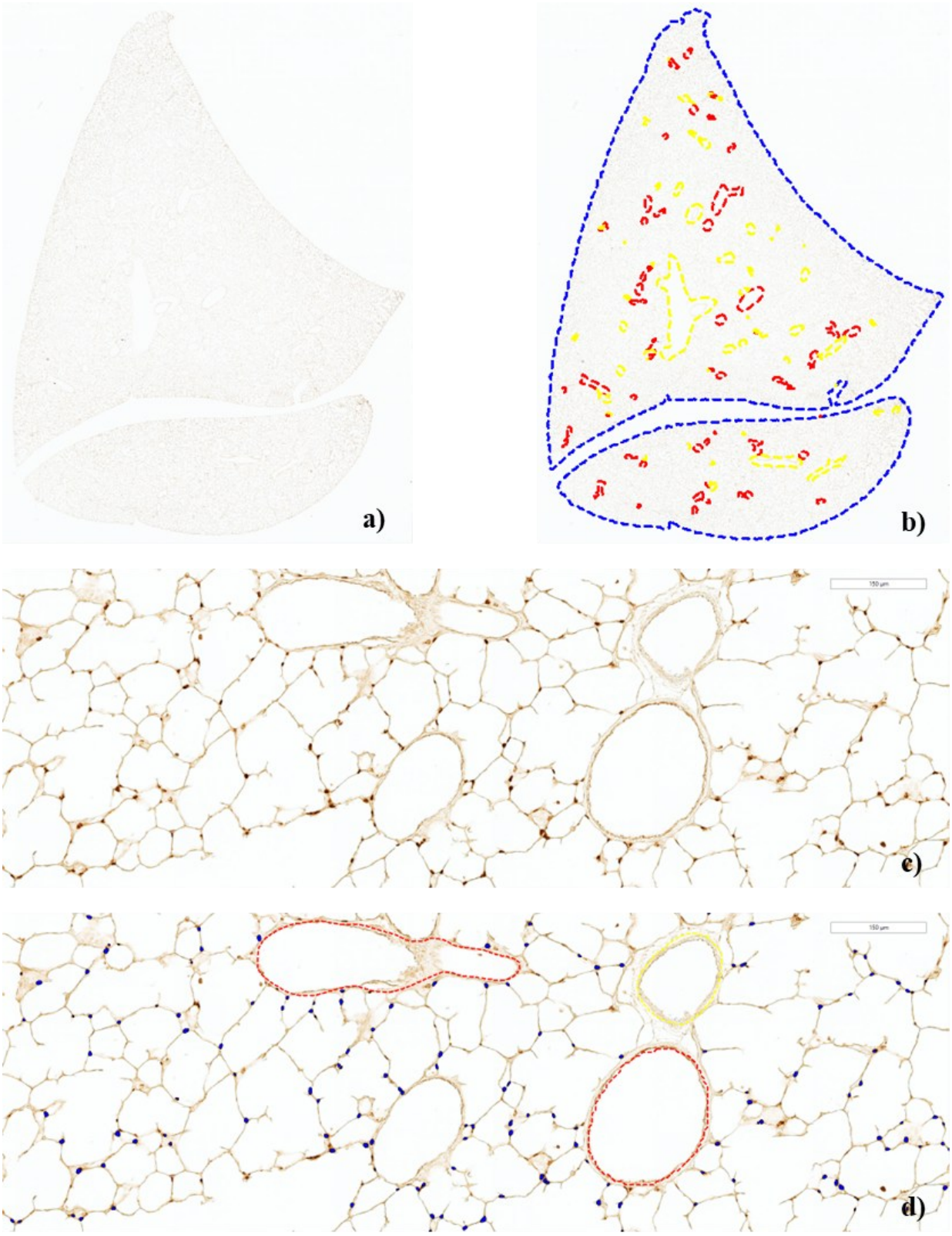

Figure 12. Detection of pulmonary tissue with the exclusion of bronchi and large blood vessels and identification of SP-C positive AT II cells. Figure a) displays a representative image of a lung section stained by IHC with SP-C and scanned by Aperio VERSA. The digitized slice was uploaded to the software, which was trained to detect the contour of the pulmonary tissue in blue, bronchi in red and large blood vessels in yellow (Figure b). Figure c) and Figure d) shows a representative image of SP-C positive AT II cells before and after the detection by the software (blue dots).

3.5.2 Development of the app for the measurement of pulmonary vascular medial thickness

Pulmonary sections stained by IHC with α-SMA (Figure 13a), a specific marker of smooth muscle cells (SMCs), were scanned using Aperio VERSA (Leica Biosystems) at a magnification of 40x. The digitized lung slices were then visualized on Aperio Imagescope (Leica Biosystems) and uploaded to Visiopharm® software, where the app for the measurement of the thickness of α-SMA positive *tunica media* in small pulmonary blood vessels was developed using the DL-based classification method. During the training phase, ROIs were drawn on pulmonary sections from different experimental conditions to ensure the adaptability of the algorithm to tissue variability and staining heterogeneity. Two classes, named "Background" and "Blood Vessels", were manually annotated within each ROI. Given that α-SMA is expressed not only by vSMCs but also by SMCs surrounding bronchi and bronchioles, accurate annotation of these structures was essential: the "Background" class was used to identify airway SMC, while the "Blood vessels" class was used to label vSMCs. An additional post-processing step, named "Change by Shape", was then added to select pulmonary blood vessels with a major axis length between 30 and 100 μm, automatically excluding out-of-range vessels.

As shown in Figure 13b, an app to detect tissue section (green ROI) was run, ensuring that all relevant pulmonary blood vessels were detected (Figure 13d) and the thickness of their *tunica media* was automatically measured across the entire section. Pulmonary vascular medial thickness was calculated by dividing α-SMA positive area by the circumference of each blood vessel detected and expressed as mean thickness.

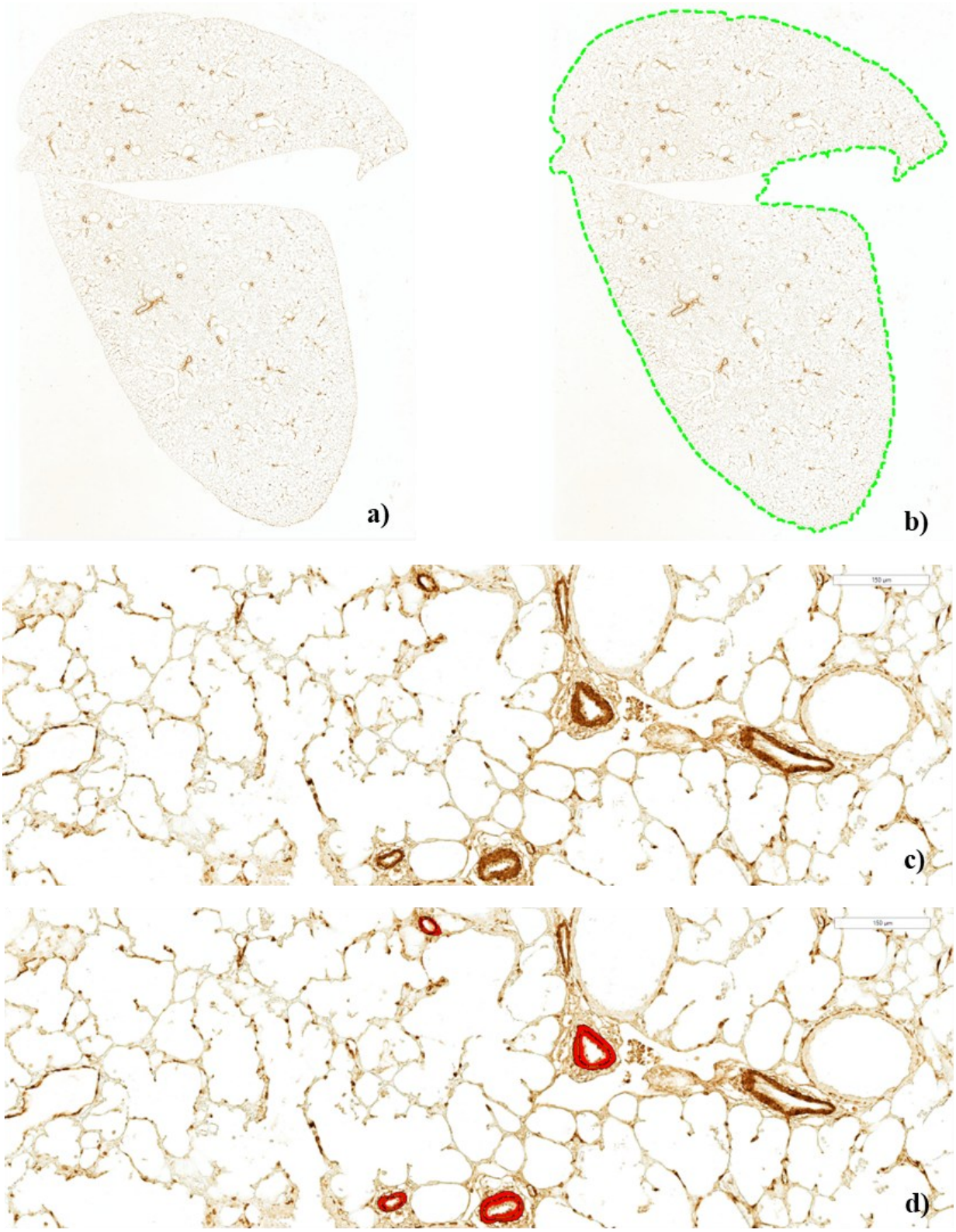

Figure 13. Detection of pulmonary tissue and identification of α-SMA-positive blood vessels. Figure a) displays a representative image of a lung section stained by IHC with α-SMA and scanned by Aperio VERSA. The digitized slice was uploaded to the software, which was trained to detect the contour of the pulmonary tissue in green (Figure b). Figure c) and Figure d) show a representative image of α-SMA positive blood vessels with a major axis length between 30 and 100 µm before and after the detection by the software (in red).

3.6 RNA extraction and quantitative Real Time-PCR (qRT-PCR)

Right lungs immersed in RNAlater solution and stored at -20°C were homogenized in QIAzol® Lysis Reagent using the gentleMACS™ Octo Dissociator (Miltenyi Biotec, Germany). After that, mRNA was extracted using the miRNeasy Mini Kit protocol (QIAGEN, Germany), using an automated method (QIAcube; QIAGEN, Germany), which includes a DNAse treatment to avoid DNA genomic contamination. The RNA concentration and quality were evaluated by using the Nanodrop™ spectrophotometer (ThermoFisher, USA). For cDNA synthesis, 25 nanograms (ng)/microliter of total RNA was reverse transcribed using RT2 First Strand Kit (QIAGEN, Germany) following the manufacturer's instructions. The reverse transcription reaction was performed by Eppendorf Mastercycler ep Gradient (Eppendorf, Germany). Then, the cDNA was mixed with RT^2 SYBR Green ROX qPCR Mastermix (QIAGEN, Germany) and added to a custom RT^2 PCR Array. Each sample was analyzed in duplicate using StepOnePlus™ Real-Time PCR Systems (ThermoFisher Scientific, USA), following the manufacturer's protocol. At the end of each PCR assay, the melting curve analysis was carried out. mRNA expression levels were normalized to a housekeeping gene and expressed as $2^{-\Delta Ct}$. For quantitative Real Time-PCR (qRT-PCR) analysis, genes related to the angiogenic and inflammatory pathways were selected.

3.7 Statistical analysis

Statistical analyses were performed using GraphPad Prism software, version 10.4.0. For multiple comparison, ordinary one-way analysis of variance (ANOVA), followed by Tukey's multiple comparisons test, was used. All data were presented as mean ± SEM and comparisons with p value < 0.05 were considered statistically significant.

4. Results

4.1 Lung function measurements

As shown in Figure 14 a-b, preterm pups exposed to normoxia and their age-matched term controls exhibited improved lung function between the two analyzed time-points, characterized by significantly increased IC (Figure 14a) and Cst (Figure 14b), along with decreased G (Figure 14c) and H (Figure 14d). Furthermore, preterm pups exposed to normoxia showed slightly decreased IC and Cst at the two analyzed time-points when compared to their age-matched term controls (Figure 14 a-b), whereas no difference in G and H was observed between these experimental groups (Figure 14 c-d).

In preterm pups exposed to hyperoxia for three days (H95% D28+3), a partial impairment of lung function was observed compared to both normoxic preterm animals (N21% D28+3) and term age-matched controls (T31). This was primarily reflected in lower IC (Figure 14a) and Cst (Figure 14b), along with higher G (Figure 14c) and H (Figure 14d) values. However, prolonged exposure to hyperoxia for seven days led to a statistically significant decline in lung function parameters, indicating a progressive worsening over time. Particularly, IC and Cst were significantly reduced (Figure 14 a-b), whereas G and H were significantly increased (Figure 14 c-d) compared to both normoxic preterm animals (N21% D28+7) and term age-matched controls (T31+4).

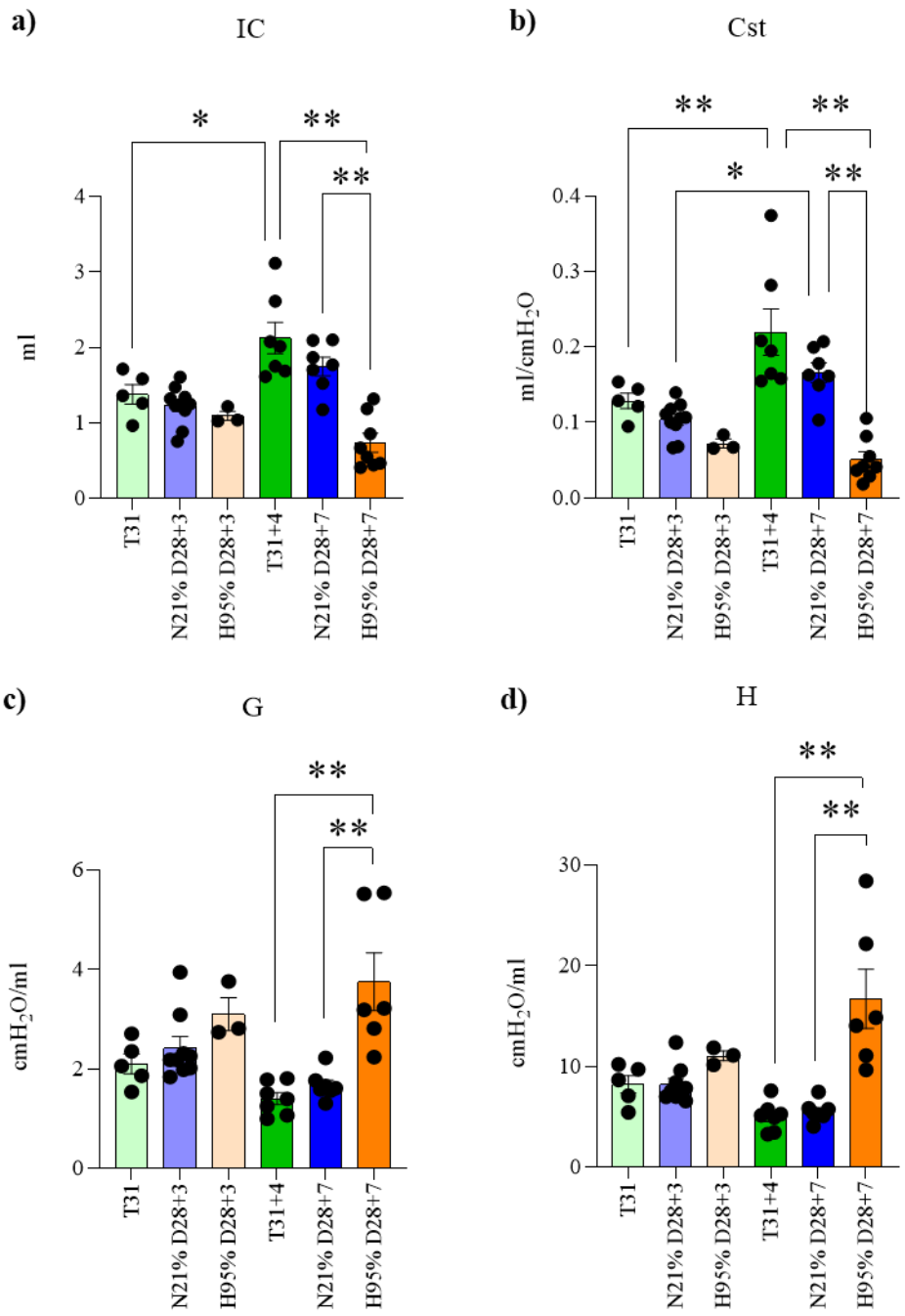

Figure 14. Lung function measurements. Before the sacrifice, term and preterm pups were anesthetized, and a cannula was secured in the trachea. Lung function was assessed using the flexiVent^{TM} system, as described in Materials and Methods. The following functional parameters were measured: a) Inspiratory Capacity (IC); b) Static Compliance (Cst); c) Tissue damping (G); d) Tissue elastance (H). The experimental groups analyzed are: term pups (T31, light green bar, n=5), preterm pups exposed to 21% O_2 for 3 days (N21% D28+3, light blue bar, n=10, 1 outlier identified in G and H), preterm pups exposed to 95% O_2 for 3 days (H95% D28+3, light orange bar, n=3), term pups left with their mothers for 4 days (T31+4, green bar, n=7), preterm pups exposed to 21% O_2 for 7 days (N21% D28+7, blue bar, n=7) and preterm pups exposed to 95% O_2 for 7 days (H95% D28+7, orange bar, n=8). Data are presented as mean ± SEM and analyzed with one-way ANOVA, corrected for multiple comparisons: * $p < 0.05$; ** $p \leq 0.01$.

4.2 Lung morphology

Structural alterations were analyzed on pulmonary sections stained with H&E and Miller's staining, whereas ultrastructural features were examined using TEM.

Similar structural features were observed in H&E-stained pulmonary slides from term and preterm pups exposed to normoxia at the two analyzed time-points (Figure 15 a-b; Figure 15 d-e). However, preterm pups exposed to hyperoxia for three days (H95% D28+3) showed airspace enlargement (Figure 15c) and increased presence of inflammatory cells within the alveolar spaces (Figure 16a) when compared to normoxic preterm animals (N21% D28+3) and their age-matched term controls (T31). After seven days of hyperoxia exposure, structural changes became more pronounced, including thickened alveolar septa, simplified and larger alveoli compared to both normoxic preterm pups (N21% D28+7) and term controls (T31+4) (Figure 15f). Furthermore, a marked increase in inflammatory cell infiltration and proteinaceous debris within alveolar spaces was found in the lungs of hyperoxia-exposed pups (H95% D28+7) (Figure 16b).

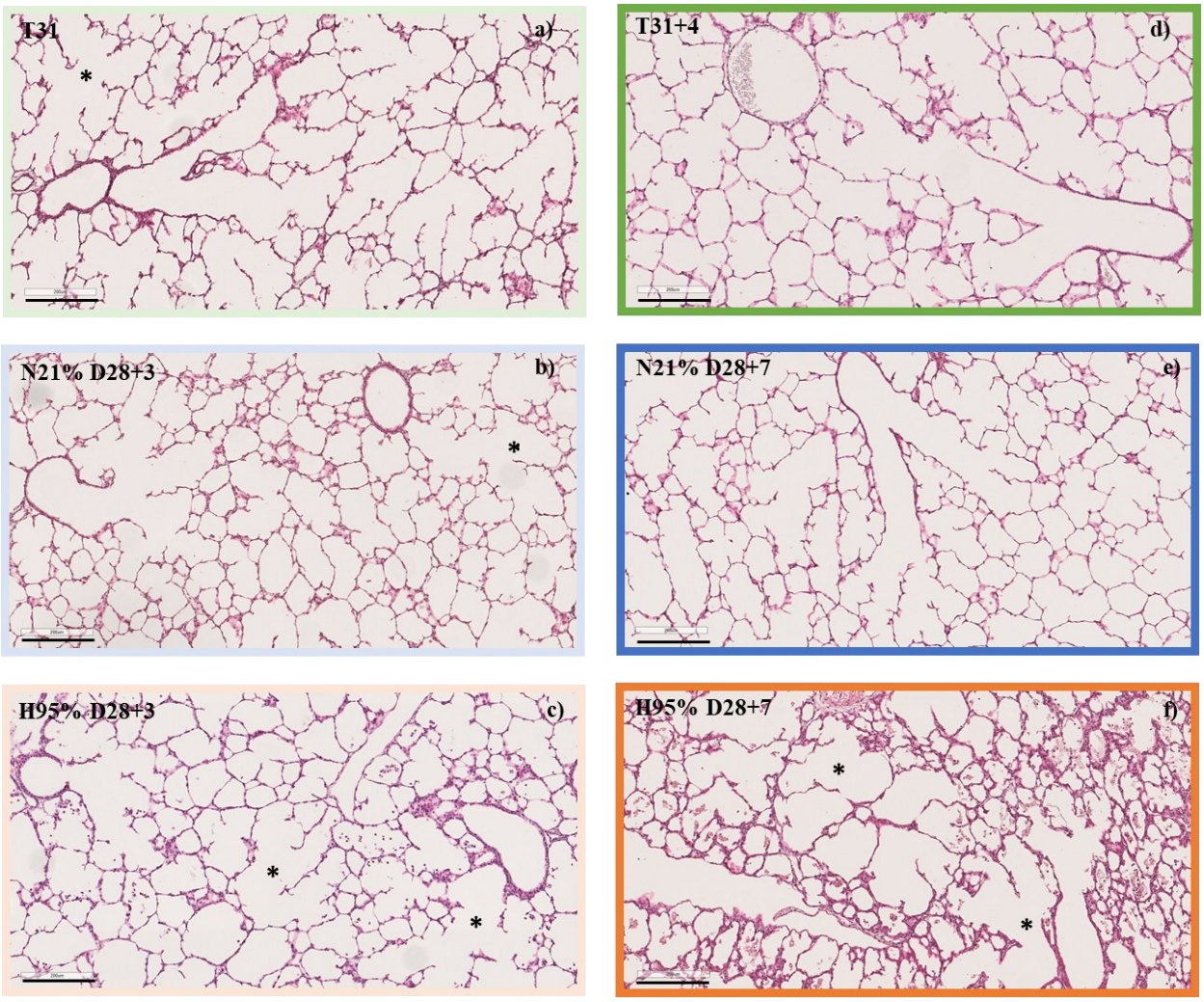

Figure 15. Representative pictures of pulmonary sections stained with H&E. Immediately after sacrifice, the left lungs of term and preterm pups were removed, fixed with formalin, and embedded in paraffin. Then, tissue slides were stained with H&E. The experimental groups analyzed are: term pups (T31), preterm pups exposed to 21% O_2 for 3 days (N21% D28+3), preterm pups exposed to 95% O_2 for 3 days (H95% D28+3), term pups left with their mothers for 4 days (T31+4), preterm pups exposed to 21% O_2 for 7 days (N21% D28+7) and preterm pups exposed to 95% O_2 for 7 days (H95% D28+7) (scalebar: black line, 200 µm; magnification 10x). Asterisks (*) indicate areas of airspace enlargement.

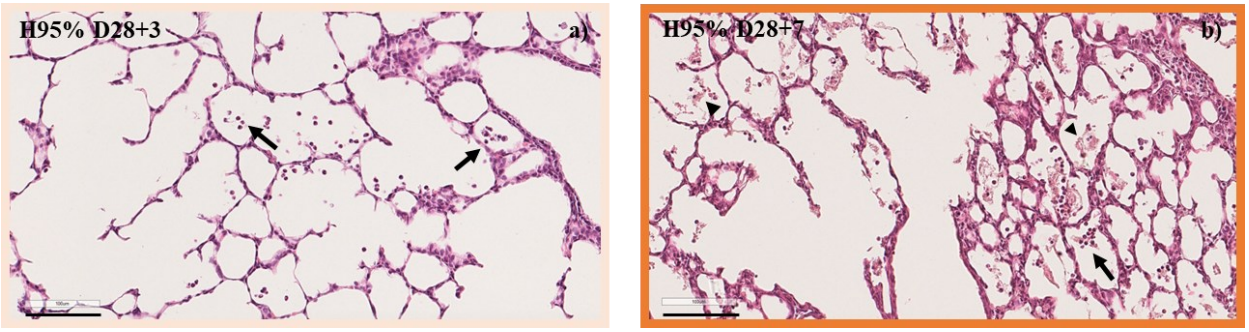

Figure 16. Representative pictures of pulmonary section stained with H&E. Immediately after sacrifice, the left lungs of term and preterm pups were removed, fixed with formalin, and embedded in paraffin. Then, tissue slides

were stained with H&E. The experimental groups analyzed are: preterm pups exposed to 95% O_2 for 3 days (H95% D28+3) and preterm pups exposed to 95% O_2 for 7 days (H95% D28+7) (scalebar: black line, 100 µm; magnification 20x). Black arrows indicate inflammatory cells; black arrowheads indicate proteinaceous debris.

Miller's staining highlighted the distribution and organization of elastic fibers in the developing lungs, appearing as thin, blue-stained structures. These fibers are predominantly located within the internal and external laminae of blood vessels, the alveolar septa, and at the tips of alveolar septa (Figure 17 a-f). No apparent differences in elastic fibers distribution and organization within the internal and external laminae of blood vessels and at the tips of alveolar septa were detected among the experimental groups analyzed. In term (T31) and preterm pups exposed to normoxia (N21% D28+3), as well as in preterm pups exposed to hyperoxia for three days (H95% D28+3), elastic fibers within the alveolar septa appeared fragmented (Figure 17 a-c), with impaired structural organization particularly evident following hyperoxia exposure (Figure 17c). In contrast, preterm pups exposed to normoxia for seven days (N21% D28+7) and their age-matched term controls (T31+4) showed a more continuous and organized elastic fiber pattern within the alveolar septa (Figure 17 d-e). Postnatal exposure to hyperoxia for seven days resulted in markedly disrupted elastin architecture. Particularly, in this experimental group (H95% D28+7), thickened, tortuous, and poorly organized elastic fibers within the alveolar septa were observed (Figure 17f) when compared to N21% D28+7 and T31+4.

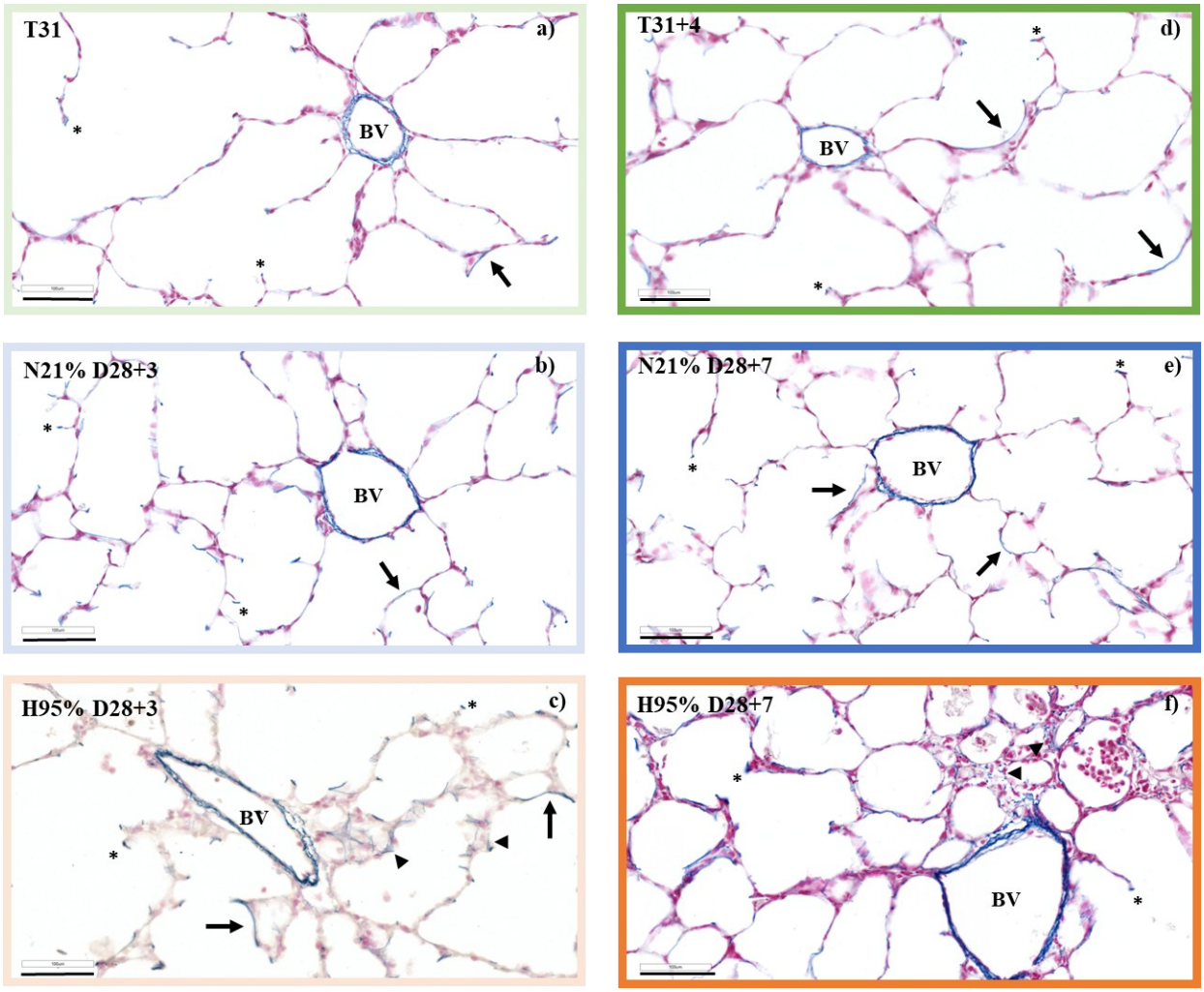

Figure 17. Representative pictures of pulmonary sections stained with Miller's staining. Immediately after sacrifice, the left lung of term and preterm pups was removed, fixed with formalin, and embedded in paraffin. Then, tissue slides were stained with Miller's staining. The experimental groups analyzed are: term pups (T31), preterm pups exposed to 21% O_2 for 3 days (N21% D28+3), preterm pups exposed to 95% O_2 for 3 days (H95% D28+3), term pups left with their mothers for 4 days (T31+4), preterm pups exposed to 21% O_2 for 7 days (N21% D28+7) and preterm pups exposed to 95% O_2 for 7 days (H95% D28+7) (scalebar: black line, 100 µm; magnification 20x). BV: blood vessel; black arrows indicate elastic fibers within the alveolar septa; black arrowheads indicate impaired organization of elastic fibers within the alveolar septa; asterisks indicate elastic fibers at the tips of alveolar septa.

In term pups (T31+4), mature AT II cells containing lamellar bodies were observed (Figure 18a). In contrast, preterm pups exposed to normoxia for seven days (N21% D28+7) exhibited a reduction in the number of mature AT II cells containing lamellar bodies compared to T31+4 (Figure 18b). This reduction was even more pronounced in preterm pups exposed to hyperoxia for seven days (H95% D28+7), which showed fewer mature AT II cells (Figure 18c).

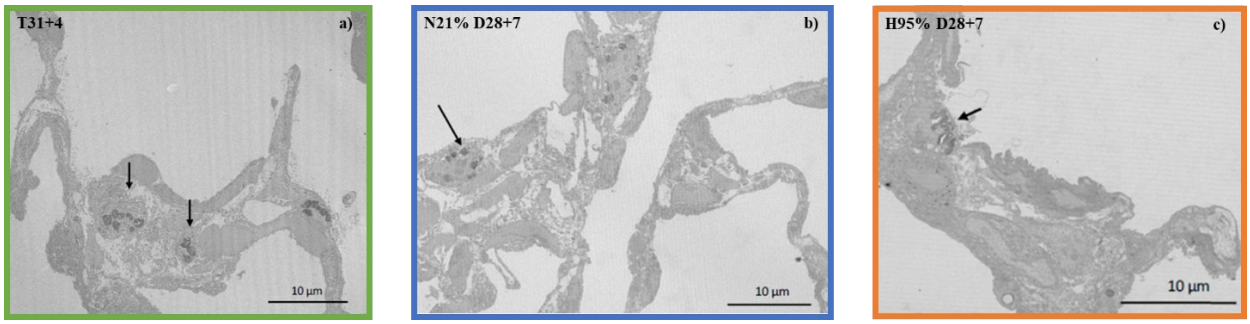

Figure 18. Representative pictures of AT II cells examined using TEM. Immediately after sacrifice, the left lung of term and preterm pups was removed, fixed with formalin, and processed for ultrastructural analysis. The experimental groups analyzed are: term pups left with their mothers for 4 days (T31+4), preterm pups exposed to 21% O_2 for 7 days (N21% D28+7) and preterm pups exposed to 95% O_2 for 7 days (H95% D28+7) (scalebar: black line, 10 µm). Black arrows indicate lamellar bodies within the cytoplasmatic region of AT II cells.

In the three experimental groups analyzed, small clusters of elastin, not yet fully organized, were observed at the tips of alveolar septa (Figure 19).

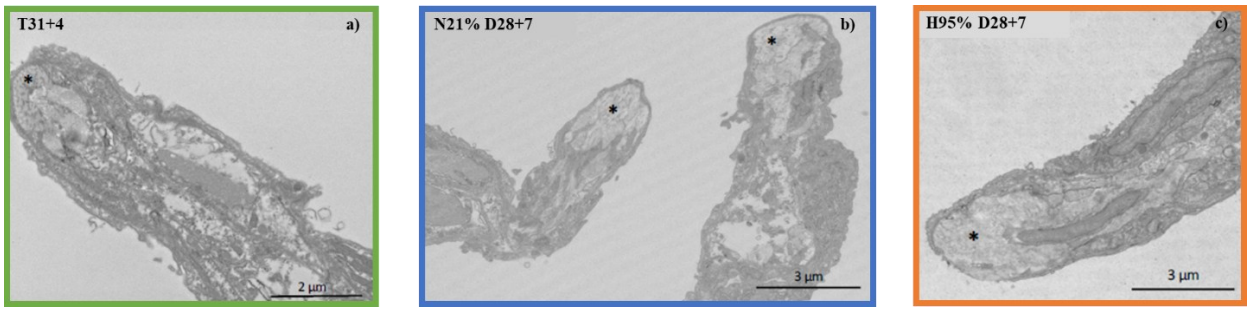

Figure 19. Representative pictures of SCs examined using TEM. Immediately after sacrifice, the left lung of term and preterm pups was removed, fixed with formalin, and processed for ultrastructural analysis. The analyzed experimental groups are: term pups left with their mothers for 4 days (T31+4), preterm pups exposed to 21% O_2 for 7 days (N21% D28+7) and preterm pups exposed to 95% O_2 for 7 days (H95% D28+7) (scalebar: black line, 2 µm for T31+4; 3 µm for N21%D28+7 and H95% D28+7). Asterisks indicate small clusters of elastin at the tips of alveolar septa.

In term (T31+4) and preterm pups exposed to normoxia for seven days (N21% D28+7), the *tunica media* of pulmonary blood vessels is characterized by SMCs interspersed with extracellular matrix, in which the elastic component is arranged into discontinuous structures (Figure 20 a-b). As shown in Figure 20 a-b, the surrounding extracellular matrix is composed of collagen, elastin, and microfibrillar structures. However, in T31+4, the elastic component generally appeared more developed within the *tunica media* and became increasingly discontinuous toward the *tunica*

adventitia (Figure 20a). In contrast, in N21% D28+7, the elastic component was arranged into more fragmented fibers (Figure 20b). After seven days of hyperoxia exposure, in preterm pups the *tunica media* showed significant alterations, including spatial disorganization and morphological heterogeneity of SMCs (Figure 20c). Moreover, the extracellular matrix appeared to be limited and the elastic component was arranged into small fibers (Fig. 20c).

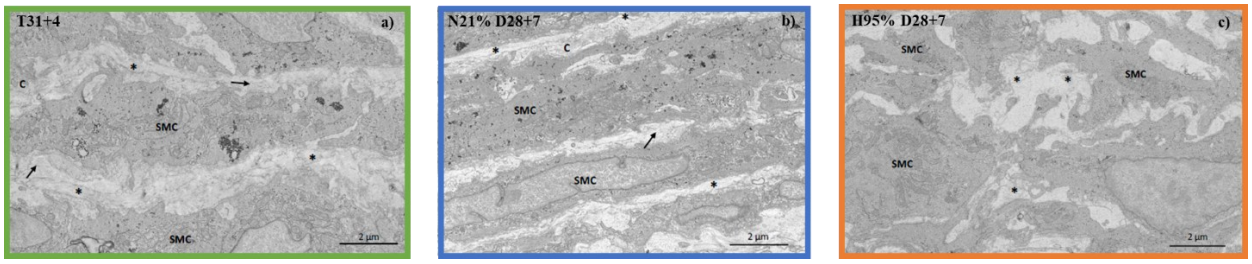

Figure 20. Representative pictures of the *tunica media* of pulmonary blood vessels examined using TEM. Immediately after sacrifice, the left lung of term and preterm pups was removed, fixed with formalin, and processed for ultrastructural analysis. The experimental groups analyzed are: term pups left with their mothers for 4 days (T31+4), preterm pups exposed to 21% O_2 for 7 days (N21% D28+7) and preterm pups exposed to 95% O_2 for 7 days (H95% D28+7) (scalebar: black line, 2 µm). C: collagen; SMC: smooth muscle cell; asterisks indicate elastin; black arrows indicate microfibrillar structure.

The internal elastic lamina was observed under the endothelial layer of the vascular wall. In term pups left at room air with their mothers until postnatal day 4 (T31+4), it is characterized by a matrix, that still appeared predominantly amorphous (Figure 21a). In preterm pups exposed to normoxia for seven days (N21% D28+7), the internal elastic lamina is composed of an amorphous matrix, where electron-dense microfibrillar component, essential for the deposition of "elastin clumps", was still detectable (Figure 21b). An extremely large number of these structures was observed at the peripheral regions of the fiber (Figure 21b). In preterm pups exposed to hyperoxia for seven days (H95% D28+7), the internal elastic lamina exhibited a variable thickness, with numerous "elastin clumps" surrounded by microfibrillar component (Figure 21c).

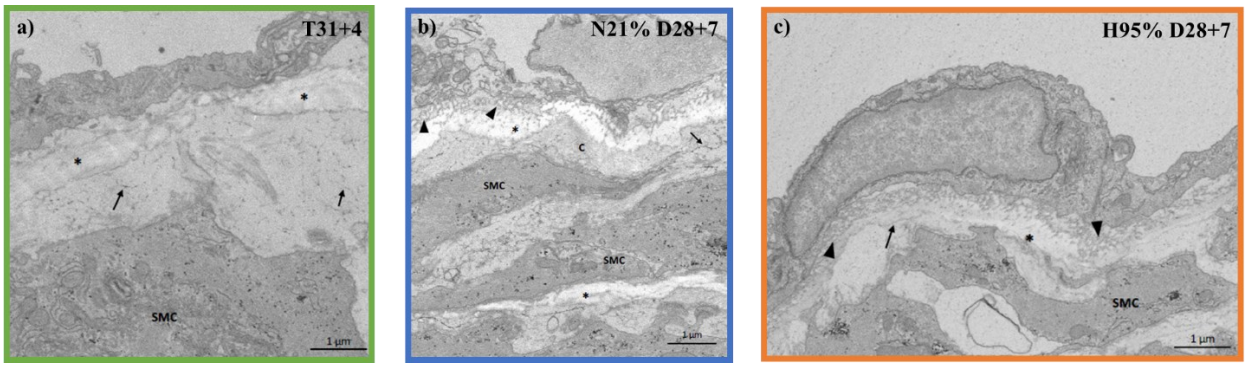

Figure 21. Representative pictures of the vascular internal elastic lamina examined using TEM. Immediately after sacrifice, the left lung of term and preterm pups was removed, fixed with formalin, and processed for ultrastructural analysis. The experimental groups analyzed are: term pups left with their mothers for 4 days (T31+4), preterm pups exposed to 21% O_2 for 7 days (N21% D28+7) and preterm pups exposed to 95% O_2 for 7 days (H95% D28+7) (scalebar: black line, 1 µm). C: collagen; SMC: smooth muscle cell; asterisks indicate elastin; black arrows indicate microfibrillar structure; black arrowheads indicate "elastin clumps".

4.3 Lung morphometry

4.3.1 Manual morphometric analysis

In term and preterm pups exposed to normoxia, MLI values were comparable at the two time-points analyzed (Figure 22a). However, exposure to high oxygen levels for three days resulted in a statistically significant increase in MLI values compared to term (T31) and preterm pups exposed to normoxia for three days (N21% D28+3) (Figure 22a). In preterm pups exposed to hyperoxia for seven days (H95% D28+7), MLI values remained elevated. This increase reached statistical significance when compared to age-matched term controls (T31+4), but not when compared to preterm pups maintained in normoxia (N21% D28+7) (Figure 22a).

In term and preterm pups exposed to normoxia, the total number of SCs remained unchanged between the two analyzed time-points (Figure 22b). After three days of postnatal hyperoxia exposure, the total number of SCs decreased, although not significantly, compared to normoxic preterm animals (N21% D28+3) and age-matched term controls (T31) (Figure 22b). However, a reduction of the total number of SCs was also observed in preterm pups exposed to hyperoxia for

seven days (H95% D28+7), reaching statistical significance when compared to age-matched term controls (T31+4) and preterm pups exposed to normoxia (N21% D28+7) (Figure 22b).

In term and preterm pups exposed to normoxia, RAC progressively increased during postnatal lung development, with a statistically significant difference observed between the two analyzed time-points in the preterm normoxic group (Figure 22c). In contrast, no significant changes in RAC were observed from postnatal day 3 to day 7 in preterm pups exposed to hyperoxia (Figure 22c). In particular, at day 7, hyperoxic preterm animals (H95% D28+7) showed a significant reduction in RAC compared to age-matched term controls (T31+4) and preterm pups exposed to normoxia (N21% D28+7) (Figure 22c).

In term and preterm pups exposed to normoxia, no difference in ALI score between the two analyzed time-points was observed (Figure 22d). However, preterm pups exposed to hyperoxia for three days (H95% D28+3) showed a non-significant increase in the ALI score when compared to term (T31) and normoxic preterm animals (N21% D28+3) (Figure 22d). In the hyperoxic experimental group, preterm pups showed a significant increase in ALI score from postnatal day 3 to day 7 (Figure 22d). A statistically significant difference was also observed when preterm pups exposed to hyperoxia for seven days (H95% D28+7) were compared to age-matched term controls (T31+4) and preterm pups exposed to normoxia (N21% D28+7) (Figure 22d).

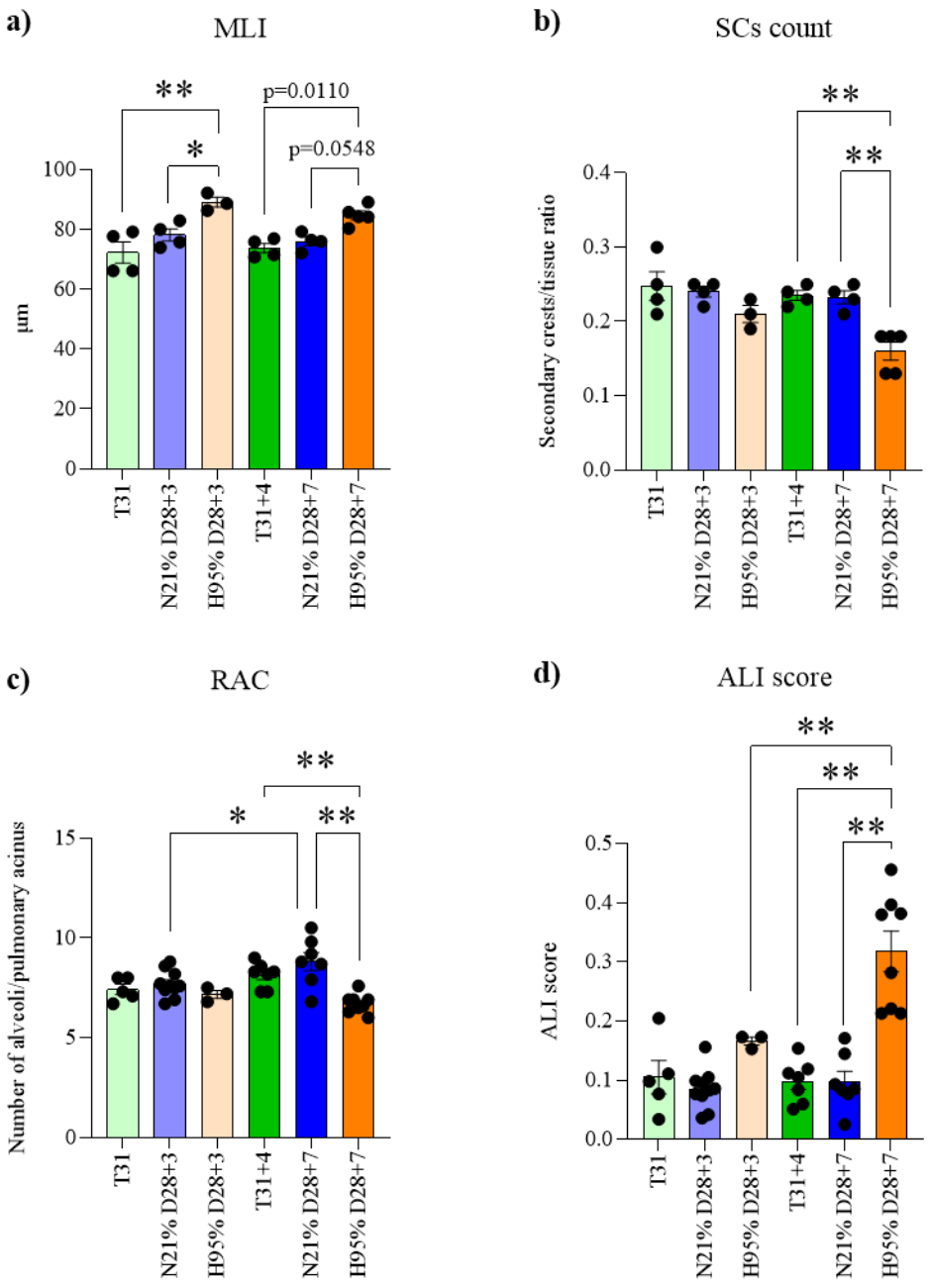

Figure 22. Manual morphometric analysis. Morphometric analysis on pulmonary sections of term and preterm pups stained with H&E was carried out as described in Materials and Methods. The following morphometric parameters were measured: a) Mean Linear Intercept (MLI); b) Secondary Crests (SCs) count; c) Radial Alveolar Count (RAC); d) Acute Lung Injury (ALI) score. The experimental groups analyzed are: term pups (T31, light green bar, n=4 for MLI and SCs count, n=5 for RAC and ALI score), preterm pups exposed to 21% O_2 for 3 days (N21% D28+3, light blue bar, n=4 for MLI and SCs count, n=10 for RAC and ALI score) or to 95% O_2 for 3 days (H95% D28+3, light orange bar, n=3), term pups left with their mothers for 4 days (T31+4, green bar, n=4 for MLI and SCs count, n=7 for RAC and ALI score), preterm pups exposed to 21% O_2 for 7 days (N21% D28+7, blue bar, n=4 for MLI and SCs count, n=7 for RAC and ALI score) or to 95% O_2 for 7 days (H95% D28+7, orange bar, n=5 for MLI and SCs count, n=8 for RAC and ALI score). Data are presented as mean ± SEM and analyzed with one-way ANOVA, corrected for multiple comparisons: * $p < 0.05$; ** $p \leq 0.01$.

4.3.2 Morphometric analysis using Visiopharm® software

SCs count using Visiopharm® software revealed a slight increasing trend in both term and preterm pups exposed to normoxia during postnatal lung development (Figure 23a). After three days of postnatal hyperoxia exposure, preterm pups showed a reduction in the total number of SCs; however, this decrease was not statistically significant when compared to term (T31) and preterm pups exposed to normoxia (N21% D28+3) (Figure 23a). At postnatal day 7, hyperoxic preterm animals (H95% D28+7) showed a significantly lower number of SCs compared to age-matched term controls (T31+4) and preterm pups exposed to normoxia (N21% D28+7) (Figure 23a).

The measurement of ST using Visiopharm® software showed a progressive reduction during postnatal lung development, as demonstrated by the statistical significance observed between the two analyzed time-points in the preterm normoxic group (Figure 23b). In contrast, in preterm pups exposed to hyperoxia, a statistically significant increase in ST was observed between postnatal day 3 and day 7 (Figure 23b). In particular, at day 7, hyperoxic preterm animals (H95% D28+7) showed significantly increased ST compared to age-matched term controls (T31+4) and preterm pups exposed to normoxia (N21% D28+7) (Figure 23b).

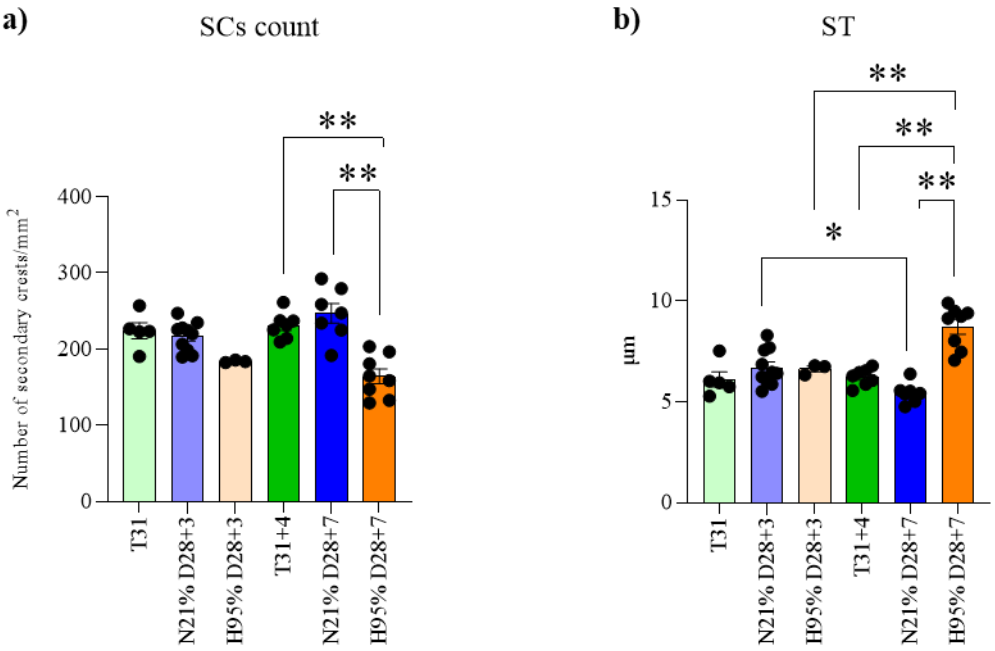

Figure 23. Morphometric analysis using Visiopharm® software. Morphometric analysis on pulmonary sections of term and preterm pups stained with H&E was carried out as described in Materials and Methods. The following morphometric parameters were measured: a) Secondary Crests (SCs) count; b) Septal Thickness (ST). The experimental groups analyzed are: term pups (T31, light green bar, n=5), preterm pups exposed to 21% O_2 for 3 days (N21% D28+3, light blue bar, n=10) or to 95% O_2 for 3 days (H95% D28+3, light orange bar, n=3), term pups left with their mothers for 4 days (T31+4, green bar, n=7), preterm pups exposed to 21% O_2 for 7 days (N21% D28+7, blue bar, n=7) or to 95% O_2 for 7 days (H95% D28+7, orange bar, n=8). Data are presented as mean ± SEM and analyzed with one-way ANOVA, corrected for multiple comparisons: ** $p \leq 0.01$.

4.4 Morphological and morphometric analysis on IHC-stained pulmonary sections

4.4.1 IHC for SP-C and quantification of AT II cells

IHC for SP-C is shown in Figure 24. In pulmonary sections from the analyzed experimental groups, a positive reaction within the cytoplasmatic region of AT II cells was observed (Figure 24), allowing for an accurate assessment of their number using Visiopharm® software. In term and preterm pups at the two analyzed time-points, the spatial distribution of AT II cells was relatively homogeneous. However, as shown in Figure 24, in preterm pups exposed to hyperoxia for seven days (H95% D28+7), these cells were no longer evenly distributed across the alveolar epithelium, with a higher cell density in peribronchial and perivascular regions.

In term (T31) and preterm pups exposed to normoxia for three days (N21% D28+3) a more intense positive reaction (Figure 24) and a relatively higher number of SP-C positive cells was measured (Figure 25). During the postnatal lung development, the total number of AT II cells progressively declined in term and preterm pups, reaching the statistical significance in the preterm normoxic group (Figure 25). After three days of postnatal exposure to hyperoxia, preterm pups (H95% D28+3) exhibited a similar degree of positivity (Figure 24). Moreover, in this experimental group, a lower number of SP-C positive AT II cells was observed. This reduction approached statistical significance (p=0,0557) compared to T31 and was not significant when compared to N21% D28+3 (Figure 25). In contrast, at postnatal day 7, H95% D28+7 showed a more pronounced

reduction (Figure 25), as evidenced by the statistically significant difference when compared to age-matched controls (T31+4) and normoxic preterm animals (N21% D28+7).

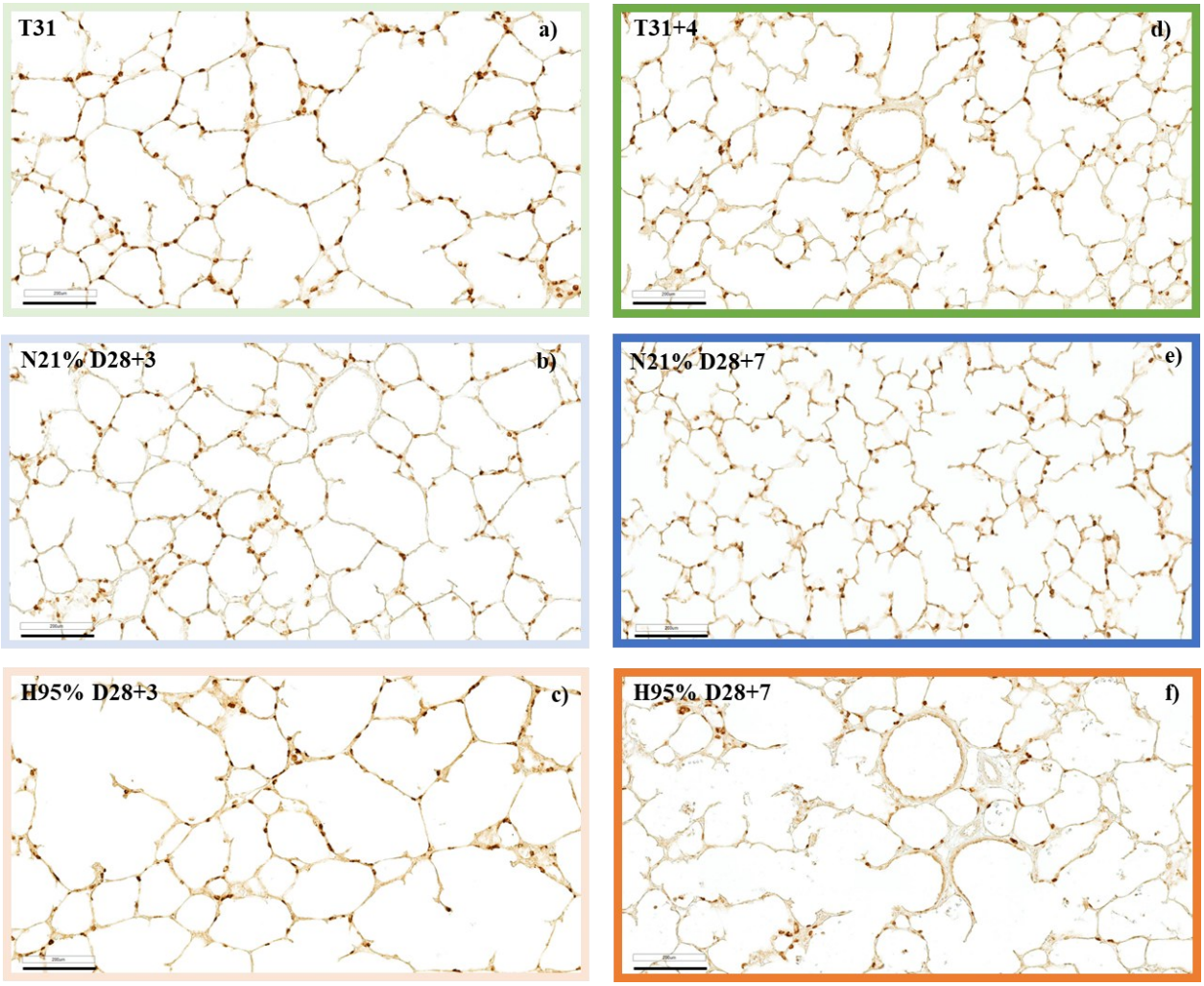

Figure 24. Representative pictures of pulmonary sections stained by IHC for SP-C. Immediately after sacrifice, the left lung of term and preterm pups was removed, fixed with formalin, and embedded in paraffin. Then, IHC for SP-C was performed as described in Materials and Methods. The experimental groups analyzed are: term pups (T31), preterm pups exposed to 21% O_2 for 3 days (N21% D28+3), preterm pups exposed to 95% O_2 for 3 days (H95% D28+3), term pups left with their mothers for 4 days (T31+4), preterm pups exposed to 21% O_2 for 7 days (N21% D28+7) and preterm pups exposed to 95% O_2 for 7 days (H95% D28+7) (scalebar black line, 200 µm; magnification: 10x). Positive reaction indicates the presence of AT II cells.

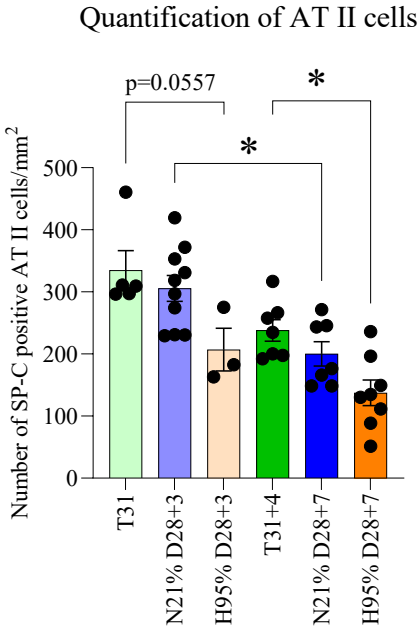

Figure 25. Quantification of AT II cells using Visiopharm® software in term pups (T31, light green bar, n=5), preterm pups exposed to 21% O_2 for 3 days (N21% D28+3, light blue bar, n=10) or to 95% O_2 for 3 days (H95% D28+3, light orange bar, n=3), term pups left with their mothers for 4 days (T31+4, green bar, n=7), preterm pups exposed to 21% O_2 for 7 days (N21% D28+7, blue bar, n=7) or to 95% O_2 for 7 days (H95% D28+7, orange bar, n=8). Data are presented as mean ± SEM and analyzed with one-way ANOVA, corrected for multiple comparisons: * $p < 0.05$.

4.4.2 IHC for α-SMA and measurement of pulmonary vascular medial thickness

The *tunica media* of blood vessels from pulmonary sections stained by IHC for α-SMA showed a positive reaction in all analyzed experimental groups (Figure 26), allowing for a precise measurement of its thickness using Visiopharm® software. Similar morphological features were observed in pulmonary sections from term and preterm pups exposed to normoxia at the two analyzed time-points (Figure 26). Automated quantification of pulmonary vascular medial thickness using Visiopharm® software confirmed these observations (Figure 27). Similarly, in preterm pups exposed to hyperoxia for three days (H95% D28+3), the thickness of α-SMA positive *tunica media* remained unchanged when compared to age-matched term controls (T31) and preterm normoxic animals (N21% D28+3) (Figure 27). In contrast, pulmonary sections from preterm pups exposed to hyperoxia for seven days (H95% D28+7) stained by IHC for α-SMA exhibited an evident thickening of *tunica media* in small blood vessels (Figure 26). These

observations were further confirmed by the automated quantitative analysis by Visiopharm® software, which demonstrated a not statistically significant increase in vascular medial thickness compared to H95% D28+3. However, a statistically significance increase was observed when compared to age-matched term controls (T31+4) and preterm normoxic animals (N21% D28+7) (Figure 27).

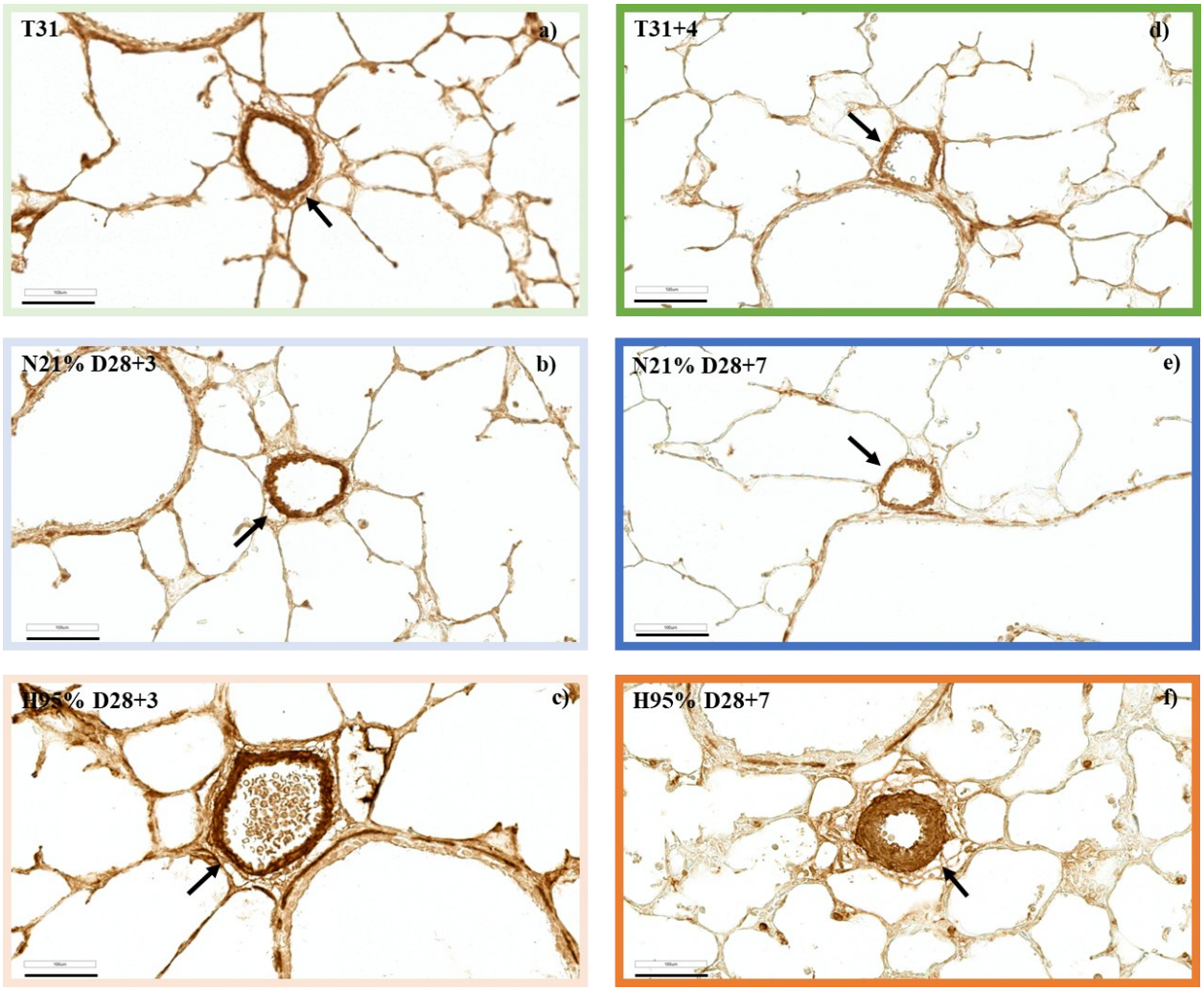

Figure 26. Representative pictures of pulmonary sections stained by IHC for α-SMA. Immediately after sacrifice, the left lung of term and preterm pups was removed, fixed with formalin, and embedded in paraffin. Then, IHC for α-SMA was performed as described in Materials and Methods. Positive staining indicates the *tunica media* of pulmonary blood vessels (with a major axis length between 30-100 µm). The experimental groups analyzed are: term pups (T31), preterm pups exposed to 21% O_2 for 3 days (N21% D28+3), preterm pups exposed to 95% O_2 for 3 days (H95% D28+3), term pups left with their mothers for 4 days (T31+4), preterm pups exposed to 21% O_2 for 7 days (N21% D28+7) and preterm pups exposed to 95% O_2 for 7 days (H95% D28+7) (scalebar black line, 100 µm; magnification: 20x). Black arrows indicate pulmonary blood vessels with a major axis length of 30-100 µm.

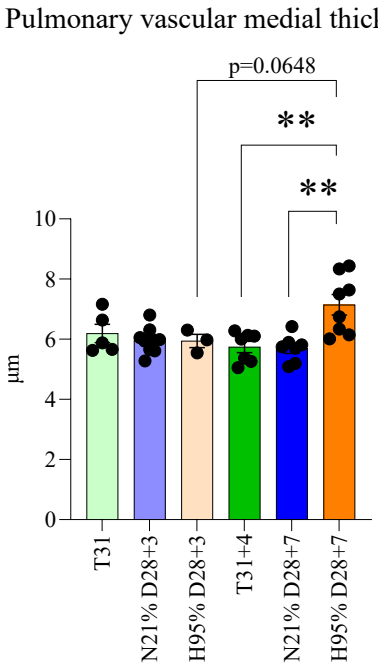

Figure 27. Measurement of pulmonary vascular medial thickness using Visiopharm® software in term pups (T31, light green bar, n=5), preterm pups exposed to 21% O_2 for 3 days (N21% D28+3, light blue bar, n=10) or to 95% O_2 for 3 days (H95% D28+3, light orange bar, n=3), in term pups left with their mothers for 4 days (T31+4, green bar, n=7), preterm pups exposed to 21% O_2 for 7 days (N21% D28+7, blue bar, n=7) or to 95% O_2 for 7 days (H95% D28+7, orange bar, n=8). Data are presented as mean ± SEM and analyzed with one-way ANOVA, corrected for multiple comparisons: * $p < 0.05$; ** $p \leq 0.01$.

4.5 qRT-PCR analysis

The mRNA expression levels of thrombospondin-1 (THBS-1), CD-34, ANGPT-1, and ANGPT-2 were assessed as factors involved in angiogenesis.

Term pups (T31) showed slightly increased THBS-1 mRNA expression level compared to preterm pups exposed to either normoxia (N21% D28+3) or hyperoxia (H95% D28+3) for three days (Figure 28a). However, in term pups maintained at room air with their mothers until postnatal day 4 (T31+4), mRNA expression of THBS-1 decreased, reaching levels comparable to those observed in preterm pups exposed to normoxia (N21% D28+7) (Figure 28a). At postnatal day 7, preterm pups exposed to hyperoxia (H95% D28+7) showed a statistically significant increase in mRNA expression level compared to T31+4 and N21%D28+7, as well as to H95% D28+3 (Figure 28a).

Similarly, in term pups (T31), a slight increase in CD-34 mRNA expression level was observed when compared to preterm pups exposed to either normoxia (N21% D28+3) or hyperoxia (H95% D28+3) for three days (Figure 28b). However, four days after natural delivery, term pups (T31+4) revealed a significantly decreased expression, reaching levels comparable to those seen in preterm pups exposed to normoxia for seven days (N21% D28+7) (Figure 28b). After seven days of postnatal hyperoxia exposure, preterm pups (H95% D28+7) showed a marked reduction in mRNA expression level compared to T31+4 and N21% D28+7 (Figure 28b).

At postnatal day 3, preterm pups exposed to either normoxia (N21% D28+3) or hyperoxia (H95% D28+3) exhibited significantly increased mRNA expression level of ANGPT-1 compared to their age-matched term controls (T31) (Figure 28c). In term pups, ANGPT-1 mRNA expression slightly increased over time. In contrast, in preterm pups, expression decreased between the two analyzed time-points, with a statistically significant reduction observed in both normoxic and hyperoxic animals (Figure 28c). Notably, at postnatal day 7, preterm pups exposed to hyperoxia (H95% D28+7) showed significantly lower mRNA expression level of ANGPT-1 compared to age-matched term controls (D31+4) and preterm pups exposed to normoxia (N21% D28+7) (Figure 28c).

In term and preterm pups exposed to normoxia, mRNA expression of ANGPT-2 remained unchanged between the two analyzed time-points (Figure 28d). However, after exposure to high oxygen levels, expression increased over time (Figure 28d). In particular, at postnatal day 7, in preterm pups exposed to hyperoxia (H95% D28+7), ANGPT-2 mRNA expression reached a significantly higher level compared to those observed in age-matched term controls (T31+4) and preterm pups exposed to normoxia (N21% D28+7) (Figure 28d).

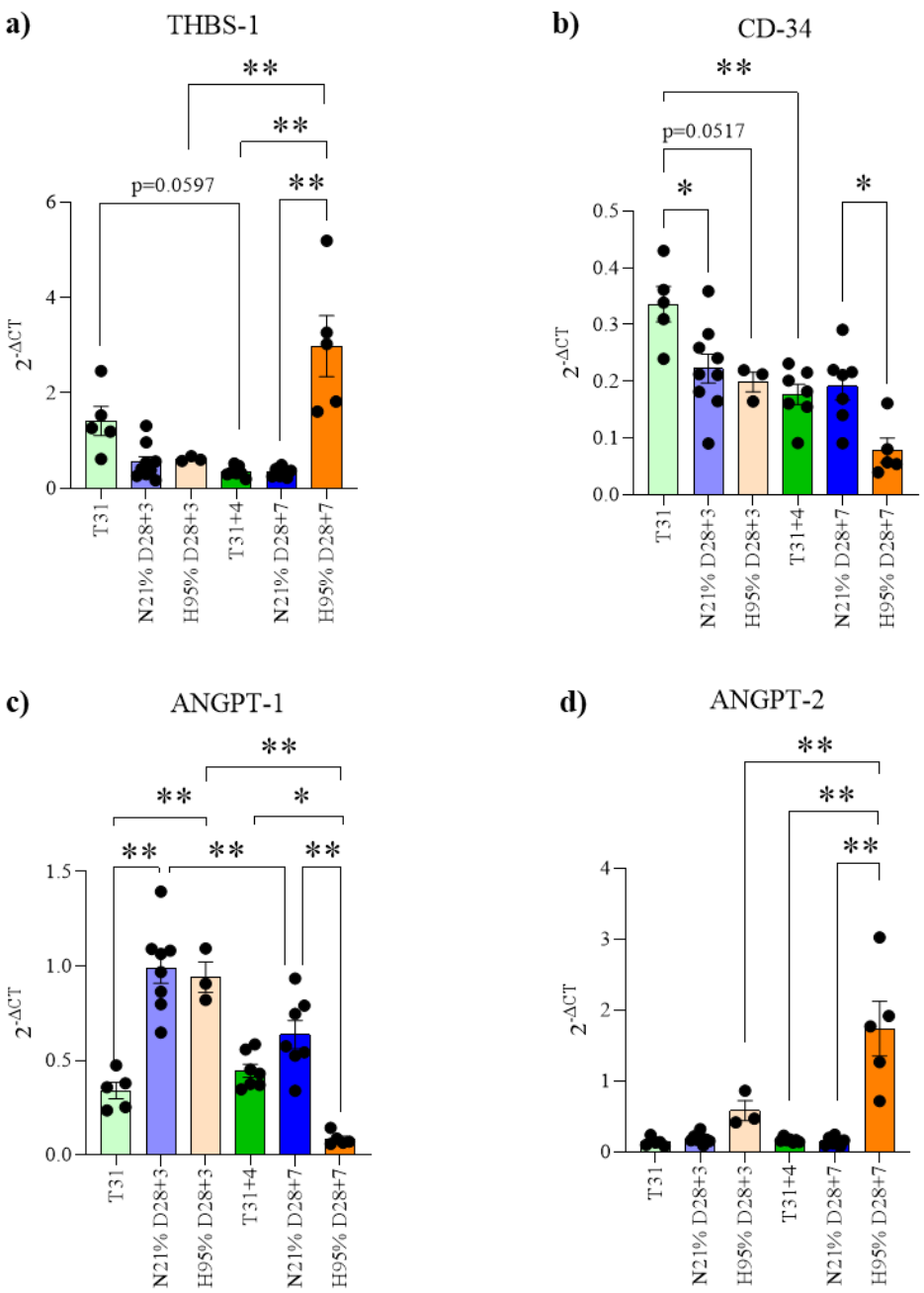

Figure 28. mRNA expression level of factors involved in angiogenesis. qRT-PCR analysis was performed in homogenates of right lung lobes as described in Materials and Methods. mRNA expression levels of the following genes were assessed: a) Thrombospondin-1 (THBS-1); b) CD-34; c) Angiopoietin-1 (ANGPT-1); d) Angiopoietin-2 (ANGPT-2). The experimental groups analyzed are: term pups (T31, light green bar, n=5), preterm pups exposed to 21% O_2 for 3 days (N21% D28+3, light blue bar, n=8) or to 95% O_2 for 3 days (H95% D28+3, light orange bar, n=3), term pups left with their mothers for 4 days (T31+4, green bar, n=7), preterm pups exposed to 21% O_2 for 7 days (N21% D28+7, blue bar, n=7) or to 95% O_2 for 7 days (H95% D28+7, orange bar, n=5). Relative changes in mRNA expression level were calculated according to the $2^{-\Delta\Delta Ct}$ method using mean values of ACTB and HPRT1 as reference genes. Data are presented as mean ± SEM and analyzed with one-way ANOVA, corrected for multiple comparisons: * $p < 0.05$; ** $p \leq 0.01$.

The mRNA expression level of IL-1β and interleukin-8 (CXCL-8) was evaluated as factors involved in inflammation.

At postnatal day 3, preterm pups exposed to either normoxia (N21% D28+3) or hyperoxia (H95% 28+3) showed higher mRNA expression levels of IL-1β and CXCL-8 compared to term age-matched controls (T31). However, this difference did not reach statistical significance (Fig. 29 a-b). In term pups, no difference in the expression of both inflammatory biomarkers was observed over time; whereas in preterm pups exposed to normoxia, mRNA expression decreased between the two analyzed time-points (Figure 29 a-b). However, at postnatal day 7, hyperoxia exposure induced a statistically significant increase in the mRNA expression of IL-1β and CXCL-8 compared to age-matched term controls (T31+4) and preterm pups exposed to normoxia (N21% D28+7) (Figure 29 a-b).

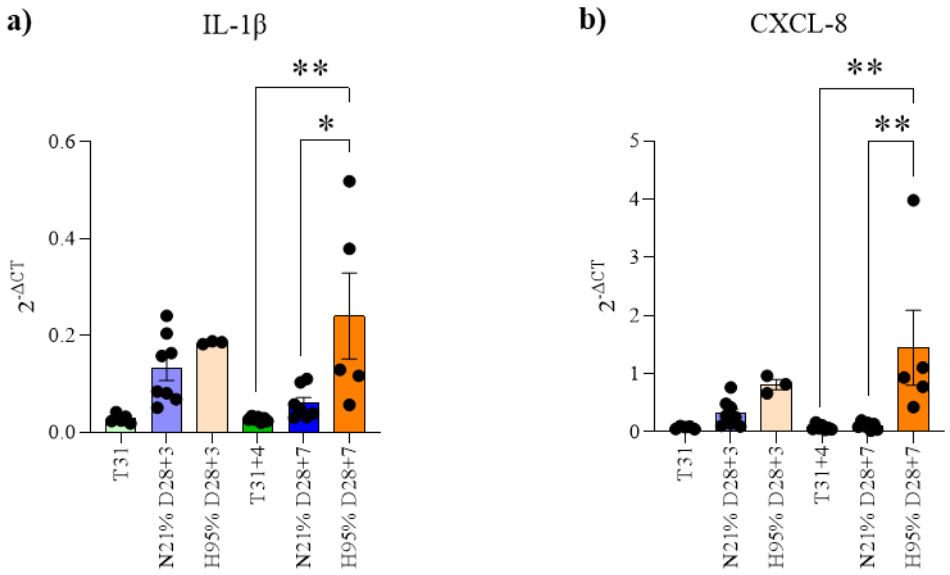

Figure 29. mRNA expression of factors involved in inflammation. qRT-PCR analysis was performed in homogenates of right lung lobes as described in Materials and Methods. mRNA expression levels of the following genes were assessed: a) Interleukin-1 β (IL-1β); b) Interleukin-8 (CXCL-8). The experimental groups analyzed are: term pups (T31, light green bar, n=5), preterm pups exposed to 21% O_2 for 3 days (N21% D28+3, light blue bar, n=8) or to 95% O_2 for 3 days (H95% D28+3, light orange bar, n=3), term pups left with their mothers for 4 days (T31+4, green bar, n=7), preterm pups exposed to 21% O_2 for 7 days (N21% D28+7, blue bar, n=7) or to 95% O_2 for 7 days (H95% D28+7, orange bar, n=5). Relative changes in mRNA expression levels were calculated according to the $2^{-\Delta\Delta Ct}$

method using mean values of ACTB and HPRT1 as reference genes. Data are presented as mean ± SEM and analyzed with one-way ANOVA, corrected for multiple comparisons: * $p < 0.05$; ** $p \leq 0.01$.

4.6 Summary table

		Experimental groups					
		T31	N21% D28+3	H95% D28+3	T31+4	N21% D28+7	H95% D28+7
Lung function measurements	IC	1.37±0.13	1.22±0.079	1.09±0.06	2.12±0.20§	1.74±0.12	0.73±0.12$^{+\ *}$
	Cst	0.12±0.01	0.10±0.01	0.07±0.01	0.21±0.03§	0.16±0.01$^{\#}$	0.05±0.01$^{+\ *}$
	G	2.10±0.20	2.42±0.22	3.10±0.32	1.40±0.12	1.67±0.10	3.75±0.58$^{+\ *}$
	H	8.33±0.87	8.19±0.60	11.06±0.48	5.06±0.55	5.54±0.39	16.72±2.94$^{+\ *}$
Manual morphometric analysis	MLI	72.34±3.54	78.20±2.04	89.12±1.69$^{+\ *}$	73.80±1.53	76.00±1.48	84.75±1.42^{+}
	Manual SCs count	0.24±0.01	0.24±0.01	0.21±0.01	0.23±0.01	0.23±0.01	0.16±0.01$^{+\ *}$
	RAC	7.42±0.25	7.70±0.21	7.16±0.20	8.14±0.23	8.81±0.45$^{\#}$	6.71±0.17$^{+\ *}$
	ALI score	0.10±0.02	0.08±0.01	0.16±0.01	0.09±0.001	0.09±0.01	0.31±0.03$^{£\ +\ *}$
Morphometric analysis using an AI-based software	Automated SCs count	224.20±10.59	216.70±6.05	184.00±1.01	231.00±6.52	247.00±12.84	164.30±9.82$^{+\ *}$
	ST	6.10±0.37	6.68±0.28	6.62±0.14	6.22±0.15	5.43±0.19$^{\#}$	8.71±0.37$^{£\ +\ *}$
	Quantification of AT II cells	334.90±31.55	305.60±20.69	207.00±34.51	238.00±17.29	200.10±19.57$^{\#}$	137.30±20.65^{+}
	Measurement of pulmonary vascular medial thickness	6.19±0.30	5.96±0.13	5.94±0.21	5.74±0.18	5.69±0.16	7.14±0.34$^{+\ *}$
qRT-PCR analysis	THBS-1	1.41±0.30	0.54±0.12	0.61±0.029	0.35±0.04	0.34±0.03	2.98±0.63$^{£\ +\ *}$
	CD-34	0.33±0.03	0.22±0.02$^{\$}$	0.19±0.01	0.17±0.01§	0.19±0.02	0.07±0.02*
	ANGPT-1	0.34±0.04	0.98±0.08$^{\$}$	0.94±0.08^{+}	0.44±0.03	0.63±0.07$^{\#}$	0.08±0.01$^{£\ +\ *}$
	ANGPT-2	0.14±0.02	0.19±0.02	0.58±0.14	0.16±0.01	0.15±0.02	1.74±0.38$^{£\ +\ *}$
	IL-1β	0.02±0.004	0.13±0.02	0.18±0.001	0.02±0.001	0.05±0.01	0.24±0.08$^{+\ *}$
	CXCL-8	0.07±0.01	0.31±0.08	0.81±0.08	0.07±0.01	0.10±0.02	1.44±0.64$^{+\ *}$

Table 2. Summary of findings from lung functions measurements, manual morphometric analysis, morphometric analysis using an AI-based software and qRT-PCR analysis. The experimental groups analyzed are: term pups (T31), preterm pups exposed to 21% O_2 for 3 days (N21% D28+3) or to 95% O_2 for 3 days (H95% D28+3), term pups left with their mothers for 4 days (T31+4), preterm pups exposed to 21% O_2 for 7 days (N21% D28+7) or to 95% O_2 for 7 days (H95% D28+7). Data are presented as mean ± SEM and analyzed with one-way ANOVA, corrected for multiple comparisons. $ $p < 0.05$ when term pups were compared to preterm pups exposed to normoxia; + $p < 0.05$ when term pups were compared to preterm pups exposed to hyperoxia; * $p < 0.05$ when preterm pups exposed to normoxia were compared to preterm pups exposed to hyperoxia; § $p < 0.05$ when T31 were compared with T31+4; # $p < 0.05$ when D28+3 were compared with D28+7; £ $p < 0.05$ when H95% D28+3 were compared with H95% D28+7.

5. Discussion

Although recent advances in neonatal intensive care have improved outcomes, BPD remains the most common chronic respiratory disease of preterm babies [31], with lifelong respiratory sequelae and a global incidence among this population ranging from 10 to 89% [37]. The development of BPD involves a complex and multifactorial pathogenesis, driven by a combination of both pre- and postnatal risk factors [38]. The resulting lung injury impairs both alveolar and vascular growth, leading to a characteristic pattern of abnormal lung development [68], [152], [153]. Given that the pathogenic mechanisms contributing to the development of the disease are not yet fully elucidated, a deeper understanding is crucial for developing effective prevention and treatment strategies for this common respiratory condition among preterm infants.

However, research on BPD is constrained by the limited availability of human samples. Fortunately, most infants with BPD survive, but this makes it ethically unfeasible to perform invasive procedures to obtain lung tissue for research during critical stages of development. Moreover, post-mortem material has become increasingly rare and difficult to obtain [120].

For this reason, several animal models, including both small and large species, have been developed to investigate the pathogenesis of BPD and to evaluate potential therapeutic interventions. Among these, the preterm rabbit model has emerged as a particularly relevant tool, as it more closely resembles the functional and structural development of the human lung compared to small animal species [121]. Moreover, the possibility of inducing prematurity, the most common risk factor for BPD, allowed us to show the translational advantage of using preterm rabbit pups for preclinical research. However, several key features of this animal model have yet to be fully characterized. Thus, to address this gap, this study aimed to evaluate the impact of preterm birth alone and in combination with hyperoxia exposure on postnatal lung development, integrating functional, histological and biomolecular outcomes and using an innovative AI-based software for morphometric analyses. Through this integrative approach, this

study provided a comprehensive characterization of the preterm rabbit model of BPD exposed to hyperoxia.

In our study, preterm pups delivered by C-section on gestational day 28 were randomized to hyperoxia (95% O_2) or normoxia (21% O_2) for three or seven days. Additional experimental groups, consisting of age-matched term born pups, were included as physiological controls of postnatal lung development. At the end of each experimental period, lung function measurements were performed using the flexiVent^{TM} system to correlate structural changes with respiratory mechanics.

Consistent with findings by Richter *et al.* [133], our data demonstrated that prolonged exposure to high oxygen levels for seven days resulted in significantly impaired lung function. However, even in the absence of hyperoxia exposure, lung function appears compromised in preterm animals. Salaets *et al.* [130] showed that preterm birth alone, without any additional postnatal insult, leads to significantly reduced lung function in rabbit pups compared to age-matched term controls. Similarly, in our study, preterm pups maintained under normoxic conditions exhibited decreased inspiratory capacity and static compliance when compared to age-matched term controls. However, these differences did not reach statistical significance (Figure 14 a-b). These findings underscore the intrinsic vulnerability of the preterm lung and highlight the ability of this model to reproduce early respiratory dysfunction widely observed in human preterm infants [151]. Moreover, a gradual functional increase was observed in term and preterm pups exposed to normoxia over time, most probably reflecting ongoing postnatal lung maturation. These data further support the translational value of the preterm rabbit model, as it not only successfully mimics the functional impairments following preterm birth and hyperoxia exposure but also the progressive improvement of lung function that occurs during the early postnatal period.

In addition to lung function measurements, this study provided a detailed histological characterization of the preterm rabbit model of BPD exposed to hyperoxia that further extends

scientific evidence currently available in the literature. Previous studies have demonstrated that this animal model successfully recapitulates the main pathological features of the human disease, including impaired lung function, arrested alveolarization, altered extracellular matrix composition, and vascular abnormalities [131], [133], [154]. Although these studies have significantly contributed to the understanding of the pathogenetic mechanisms, conventional morphometric techniques were applied. The traditional approach, based on manual morphometric analysis, is well established in scientific literature and allows a direct interpretation of structural alterations. However, it is time-consuming and could be operator-dependent, significantly limiting reliability and reproducibility of data across different studies. To overcome these limitations, in this study the use of Visiopharm® software was implemented. It allowed us to perform faster and more accurate morphometric analyses, thus minimizing observer bias and variability. Moreover, the identification of subtle structural alterations, that could remain undetected by a human observer, represents another advantage of the automated quantitative analysis when compared to the conventional approach. Nevertheless, the development of an app using the DL-based classification method requires a training phase and a large, well-annotated and high-quality input dataset. This initial phase could be time-consuming, but it is essential to properly train the algorithm to detect the structures of interest. The adoption of an AI-based software, such as Visiopharm®, for histological analyses in preclinical models of BPD is still largely unexplored. Therefore, the approach used in this study, integrating conventional morphometric techniques with automated quantitative analyses, represents an innovative step forward, highlighting the potential of AI as a promising tool to improve accuracy and reproducibility of histological analyses in preclinical research area.

Morphologically, we observed that preterm pups exposed to hyperoxia for three days exhibited structural abnormalities, which became more pronounced after seven days of exposure, indicating a progressive worsening of oxygen-induced lung injury. These morphological changes included

enlarged airspaces, simplified alveoli, thickened alveolar septa, infiltration of inflammatory cells, and accumulation of proteinaceous debris, hallmarks consistent with the histopathological features of the "new" BPD described in human preterm infants [69], [152].

Among the extracellular matrix components primarily affected by hyperoxia exposure, elastic fibers appear to be particularly vulnerable. These fibers, essential for maintaining lung elasticity and supporting alveolar recoil, are composed of a core of elastin, a highly insoluble and cross-linked protein, surrounded by a scaffold of microfibrillar glycoproteins that ensure their structural integrity and guide fiber assembly [155]. Alterations in elastin deposition during critical stages of lung development can severely disrupt pulmonary architecture and respiratory mechanics [155]. In this context, Bruce *et al.* demonstrated that postnatal exposure to hyperoxia in developing rat lungs leads to fragmented, disorganized fibers and reduces elastin content per lung [156]. Although the precise mechanisms responsible for these changes remain incompletely understood, proteolytic damage secondary to inflammation is thought to play a critical role. Supporting this hypothesis, the same group reported altered urinary excretion of elastin cross-links in premature infants who subsequently developed BPD, indicating increased elastin degradation during the early postnatal period [157]. In addition to increased elastase activity, hyperoxia has also been shown to impair elastin cross-linking, further contributing to the accumulation of structurally immature and disorganized fibers [158].

Here, we did not quantify elastin content per lung; however, morphological analysis showed similar alterations in elastic fiber organization after postnatal exposure to high oxygen levels. Specifically, preterm pups exposed to hyperoxia for three days exhibited disorganized elastic fibers within the alveolar walls (Figure 17c). These morphological abnormalities became more pronounced after seven days of exposure, with the presence of fragmented, thickened, and tortuous fibers (Figure 17f). These findings are in line with the work of Mascaretti *et al.*, who reported an evident elastic fiber disorganization in preterm rabbit lungs following hyperoxia

exposure [131]. They observed a disruption in fiber distribution within the alveolar walls and secondary septa, suggesting that hyperoxia interferes with the elastin deposition and maturation that occurs during postnatal lung development.

Even in the absence of hyperoxia, our results indicated a degree of elastic fiber immaturity. Preterm pups exposed to normoxia for three days and their age-matched term controls exhibited fragmented elastic fibers within the alveolar septa (Figure 17 a-b). However, as lung development progresses, increasing structural complexity and improved elastic fiber organization were observed (Figure 17 d-e), supporting the role of postnatal lung maturation in proper fiber assembly. Ultrastructural observations further confirmed this, showing clusters of immature elastin at the tips of alveolar septa (Figure 19). These results suggest that elastic fibers undergo progressive maturation after birth and that hyperoxia can significantly disrupt this process, leading to impaired alveolarization, with fewer and larger alveoli.

Manual morphometric analyses confirmed that postnatal exposure to hyperoxia leads to airspaces enlargement, impaired secondary septation and arrested alveolar development, as demonstrated by a significant increase in MLI (Figure 22a), along with a reduction in SCs count (Figure 22b) and RAC (Figure 22c). Moreover, a significantly increased ALI score was observed, consistent with persistent pulmonary inflammation and tissue damage.

To further investigate the inflammatory response contributing to these structural abnormalities, we analyzed the mRNA expression levels of IL-1β and CXCL-8, two key pro-inflammatory cytokines. At postnatal day 3, the mRNA expression of both genes was increased in preterm pups, without reaching statistical significance (Figure 29a-b). These findings are consistent with the transcriptomic analysis by Storti *et al.*, who demonstrated that preterm birth alone significantly alters pulmonary gene expression, leading to the early activation of the inflammatory pathway that persists until the first postnatal week [159]. Over time, we observed a progressive decline in mRNA expression levels of IL-1β and CXCL-8 under normoxic conditions, but they were

significantly upregulated after seven days of hyperoxia exposure (Figure 29a-b). These data are supported by the longitudinal transcriptomic analysis of Boggi *et al.*, confirming the sustained activation of several pro-inflammatory pathways and genes in hyperoxia-exposed preterm rabbit pups [160].

Visiopharm® software was employed for the quantification of SCs and for the measurement of ST. This analysis confirmed the significant decrease in SCs count observed using conventional morphometric techniques (Figure 23a) and showed an increase in ST (Figure 23b), further supporting disrupted secondary septation and indicating a fibrotic response to postnatal hyperoxia exposure. Moreover, a progressive decline in ST was observed over time in preterm pups exposed to normoxia (Figure 23b), suggesting that structural alveolar maturation continues during postnatal period.

Our findings demonstrated that exposure to high oxygen levels in preterm rabbit pups led to early and progressive structural alterations, as previously described by Jiménez *et al.* [154]. Their work emphasized the time-dependent detrimental effect of hyperoxia on postnatal lung development, highlighting how prolonged oxygen exposure disrupts alveolarization and microvascular growth, ultimately leading to a BPD-like phenotype. They also observed that preterm pups maintained under normoxic conditions exhibited a progressive increase in RAC over time [154], reflecting ongoing alveolar development and increasing structural complexity. This result is consistent with our morphometric data (Figure 22c) and further underscores the impact of hyperoxia exposure on the impairment of postnatal lung maturation.

The structural abnormalities observed in our study closely paralleled the progressive decline in lung function, thus establishing a direct association between impaired lung architecture and compromised respiratory mechanics. Particularly, increased MLI, decreased count of SCs and RAC, along with disrupted elastic fiber organization observed after hyperoxia exposure, are consistent with altered gas exchange capacity. Moreover, increased ALI score and thickened

alveolar septa are known to adversely affect the mechanical properties of the lung tissue. These morphometric alterations are strongly correlated with the functional deficits observed in hyperoxia-exposed pups. In contrast, preterm pups exposed to normoxia, as well as their age-matched term controls, exhibited gradual improvement in lung function over time, which was accompanied by a greater complexity of elastic fiber architecture, a progressive increase in RAC and a decrease in ST, reflecting ongoing postnatal lung maturation. However, although preterm pups showed a slight reduction in lung function when compared to age-matched term controls, these functional differences were not accompanied by significant morphological changes.

Additionally, to better understand the cellular mechanisms contributing to the functional impairment and the structural abnormalities observed in our experimental model, particular attention was paid to AT II cells. These cells are not only responsible for the synthesis and secretion of pulmonary surfactant, essential for reducing surface tension and preventing alveolar collapse, but they also play a critical role in maintaining alveolar structure [5]. In our study, AT II cells were detected by IHC using SP-C as a specific marker, and cell density was automatically quantified by dividing the number of SP-C positive cells by the total section area expressed in mm^2.

We observed a progressive decline in AT II cell density in term and preterm pups exposed to normoxia between the two analyzed time-points, reaching the statistical significance in the normoxic experimental group (Figure 25). These findings are in line with a previous work by Randell *et al.*, who demonstrated that in the developing rat lungs, the number of AT II cells was higher at birth and subsequently declined during the first postnatal week, remaining at a constant level until the adult life [161]. This decrease has been hypothesized to result either from an inhibition of AT II cells production during the perinatal period or from postnatal lung maturation, involving the differentiation of these cells into AT I cells to support the increasing need for an efficient gas exchange [161].

However, it was demonstrated that AT II cells are critical targets of hyperoxia-induced impairment of postnatal lung development [162]. In our study, preterm pups exposed to hyperoxia for three days exhibited a reduced density of SP-C positive AT II cells, and this reduction became significantly more pronounced after seven days of hyperoxia (Figure 25). These results suggest that postnatal exposure to high oxygen levels exacerbates the decline in AT II cell number, potentially through multiple mechanisms, including OS-induced cellular injury, apoptosis, inhibited proliferation, and disrupted differentiation. Supporting this, recent studies have demonstrated that hyperoxia not only induces apoptosis and inhibits proliferation of AT II cells [163], but also stimulates their transdifferentiation into AT I cells [164]. Although it represents an adaptive mechanism aimed at maintaining alveolar structure integrity, this compensatory response appeared to be structurally and functionally inefficient [164]. Therefore, despite the initial attempt to preserve alveolar architecture, the loss of AT II cells likely contributes to persistent respiratory dysfunction. This was further reinforced by Vaughan *et al.*, who highlighted the essential role of AT II cells in alveolar maintenance and proposed that their depletion in early life could predispose individuals to chronic lung disease in adulthood [165].

Moreover, in preterm pups exposed to hyperoxia for seven days, we observed that AT II cells were heterogeneously distributed within the alveolar epithelium, showing a higher density in the peribronchial and perivascular regions (Figure 24f). We speculated that this altered spatial distribution could represent an adaptive mechanism aimed at preserving the AT II cells population within specific pulmonary areas that could be more resistant to the oxygen-induced lung injury.

In line with ultrastructural findings reported by Hou *et al.* [164], our analysis by TEM also revealed functionally injured AT II cells in preterm pups exposed to hyperoxia, characterized by a reduced number of mature AT II cells containing lamellar bodies (Figure 18c). However, these results must be interpreted cautiously, as ultrastructural analysis was conducted on a single lung sample per experimental condition and was limited to the latest time-point investigated.

Moreover, no quantitative analysis was performed on samples processed for TEM; therefore, the number of mature AT II cells was semi-quantitatively assessed. Further studies including larger sample size, multiple developmental time-points and quantitative analysis are needed to confirm these observations. Nevertheless, these findings support the idea that AT II cells are critical targets of oxygen-induced injury. The observed decrease in AT II cell density, their altered spatial distribution, and reduction in mature AT II cells containing lamellar bodies represent significant structural abnormalities that can contribute to the pathogenesis of BPD by disrupting alveolar integrity, compromising surfactant production, and ultimately leading to impaired lung function.

As extensively reported in scientific literature, the "new" BPD is characterized by arrested alveolarization and impaired pulmonary vascular growth [68], [69], [152], resulting in a reduced surface area for gas exchange in the developing lung. Under physiological conditions, vascular development is finely regulated by a balance between pro- and anti-angiogenic factors. Given that disrupted vascular growth is a key pathological mechanism contributing to the development of BPD [75], we analyzed the mRNA expression level of factors involved in the angiogenic signaling pathway.

We firstly assessed the expression of THBS-1, encoding thrombospondin-1, an anti-angiogenic and pro-fibrotic protein with a well-known pathogenic role in experimental and human BPD [166]. It showed a slight early upregulation in term pups but declined over time (Figure 28a), reaching levels comparable to those observed in the normoxic experimental group. It has been hypothesized that this temporal downregulation could reflect the normal postnatal lung development. However, after seven days of hyperoxia exposure, mRNA expression level of THBS-1 was significantly increased (Figure 28a), consistent with findings by De Paepe *et al.*, who reported a significant upregulation of anti-angiogenic factors, including THBS-1, in lung samples from short-ventilated preterm infants [167].

In addition to THBS-1, we also analyzed the mRNA expression level of CD-34, a transmembrane glycoprotein expressed on hematopoietic stem cells and vascular endothelial cells [168]. CD34+ precursors derived from cord blood have been shown to differentiate into endothelial cells in response to angiogenic stimuli, such as angiopoietins [169], highlighting their functional relevance in vascular development. In our study, at postnatal day 3, preterm pups exhibited a significantly lower mRNA expression level of CD-34 when compared to age-matched term controls (Figure 28b), indicating impaired endothelial precursor recruitment. Moreover, while in term pups a physiological downregulation of mRNA expression level was observed, in preterm pups CD-34 mRNA remained low and was even more reduced after postnatal hyperoxia exposure for seven days (Figure 28b), suggesting that hyperoxia could also contribute to disrupted vascular growth through impaired recruitment of endothelial cell precursors.

In the context of the Ang-Tie signaling pathway, which plays an essential role in vascular maturation, remodeling, and stability [18], we analyzed mRNA expression levels of ANGPT-1 and ANGPT-2. At postnatal day 3, in preterm pups, ANGPT-1 mRNA was significantly higher compared to age-matched term controls (Figure 28c), possibly reflecting a compensatory mechanism aimed at promoting vascular maturation and stabilization in the developing lungs of preterm animals. However, it declined over time and was further reduced after seven days of hyperoxia exposure (Figure 28c). In contrast, ANGPT-2, a context-dependent antagonist of ANGPT-1 that promotes vascular destabilization [20] and inflammation [22], showed a significant upregulation in preterm pups exposed to hyperoxia for seven days (Figure 28d). The opposing expression pattern of ANGPT-1 and ANGPT-2 observed under hyperoxic conditions indicates a dysregulated Ang-Tie signaling pathway, which may contribute to impaired vascular maturation and endothelial destabilization. This imbalance leads to increased vascular permeability, promoting inflammatory cell infiltration and exacerbating acute lung injury, which plays a critical role in the pathogenesis of BPD.

Previous studies have hypothesized that impaired angiogenesis and arrested lung growth could reduce the cross-sectional area of the pulmonary vasculature, promoting the development of PH in preterm infants [89]. This condition is associated with vascular structural alterations, such as SMC proliferation and medial thickening, contributing to increased pulmonary vascular resistance and arterial pressure [89]. In the context of hypertension, these morphological changes involve a complex interplay of mechanisms such as endothelial dysfunction, inflammation, OS, and upregulation of growth factors promoting extracellular matrix deposition and SMC proliferation [170].

Consistent with findings by Jiménez et al. [154], we also observed a significant vascular remodeling after seven days of hyperoxia exposure. It was further confirmed by a previous work, which demonstrated that, in an experimental model of PH, prolonged exposure to hyperoxia induces a selective reorganization of non-muscular segments of the pulmonary microvasculature, promoting the development of a contractile phenotype [171]. To quantitatively assess structural vascular changes, in our study, SMCs in the *tunica media* of small pulmonary blood vessels were identified by IHC using α-SMA as a specific marker. Automated quantitative analysis using Visiopharm® software showed a statistically significant increase in the thickness of the *tunica media* in preterm pups exposed to hyperoxia for seven days (Figure 27). This effect was particularly evident in the pulmonary microvasculature (blood vessels with a major axis length of 30-100 μm) (Figure 26).

Ultrastructural analysis by TEM provided a more detailed characterization of structural abnormalities within the *tunica media* induced by postnatal hyperoxia exposure. Specifically, SMCs appeared spatially disorganized and morphologically heterogeneous, while the extracellular matrix was significantly reduced, with the elastic component fragmented and arranged into small, discontinuous fibers (Figure 20c).

We also observed ultrastructural alterations within the internal elastic lamina of pulmonary blood vessels, a key component separating the *tunica intima* from the *tunica media* and contributing to the elastic properties of the vessel wall. In preterm pups exposed to hyperoxia for seven days, the internal elastic lamina exhibited variable thickness and was characterized by numerous "elastin clumps" surrounded by abundant microfibrillar component (Figure 21c). These results highlighted that postnatal exposure to hyperoxia induces significant vascular alterations, as evidenced by increased thickness of the *tunica media*, SMCs disorganization, and disrupted maturation of the extracellular matrix components. Particularly, we hypothesized that the abnormal arrangement and fragmentation of elastic fibers observed within the *tunica media* and the internal elastic lamina indicate impaired elastin synthesis and assembly, contributing to increased vascular stiffness and reduced elasticity. Consistent with this hypothesis, Wagenseil *et al.* showed that elastin is organized into elastic fibers in the vascular wall during arterial development through a complex process involving the coordinated action of different proteins [172]. Thus, any alterations in elastin content, synthesis, and assembly during this critical developmental period can result in persistent changes, including increased arterial stiffness and a higher risk of developing hypertension. In the context of BPD, disrupted elastic fiber deposition in the vascular wall induced by early postnatal exposure to hyperoxia could represent a key pathogenetic mechanism contributing to the development of long-term pulmonary vascular dysfunction.

6. Conclusions and limitations

In conclusion, the integrative approach used in this study has allowed us to delineate a comprehensive characterization of the preterm rabbit model of BPD exposed to hyperoxia. Our findings demonstrated that preterm birth alone, without any additional insult, was associated with intrinsically impaired lung function, that was further exacerbated by postnatal exposure to hyperoxia. Preterm pups exposed to hyperoxia showed all the main structural abnormalities characteristic of the human disease, that were confirmed by both conventional morphometric techniques and automated quantitative analysis using Visiopharm® software. Moreover, after postnatal exposure to hyperoxia a significant reduction in AT II cell density and thickening of *tunica media* of small pulmonary blood vessels were observed. These results were subsequently supported by ultrastructural analysis, showing morphological alterations in the vascular wall, as well as a reduction in mature AT II cell number. At the biomolecular level, an imbalance of angiogenesis-regulating genes favoring anti-angiogenic factors was observed in preterm pups exposed to hyperoxia. Moreover, preterm birth alone was associated with an upregulation of pro-inflammatory cytokines, that was further worsened by postnatal exposure to hyperoxia.

Collectively, these findings demonstrated that hyperoxia exposure exacerbates the developmental immaturity of the preterm lungs, leading to functional, structural and biomolecular changes characteristic of the human BPD. Therefore, this study has provided relevant insights into the effects of preterm birth alone and in combination with hyperoxia exposure on postnatal lung development, thus advancing our understanding of the pathogenetic mechanisms contributing to the development of the disease and supporting the translational relevance of this animal model for preclinical studies of BPD.

However, the present study has some limitations. First, the restricted availability of rabbit-specific antibodies and reagents represented a significant challenge, particularly for IHC, limiting our ability to perform a more detailed investigation of the structural abnormalities observed. In our

study, preterm pups were exposed to high levels of oxygen (95% O_2), which are no longer routinely applied in NICUs. Considering the chronic nature of BPD, the relatively short experimental time did not allow us to adequately investigate pathogenetic mechanisms contributing to the progression of the disease. Although postnatal exposure to hyperoxia successfully mimics the main pathological features of the human BPD, it does not adequately replicate the complex and multifactorial etiology of the disease. Therefore, future studies should aim to refine the preterm rabbit model by combining hyperoxia with additional injurious stimuli and by extending the experimental period. These advancements would further enhance the translational relevance of this animal model, allowing it to more accurately reproduce the clinical scenario. Another limitation is that the ultrastructural analysis by TEM was performed on a single lung sample per group and was limited to the latest time-point investigated. The tissue processing requirement for TEM precluded the possibility of integrating ultrastructural data with functional, histological, and biomolecular findings from the same experimental subject. Future studies should aim to increase the sample size and include the earlier time-point, which was not investigated by ultrastructural analysis in the present study.

Lastly, the implementation of Visiopharm® software for histological analysis represents an innovative step forward in preclinical research on BPD. This promising tool allows for a faster and more reproducible quantitative assessment of lung structure, minimizing observer bias and variability. In our study, the algorithm was trained to properly detect the structures of interest on pulmonary sections from different experimental conditions and the training dataset was continuously refined for each application. Nevertheless, its accuracy is strictly dependent on sample processing, quality of tissue staining, image acquisition and manual annotation during the training phase. Therefore, further validation steps are needed to ensure the robustness of data so that Visiopharm® software could be widely employed for histological analysis in preclinical studies of BPD. Moreover, given that pulmonary inflammation and impaired vascular growth are

key pathological features of the human and experimental disease, future studies should aim to implement Visiopharm® software to better characterize inflammatory cell populations using specific immunohistochemical markers and to automatically count pulmonary blood vessels number. These advancements would provide a more comprehensive understanding of cellular and structural mechanisms contributing to the pathogenesis of BPD.

References

[1] J. C. Schittny, “Development of the lung,” 2017. doi: 10.1007/s00441-016-2545-0.

[2] D. Warburton *et al.*, “Lung organogenesis,” no. C, 2010. doi: 10.1016/S0070-2153(10)90003-3.

[3] J. Pereda, L. Sulz, S. San Martin, and C. Godoy-Guzmán, “The human lung during the embryonic period: vasculogenesis and primitive erythroblasts circulation,” 2013, doi: 10.1111/joa.12042.

[4] H. Kitaoka, P. H. Burri, and E. R. Weibel, “Development of the human fetal airway tree: analysis of the numerical density of airway endtips,” 1996, doi: 10.1002/(SICI)1097-0185(199602)244:2<207::AID-AR8>3.0.CO;2-Y.

[5] R. J. Mason, “Biology of alveolar type II cells,” 2006. doi: 10.1111/j.1440-1843.2006.00800.x.

[6] P. H. Burri, “Fetal and postnatal development of the lung,” 1984. doi: 10.1146/annurev.ph.46.030184.003153.

[7] P. H. Burri, J. Dbaly, and E. R. Weibel, “The postnatal growth of the rat lung. 1. Morphometry,” 1973. doi: 10.1002/ar.1091780405.

[8] P. H. Burri, “The postnatal growth of the rat lung. 3. Morphology,” 1974. doi: 10.1002/ar.1091800109.

[9] J. Kovar, P. D. Sly, and K. E. Willet, “Postnatal alveolar development of the rabbit,” 2002, doi: 10.1152/japplphysiol.01044.2001.-Previous.

[10] P. H. Burri, “Structural aspects of postnatal lung development - Alveolar formation and growth,” 2006. doi: 10.1159/000092868.

[11] A. L. Rippa, E. V. Alpeeva, A. V. Vasiliev, and E. A. Vorotelyak, “Alveologenesis: what governs secondary septa formation,” 2021. doi: 10.3390/ijms222212107.

[12] H. Boström *et al.*, “PDGF-A signaling is a critical event in lung alveolar myofibroblast development and alveogenesis,” 1996. doi: 10.1016/s0092-8674(00)81270-2.

[13] S. A. Tschanz, L. A. Salm, M. Roth-Kleiner, S. F. Barré, P. H. Burri, and J. C. Schittny, “Rat lungs show a biphasic formation of new alveoli during postnatal development,” 2014, doi: 10.1152/japplphysiol.01355.2013.-Roughly.

[14] A. Hislop, “Developmental biology of the pulmonary circulation,” 2005. doi: 10.1016/j.prrv.2004.11.009.

[15] Ferrara N., H. P. Gerber, and J. LeCouter, “The biology of VEGF and its receptors,” 2003. doi: 10.1038/nm0603-669.

[16] P. Carmeliet *et al.*, “Abnormal blood vessel development and lethality in embryos lacking a single VEGF allele,” 1996, doi: 10.1038/380435a0.

[17] N. Ferrara *et al.*, “Heterozygous embryonic lethality induced by targeted inactivation of the VEGF gene,” 1996, doi: 10.1038/380439a0.

[18] H. G. Augustin, G. Young Koh, G. Thurston, and K. Alitalo, “Control of vascular morphogenesis and homeostasis through the angiopoietin - Tie system,” 2009. doi: 10.1038/nrm2639.

[19] C. Suri *et al.*, “Requisite role of angiopoietin-1, a ligand for the TIE2 receptor, during embryonic angiogenesis,” 1996, doi: 10.1016/S0092-8674(00)81813-9.

[20] M. Scharpfenecker, U. Fiedler, Y. Reiss, and H. G. Augustin, “The Tie-2 ligand angiopoietin-2 destabilizes quiescent endothelium through an internal autocrine loop mechanism,” 2005, doi: 10.1242/jcs.01653.

[21] I. B. Lobov, P. C. Brooks, and R. A. Lang, “Angiopoietin-2 displays VEGF-dependent modulation of capillary structure and endothelial cell survival in vivo,” 2002. doi: 10.1073/pnas.172161899.

[22] U. Fiedler *et al.*, “Angiopoietin-2 sensitizes endothelial cells to TNF-α and has a crucial role in the induction of inflammation,” 2006, doi: 10.1038/nm1351.

[23] World Health Organization, “Preterm birth.” Accessed: May 12, 2025. [Online]. Available: https://www.who.int/news-room/fact-sheets/detail/preterm-birth/

[24] J. Perin *et al.*, “Global, regional, and national causes of under-5 mortality in 2000–19: an updated systematic analysis with implications for the Sustainable Development Goals,” 2022, doi: 10.1016/S2352-4642(21)00311-4.

[25] E. O. Ohuma *et al.*, “National, regional, and global estimates of preterm birth in 2020, with trends from 2010: a systematic analysis,” 2023, doi: 10.1016/S0140-6736(23)00878-4.

[26] R. L. Goldenberg, J. F. Culhane, J. D. Iams, and R. Romero, “Epidemiology and causes of preterm birth,” 2008. doi: 10.1016/S0140-6736(08)60074-4.

[27] R. A. Mahmoud, C. C. Roehr, and G. Schmalisch, “Current methods of non-invasive ventilatory support for neonates,” 2011. doi: 10.1016/j.prrv.2010.12.001.

[28] R. M. DiBlasi, “Nasal Continuous Positive Airway Pressure (CPAP) for the respiratory care of the newborn infant,” 2009. [Online]. Available: www.liebertpub.com

[29] E. Herting, C. Härtel, and W. Göpel, “Less invasive surfactant administration (LISA): Chances and limitations,” 2019. doi: 10.1136/archdischild-2018-316557.

[30] C. S. M. Lau, R. S. Chamberlain, and S. Sun, “Less Invasive Surfactant Administration Reduces the Need for Mechanical Ventilation in Preterm Infants: A Meta-Analysis,” 2017, doi: 10.1177/2333794X17696683.

[31] B. Thébaud *et al.*, “Bronchopulmonary dysplasia,” 2019. doi: 10.1038/s41572-019-0127-7.

[32] M. Gilfillan, A. Bhandari, and V. Bhandari, “Diagnosis and management of bronchopulmonary dysplasia,” 2021. doi: 10.1136/bmj.n1974.

[33] W. H. Northway Jr., R. C. Rosan, and D. Y. Porter, “Pulmonary disease following respirator therapy of hyaline-membrane dysease,” 1967, doi: 10.1056/NEJM196702162760701.

[34] A. T. Shennan, M. S. Dunn, A. Ohisson, K. Lennox, and E. M. Hoskins, “Abnormal pulmonary outcomes in premature infants: prediction from oxygen requirement in the neonatal period,” 1988. [Online]. Available: http://publications.aap.org/pediatrics/article-pdf/82/4/527/1037169/527.pdf

[35] A. H. Jobe and E. Bancalari, “Bronchopulmonary dysplasia,” 2001. doi: 10.1164/ajrccm.163.7.2011060.

[36] J. Ibrahim and V. Bhandari, “The definition of bronchopulmonary dysplasia: an evolving dilemma,” 2018. doi: 10.1038/s41390-018-0167-9.

[37] C. Siffel, K. D. Kistler, J. F. M. Lewis, and S. P. Sarda, “Global incidence of bronchopulmonary dysplasia among extremely preterm infants: a systematic literature review,” 2021, doi: 10.1080/14767058.2019.1646240.

[38] R. Kalikkot Thekkeveedu, M. C. Guaman, and B. Shivanna, “Bronchopulmonary dysplasia: A review of pathogenesis and pathophysiology,” 2017. doi: 10.1016/j.rmed.2017.10.014.

[39] G. Klinger, N. Sokolover, V. Boyko, L. Sirota, L. Lerner-Geva, and B. Reichman, “Perinatal risk factors for bronchopulmonary dysplasia in a national cohort of very-low-birthweight infants,” 2013, doi: 10.1016/j.ajog.2012.11.026.

[40] V. Bhandari *et al.*, “Familial and genetic susceptibility to major neonatal morbidities in preterm twins,” 2006, doi: 10.1542/peds.2005-1414.

[41] R. A. Parker, D. P. Lindstrom, and R. B. Cotton, “Evidence from twin study implies possible genetic susceptibility to bronchopulmonary dysplasia,” 1996. doi: 10.1016/s0146-0005(96)80049-8.

[42] C. V. Lal and N. Ambalavanan, “Genetic predisposition to bronchopulmonary dysplasia,” 2015. doi: 10.1053/j.semperi.2015.09.004.

[43] D. Sharma, S. Shastri, N. Farahbakhsh, and P. Sharma, “Intrauterine growth restriction–part 1,” 2016. doi: 10.3109/14767058.2016.1152249.

[44] J. B. Armengaud, C. Yzydorczyk, B. Siddeek, A. C. Peyter, and U. Simeoni, “Intrauterine growth restriction: Clinical consequences on health and disease at adulthood,” 2021, doi: 10.1016/j.reprotox.2020.10.005.

[45] A. Malhotra, B. J. Allison, M. Castillo-Melendez, G. Jenkin, G. R. Polglase, and S. L. Miller, “Neonatal morbidities of fetal growth restriction: pathophysiology and impact,” 2019. doi: 10.3389/fendo.2019.00055.

[46] R. L. Goldenberg, J. C. Hauth, and W. W. Andrews, “Intrauterine infection and preterm delivery,” 2000. doi: 10.1056/NEJM200005183422007.

[47] C. J. Kim, R. Romero, P. Chaemsaithong, N. Chaiyasit, B. H. Yoon, and Y. M. Kim, “Acute chorioamnionitis and funisitis: definition, pathologic features, and clinical significance,” 2015. doi: 10.1016/j.ajog.2015.08.040.

[48] K. L. Watterberg, L. M. Demers, S. M. Scott, and S. Murphy, “Chorioamnionitis and early lung inflammation in infants in whom Bronchopulmonary Dysplasia develops,” 1996.

[Online]. Available: http://publications.aap.org/pediatrics/article-pdf/97/2/210/1047597/210.pdf

[49] E. Bancalari, "Antenatal Infections and Respiratory Outcome in Preterm Infants," 2020. doi: 10.1055/s-0040-1714347.

[50] C. Newman, V. Petruzzi, P. T. Ramirez, and C. Hobday, "Hypertensive disorders of pregnancy," 2024. doi: 10.14797/mdcvj.1305.

[51] G. M. Rocha *et al.*, "Hypertensive disorders during pregnancy and risk of Bronchopulmonary Dysplasia in very preterm infants," 2019, doi: 10.1055/s-0038-1660865.

[52] C. A. Turpin, S. A. Sakyi, W. K. Owiredu, R. K. Ephraim, and E. O. Anto, "Association between adverse pregnancy outcome and imbalance in angiogenic regulators and oxidative stress biomarkers in gestational hypertension and preeclampsia," 2015, doi: 10.1186/s12884-015-0624-y.

[53] C. T. McEvoy and E. R. Spindel, "Pulmonary effects of maternal smoking on the fetus and child: effects on lung development, respiratory morbidities, and life long lung health," 2017. doi: 10.1016/j.prrv.2016.08.005.

[54] T. Isayama *et al.*, "Adverse impact of maternal cigarette smoking on preterm infants: a population-based cohort Study," 2015, doi: 10.1055/s-0035-1548728.

[55] S. Perrone, M. Tataranno, and G. Buonocore, "Oxidative stress and bronchopulmonary dysplasia," 2012, doi: 10.4103/2249-4847.101683.

[56] J. Wang and W. Dong, "Oxidative stress and bronchopulmonary dysplasia," 2018. doi: 10.1016/j.gene.2018.08.031.

[57] V. Bhandari, "Hyperoxia-derived lung damage in preterm infants," 2010, doi: 10.1016/j.siny.2010.03.009.

[58] J. Balany and V. Bhandari, "Understanding the impact of infection, inflammation, and their persistence in the pathogenesis of bronchopulmonary dysplasia," 2015. doi: 10.3389/fmed.2015.00090.

[59] R. Kalikkot Thekkeveedu, A. El-Saie, V. Prakash, L. Katakam, and B. Shivanna, "Ventilation-Induced Lung Injury (VILI) in neonates: evidence-based concepts and lung-protective strategies," 2022. doi: 10.3390/jcm11030557.

[60] A. H. Van Kaam, "Optimal strategies of mechanical ventilation: can we avoid or reduce lung injury?," 2024. doi: 10.1159/000539346.

[61] G. F. Curley, J. G. Laffey, H. Zhang, and A. S. Slutsky, "Biotrauma and ventilator-induced lung injury: clinical implications," 2016, doi: 10.1016/j.chest.2016.07.019.

[62] A. S. Slutsky and L. N. Tremblay, "Multiple system organ failure. Is mechanical ventilation a contributing factor?," 1998. doi: 10.1164/ajrccm.157.6.9709092.

[63] U. Salimi, K. Dummula, M. H. Tucker, C. S. Dela Cruz, and V. Sampath, "Postnatal sepsis and Bronchopulmonary Dysplasia in premature infants: mechanistic Insights into 'new BPD,'" 2022, doi: 10.1165/rcmb.2021-0353PS.

[64] A. Ohlin, L. Björkman, F. Serenius, J. Schollin, and K. Källén, “Sepsis as a risk factor for neonatal morbidity in extremely preterm infants,” 2015, doi: 10.1111/apa.13104.

[65] S. E. G. Hamrick *et al.*, “Patent ductus arteriosus of the preterm infant,” 2020, doi: 10.1542/peds.2020-1209.

[66] S. J. Gentle, C. P. Travers, M. Clark, W. A. Carlo, and N. Ambalavanan, “Patent ductus arteriosus and development of Bronchopulmonary Dysplasia-associated pulmonary hypertension,” 2023, doi: 10.1164/rccm.202203-0570OC.

[67] M. Pammi *et al.*, “Airway microbiome and development of Bronchopulmonary Dysplasia in preterm infants: a systematic review,” 2019, doi: 10.1016/j.jpeds.2018.08.042.

[68] A. J. Jobe, “The new BPD: an arrest of lung development,” 1999, doi: 10.1203/00006450-199912000-00007.

[69] A. N. Husain and T. Stocker, “Pathology of arrested acinar development in postsurfactant Bronchopulmonary Dysplasia,” 1998. doi: 10.1016/s0046-8177(98)90280-5.

[70] M. Pierce and E. Bancalari, “The role of inflammation in the pathogenesis of Bronchopulmonary Dysplasia,” 1995. doi: 10.1002/ppul.1950190611.

[71] C. P. Speer, “New Insights into the Pathogenesis of Pulmonary Inflammation in Preterm Infants,” 2001. doi: 10.1159/000047092.

[72] C. P. Speer, “Inflammation and bronchopulmonary dysplasia,” 2003. doi: 10.1016/S1084-2756(02)00190-2.

[73] O. D. Saugstad, “Bronchopulmonary dysplasia and oxidative stress: are we closer to an understanding of the pathogenesis of BPD?,” 1997. doi: 10.1111/j.1651-2227.1997.tb14897.x.

[74] B. Reyburn *et al.*, “Nasal ventilation alters mesenchymal cell turnover and improves alveolarization in preterm lambs,” 2008, doi: 10.1164/rccm.200802-359OC.

[75] Abman S. H., “Bronchopulmonary dysplasia ‘a vascular hypothesis,’” 2001, doi: 10.1164/ajrccm.164.10.2109111c.

[76] M. Jakkula *et al.*, “Inhibition of angiogenesis decreases alveolarization in the developing rat lung,” Sep. 2000. doi: 10.1152/ajplung.2000.279.3.L600.

[77] B. Thébaud *et al.*, “Vascular endothelial growth factor gene therapy increases survival, promotes lung angiogenesis, and prevents alveolar damage in hyperoxia-induced lung injury: evidence that angiogenesis participates in alveolarization,” 2005, doi: 10.1161/CIRCULATIONAHA.105.541524.

[78] A. J. Bhatt, G. S. Pryhuber, H. Huyck, R. H. Watkins, L. A. Metlay, and W. M. Maniscalco, “Disrupted pulmonary vasculature and decreased Vascular Endothelial Growth Factor, Flt-1, and TIE-2 in human infants dying with Bronchopulmonary Dysplasia,” 2001, doi: 10.1164/rccm2101140.

[79] B. Thébaud and S. H. Abman, “Bronchopulmonary dysplasia: where have all the vessels gone? Roles of angiogenic growth factors in chronic lung disease,” 2007. doi: 10.1164/rccm.200611-1660PP.

[80] A. Bhandari and S. McGrath-Morrow, “Long-term pulmonary outcomes of patients with bronchopulmonary dysplasia,” 2013. doi: 10.1053/j.semperi.2013.01.010.

[81] L. M. Davidson and S. K. Berkelhamer, “Bronchopulmonary dysplasia: chronic lung disease of infancy and long-term pulmonary outcomes,” 2017. doi: 10.3390/jcm6010004.

[82] E. Baraldi and M. Filippone, “Chronic lung disease after premature birth,” 2007. doi: 10.1056/NEJMra067279.

[83] L. W. Doyle, B. Faber, C. Callanan, N. Freezer, G. W. Ford, and N. M. Davis, “Bronchopulmonary dysplasia in very low birth weight subjects and lung function in late adolescence,” 2006, doi: 10.1542/peds.2005-2522.

[84] M. Vom Hove, F. Prenzel, H. H. Uhlig, and E. Robel-Tillig, “Pulmonary outcome in former preterm, very low birth weight children with bronchopulmonary dysplasia: a case-control follow-up at school age,” 2014, doi: 10.1016/j.jpeds.2013.07.045.

[85] S. G. Royce *et al.*, “Airway remodeling and hyperreactivity in a model of bronchopulmonary dysplasia and their modulation by IL-1 receptor antagonist,” 2016, doi: 10.1165/rcmb.2016-0031OC.

[86] E. Priante, L. Moschino, V. Mardegan, P. Manzoni, S. Salvadori, and E. Baraldi, “Respiratory outcome after preterm birth: a long and difficult journey,” 2016. doi: 10.1055/s-0036-1586172.

[87] S. A. McGrath-Morrow and J. M. Collaco, “Bronchopulmonary dysplasia: what are its links to COPD?,” 2019. doi: 10.1177/1753466619892492.

[88] R. Bhat, A. A. Salas, C. Foster, W. A. Carlo, and N. Ambalavanan, “Prospective analysis of pulmonary hypertension in extremely low birth weight infants,” 2012, doi: 10.1542/peds.2011-1827.

[89] N. Ambalavanan and P. Mourani, “Pulmonary hypertension in bronchopulmonary dysplasia,” 2014, doi: 10.1002/bdra.23241.

[90] L. Strueby and B. Thébaud, “Advances in bronchopulmonary dysplasia,” 2014. doi: 10.1586/17476348.2014.899907.

[91] W. Durlak and B. Thébaud, “BPD: latest strategies of prevention and treatment,” 2024. doi: 10.1159/000540002.

[92] D. J. Henderson-Smart, A. G. De Paoli, and D. Haughton, “Methylxanthine treatment for apnoea in preterm infants,” 2010. doi: 10.1002/14651858.CD000140.pub2.

[93] B. Schmidt *et al.*, “Caffeine therapy for apnea of prematurity,” 2006. doi: 10.1056/NEJMoa054065.

[94] C. Tian, D. Li, and J. Fu, “Molecular mechanism of caffeine in preventing Bronchopulmonary Dysplasia in premature infants,” 2022. doi: 10.3389/fped.2022.902437.

[95] L. W. Doyle, S. Ranganathan, and J. L. Y. Cheong, “Neonatal caffeine treatment and respiratory function at 11 years in children under 1, 251 g at Birth,” 2017, doi: 10.1164/rccm.201704-0767OC.

[96] E. Schwartz, R. Zelig, A. Parker, and S. Johnson, “Vitamin A supplementation for the prevention of bronchopulmonary dysplasia in preterm infants: An update,” 2017. doi: 10.1177/0884533616673613.

[97] F. Chytil, “The lungs and vitamin A,” 1992. doi: 10.1152/ajplung.1992.262.5.L517.

[98] A. Abdelkader, A. A. Wahba, M. El-Tonsy, A. A. Zewail, and M. Shams Eldin, “Recurrent respiratory infections and vitamin A levels: a link? It is cross-sectional,” 2022, doi: 10.1097/MD.0000000000030108.

[99] R. P. Verma, K. M. Mcculloch, L. Worrell, and D. Vidyasagar, “Vitamin A deficiency and severe Bronchopulmonary Dysplasia in very low birth weight infants,” 1996. doi: 10.1055/s-2007-994376.

[100] Y. Ding, Z. Chen, and Y. Lu, “Vitamin A supplementation prevents the bronchopulmonary dysplasia in premature infants: a systematic review and meta-analysis,” 2021. doi: 10.1097/MD.0000000000023101.

[101] M. Filippone, D. Nardo, L. Bonadies, S. Salvadori, and E. Baraldi, “Update on postnatal corticosteroids to prevent or treat Bronchopulmonary Dysplasia,” 2019. doi: 10.1055/s-0039-1691802.

[102] E. S. Shinwell *et al.*, “Early postnatal dexamethasone treatment and increased incidence of cerebral palsy,” 2000. doi: 10.1136/fn.83.3.f177.

[103] L. W. Doyle, J. L. Cheong, R. A. Ehrenkranz, and H. L. Halliday, “Early (< 8 days) systemic postnatal corticosteroids for prevention of bronchopulmonary dysplasia in preterm infants,” 2017. doi: 10.1002/14651858.CD001146.pub5.

[104] L. W. Doyle, J. L. Cheong, S. Hay, B. J. Manley, and H. L. Halliday, “Late (≥ 7 days) systemic postnatal corticosteroids for prevention of bronchopulmonary dysplasia in preterm infants,” 2021. doi: 10.1002/14651858.CD001145.pub5.

[105] D. Bassler *et al.*, “Long-term effects of inhaled budesonide for Bronchopulmonary Dysplasia,” 2018, doi: 10.1056/nejmoa1708831.

[106] F. Ricci *et al.*, “In vitro and in vivo characterization of poractant alfa supplemented with budesonide for safe and effective intratracheal administration,” 2017, doi: 10.1038/pr.2017.171.

[107] R. Venkataraman, M. Kamaluddeen, S. U. Hasan, H. L. Robertson, and A. Lodha, “Intratracheal administration of budesonide-surfactant in prevention of Bronchopulmonary Dysplasia in very low birth weight infants: a systematic review and meta-analysis,” 2017. doi: 10.1002/ppul.23680.

[108] B. J. Manley *et al.*, “Intratracheal budesonide mixed with surfactant to increase survival free of bronchopulmonary dysplasia in extremely preterm infants: study protocol for the international, multicenter, randomized PLUSS trial,” 2023, doi: 10.1186/s13063-023-07257-5.

[109] B. J. Manley *et al.*, “Intratracheal Budesonide Mixed with Surfactant for Extremely Preterm Infants: The PLUSS Randomized Clinical Trial,” 2024, doi: 10.1001/jama.2024.17380.

[110] L. Strueby and B. Thébaud, “Mesenchymal stromal cell-based therapies for chronic lung disease of prematurity,” 2016. doi: 10.1055/s-0036-1586115.

[111] F. Lesage and B. Thébaud, “Nanotherapies for micropreemies: Stem cells and the secretome in bronchopulmonary dysplasia,” 2018. doi: 10.1053/j.semperi.2018.09.007.

[112] G. R. Willis *et al.*, “Mesenchymal stromal cell exosomes ameliorate experimental bronchopulmonary dysplasia and restore lung function through macrophage immunomodulation,” 2018, doi: 10.1164/rccm.201705-0925OC.

[113] S. Zhang, X. Luan, H. Li, and Z. Jin, “Insulin-like growth factor-1: a potential target for bronchopulmonary dysplasia treatment,” 2022, doi: 10.3892/etm.2022.11114.

[114] E. Capoluongo, F. Ameglio, and C. Zuppi, “Insulin-like growth factor-1 and complications of prematurity: a focus on bronchopulmonary dysplasia,” 2008. doi: 10.1515/CCLM.2008.211.

[115] G. Seedorf *et al.*, “rhIGF-1/BP3 preserves lung growth and prevents pulmonary hypertension in experimental Bronchopulmonary Dysplasia,” 2020, doi: 10.1164/RCCM.201910-1975OC.

[116] D. Ley *et al.*, “rhIGF-1/rhIGFBP-3 in preterm infants: a phase 2 randomized controlled trial,” 2019, doi: 10.1016/j.jpeds.2018.10.033.

[117] M. S. Rindfleisch, J. D. Hasday, V. Taciak, K. Broderick, and R. M. Viscardi, “Potential role of Interleukin-1 in the development of Bronchopulmonary Dysplasia,” Mary Ann Liebert, Inc, 1996. doi: 10.1089/jir.1996.16.365.

[118] M. F. Nold *et al.*, “Interleukin-1 receptor antagonist prevents murine bronchopulmonary dysplasia induced by perinatal inflammation and hyperoxia,” 2013, doi: 10.1073/pnas.1306859110.

[119] E. A. Green *et al.*, “Anakinra Pilot – a clinical trial to demonstrate safety, feasibility and pharmacokinetics of interleukin 1 receptor antagonist in preterm infants,” 2022, doi: 10.3389/fimmu.2022.1022104.

[120] C. Nardiello, I. Mižíková, and R. E. Morty, “Looking ahead: where to next for animal models of bronchopulmonary dysplasia?,” 2017. doi: 10.1007/s00441-016-2534-3.

[121] T. Salaets, A. Gie, B. Tack, J. Deprest, and J. Toelen, “Modelling Bronchopulmonary Dysplasia in animals: arguments for the preterm rabbit model,” 2017, doi: 10.2174/1381612823666170926123550.

[122] R. E. Morty, “Using experimental models to identify pathogenic pathways and putative disease management targets in bronchopulmonary dysplasia,” 2020. doi: 10.1159/000506989.

[123] J. Berger and V. Bhandari, “Animal models of bronchopulmonary dysplasia. The term mouse models,” 2014, doi: 10.1152/ajplung.00159.2014.-The.

[124] M. O’reilly and B. Thébaud, “Animal models of bronchopulmonary dysplasia. The term rat models,” 2014, doi: 10.1152/ajplung.00160.2014.-Bronchopulmo.

[125] K. H. Albertine, “Progress in understanding the pathogenesis of BPD using the baboon and sheep models,” 2013. doi: 10.1053/j.semperi.2013.01.001.

[126] B. A. Yoder and J. J. Coalson, “Animal models of bronchopulmonary dysplasia. The preterm baboon models,” 2014, doi: 10.1152/ajplung.00171.2014.-Much.

[127] K. H. Albertine, “Utility of large-animal models of BPD: chronically ventilated preterm lambs,” 2015, doi: 10.1152/ajplung.00178.2014.-This.

[128] L. Frank and I. R. S. Sosenko, “Failure of premature rabbits to increase antioxidant enzymes during hyperoxic exposure: increased susceptibility to pulmonary oxygen toxicity compared with term rabbits,” 1991. doi: 10.1203/00006450-199103000-00014.

[129] G. F. Ross, M. Ikegami, W. Steinhilber, and A. H. Jobe, “Surfactant protein C in fetal and ventilated preterm rabbit lungs,” 1999. doi: 10.1152/ajplung.1999.277.6.L1104.

[130] T. Salaets *et al.*, “Preterm birth impairs postnatal lung development in the neonatal rabbit model,” 2020, doi: 10.1186/s12931-020-1321-6.

[131] R. S. Mascaretti, M. M. G. B. Mataloun, M. Dolhnikoff, and C. M. Rebello, “Lung morphometry, collagen and elastin content: changes after hyperoxic exposure in preterm rabbits,” 2009, doi: 10.1590/S1807-59322009001100010.

[132] R. M. Manzano *et al.*, “A hyperoxic lung injury model in premature rabbits: The influence of different gestational ages and oxygen concentrations,” 2014, doi: 10.1371/journal.pone.0095844.

[133] J. Richter *et al.*, “Functional assessment of hyperoxia-induced lung injury after preterm birth in the rabbit,” 2014, doi: 10.1152/ajplung.00315.2013.-The.

[134] S. Dutta and P. Sengupta, “Rabbits and men: relating their ages,” 2018. doi: 10.1515/jbcpp-2018-0002.

[135] C. Catozzi *et al.*, “Single, double, and triple-hit strategies to establish a long-term premature rabbit model of bronchopulmonary dysplasia,” 2025, doi: 10.1186/s12931-024-03053-0.

[136] W. M. Thurlbeck, “Internal surface area and other measurements in emphysema,” 1967. doi: 10.1136/thx.22.6.483.

[137] J. L. Emery and A. Mithal, “The number of alveoli in the terminal respiratory unit of man during late intrauterine life and childhood,” 1960. doi: 10.1136/adc.35.184.544.

[138] W. M. Thurlbeck, “Measurement of pulmonary emphysema,” 1966. doi: 10.1164/arrd.1967.95.5.752.

[139] M. Lucattelli *et al.*, “Is neutrophil elastase the missing link between emphysema and fibrosis? Evidence from two mouse models,” 2005, doi: 10.1186/1465-9921-6-83.

[140] G. Matute-Bello *et al.*, “An official american thoracic society workshop report: features and measurements of experimental acute lung injury in animals,” 2011. doi: 10.1165/rcmb.2009-0210ST.

[141] J. J. Coalson, “Pathology of Bronchopulmonary Dysplasia,” 2006. doi: 10.1053/j.semperi.2006.05.004.

[142] K. Bera, K. A. Schalper, D. L. Rimm, V. Velcheti, and A. Madabhushi, “Artificial intelligence in digital pathology — new tools for diagnosis and precision oncology,” 2019, doi: 10.1038/s41571-019-0252-y.

[143] R. S. Doğan and B. Yılmaz, “Histopathology image classification: highlighting the gap between manual analysis and AI automation,” 2023, doi: 10.3389/fonc.2023.1325271.

[144] H. Reza Tizhoosh and L. Pantanowitz, “Artificial intelligence and digital pathology: challenges and opportunities,” 2018, doi: 10.4103/jpi.jpi_53_18.

[145] J. S. Reis-Filho and J. N. Kather, “Overcoming the challenges to implementation of artificial intelligence in pathology,” 2023, doi: 10.1093/jnci/djad048.

[146] M. Shah, D. Jain, S. Prasath, and K. Dufendach, “Artificial intelligence in bronchopulmonary dysplasia- current research and unexplored frontiers,” 2023. doi: 10.1038/s41390-022-02387-z.

[147] H. Y. Chou *et al.*, “Deep learning model for prediction of Bronchopulmonary Dysplasia in preterm infants using chest radiographs,” 2024, doi: 10.1007/s10278-024-01050-9.

[148] A. Perri *et al.*, “The future of neonatal lung ultrasound: validation of an artificial intelligence model for interpreting lung scans. A multicentre prospective diagnostic study,” 2023, doi: 10.1002/ppul.26563.

[149] M. S. Dunnill, “Quantitative methods in the study of pulmonary pathology,” 1962. doi: 10.1136/thx.17.4.320.

[150] S. Fineschi *et al.*, “Receptor for advanced glycation end products contributes to postnatal pulmonary development and adult lung maintenance program in mice,” 2013, doi: 10.1165/rcmb.2012-0111OC.

[151] T. P. Cooney and W. M. Thurlbeck, “The radial alveolar count method of Emery and Mithal: a reappraisal 2-Intrauterine and early postnatal lung growth,” 1982. doi: 10.1136/thx.37.8.580.

[152] J. J. Coalson, “Pathology of new bronchopulmonary dysplasia,” 2003. doi: 10.1016/S1084-2756(02)00193-8.

[153] N. Dankhara, I. Holla, S. Ramarao, and R. Kalikkot Thekkeveedu, “Bronchopulmonary Dysplasia: pathogenesis and pathophysiology,” 2023. doi: 10.3390/jcm12134207.

[154] J. Jiménez *et al.*, “Progressive vascular functional and structural damage in a bronchopulmonary dysplasia model in preterm rabbits exposed to hyperoxia,” 2016, doi: 10.3390/ijms17101776.

[155] R. P. Mecham, “Elastin in lung development and disease pathogenesis,” 2018. doi: 10.1016/j.matbio.2018.01.005.

[156] M. C. Bruce, R. Pawlowski, and J. F. Tomashefski, “Changes in Lung Elastic Fiber Structure and Concentration Associated with Hyperoxic Exposure in the Developing Rat Lung 1-3,” Oct. 1989. doi: 10.1164/ajrccm/140.4.1067.

[157] M. C. Bruce *et al.*, “Altered urinary excretion of elastin cross-links in premature infants who develop Bronchopulmonary Dysplasia,” 1985. doi: 10.1164/arrd.1985.131.4.568.

[158] I. Mižíková *et al.*, “Collagen and elastin cross-linking is altered during aberrant late lung development associated with hyperoxia,” 2015, doi: 10.1152/ajplung.00039.2015.-Maturation.

[159] M. Storti *et al.*, “Time-resolved transcriptomic profiling of the developing rabbit’s lungs: impact of premature birth and implications for modelling bronchopulmonary dysplasia,” 2023, doi: 10.1186/s12931-023-02380-y.

[160] C. Boggi *et al.*, “Longitudinal transcriptomic analysis of the hyperoxia-exposed preterm rabbit as a model of BPD,” 2025, doi: 10.3389/fped.2025.1567091.

[161] S. H. Randell, R. Silbajoris, and S. L. Young, “Ontogeny of rat lung type II cells correlated with surfactant lipid and surfactant apoprotein expression,” 1991. doi: 10.1152/ajplung.1991.260.6.L562.

[162] M. Yee *et al.*, “Type II epithelial cells are critical target for hyperoxia-mediated impairment of postnatal lung development,” 2006, doi: 10.1152/ajplung.00126.2006.-Type.

[163] X. xiang Liu, X. rong Yu, X. hong Jia, K. xuan Wang, Z. yan Yu, and C. jun Lv, “Effect of hyperoxia on the viability and proliferation of the primary type II alveolar epithelial cells,” 2013, doi: 10.1007/s12013-013-9658-9.

[164] A. Hou *et al.*, “Hyperoxia stimulates the transdifferentiation of type II alveolar epithelial cells in newborn rats,” 2015, doi: 10.1152/ajplung.00099.2014.-Supple.

[165] A. E. Vaughan and Chapman H. A., “Failure of alveolar type 2 cell maintenance links neonatal distress with adult lung disease,” 2017. doi: 10.1165/rcmb.2016-0411ED.

[166] B. A. Ruschkowski *et al.*, “Thrombospondin-1 plays a major pathogenic role in experimental and human Bronchopulmonary Dysplasia,” 2022, doi: 10.1164/RCCM.202104-1021OC.

[167] M. E. De Paepe, D. Greco, and Q. Mao, “Angiogenesis-related gene expression profiling in ventilated preterm human lungs,” 2010, doi: 10.3109/01902141003714031.

[168] L. Fina *et al.*, “Expression of the CD34 gene in vascular endothelial cells,” 1990.

[169] P. Hildbrand *et al.*, “The role of angiopoietins in the development of endothelial cells from cord blood CD34+ progenitors,” 2004, doi: 10.1182/blood-2003-12-4219.

[170] N. F. Renna, N. De Las Heras, and R. M. Miatello, “Pathophysiology of vascular remodeling in hypertension,” 2013. doi: 10.1155/2013/808353.

[171] R. Jones, “Ultrastructural analysis of contractile cell development in lung microvessels in hyperoxic pulmonary hypertension. Fibroblasts and intermediate cells selectively reorganize nonmuscular segments,” 1992.

[172] J. E. Wagenseil and R. P. Mecham, “Elastin in large artery stiffness and hypertension,” 2012, doi: 10.1007/s12265-012-9349-8.